Available online at www.sciencedirect.com
ScienceDirect
Ore Geology Reviews 32 (2007) 81–124
ORE GEOLOGY REVIEWS
www.elsevier.com/locate/oregeorev

Low-sulfidation type Au–Ag mineralization at Bergama, Izmir, Turkey

Huseyin Yilmaz [a,*], Tolga Oyman [a], Greg B. Arehart [b], A. Riza Colakoglu [c], Zeki Billor [d]

[a] Dokuz Eylul University, Faculty of Engineering, Department of Geological Engineering, Bornova-35100, Izmir, Turkey
[b] University of Nevada, Department of Geological Sciences, MS-172, Reno-NV, 89557-0138, United States
[c] Yuzuncu Yýl University, Faculty of Engineering, Department of Geological Engineering, Van, Turkey
[d] Cukurova University, Faculty of Engineering, Department of Geological Engineering, Adana, Turkey

Received 8 November 2005; accepted 11 October 2006
Available online 10 January 2007

Abstract

Bergama, the center of Bergama County, is located in western Turkey and includes the villages of Ovacik, Narlica and Saganci. The Ovacik epithermal gold–silver deposit is located in the Western Anatolian Volcanic and Extensional Province, adjacent to the ENE-trending Bergama graben, some 100 km north of the city of Izmir. Gold of economic grades at the Ovacik deposit (reserves 4.19 Mt at 7.6 g/t) occurs in epithermal quartz veins which display low-temperature epithermal textures, including crustiform banding, quartz pseudomorphs after bladed calcite, and multiphase hydrothermal breccias. Alteration minerals at both Ovacik and Narlica are dominated by smectite, mixed-layer illite/smectite, chalcedonic quartz and adularia, whereas major kaolinite and minor mixed-layer smectite/illite (>13.4 Å) occur at Saganci. The total sulfide content at Ovacik is low (<2%) and is dominated by pyrite with traces of electrum, chalcopyrite, arsenopyrite, acanthite, tetrahedrite, pyrargyrite, stibnite, galena, chalcocite, bornite, covellite and sphalerite, occurring mainly within breccia clasts. Pyrite and marcasite appear to be the most common opaque minerals at Narlica and form dark sulfide-rich bands along with traces of electrum, native silver and chalcopyrite; pyrite is the only sulfide identified at Saganci. $^{40}Ar/^{39}Ar$ dating of adularia from gold-bearing quartz veins indicates an age of mineralization of about 18.2 ± 0.2 Ma. Fluid inclusion studies at Ovacik reveal that main-stage quartz contains predominantly liquid-rich inclusions with homogenization temperatures (T_h) ranging from 150 to 305 °C, with the majority of T_h varying between 165 to 205 °C: ice-melting temperatures (T_m) ranging from −0.4 to −1.2 °C (salinity <2 wt.% NaCl equiv.) are dominant. Higher T_h (220 to 248 °C) at the Narlica deposit may be attributed to the deeper level of exposure.

Geochemical variations in altered wall rocks at Ovacik and Narlica are generally characterized by two-fold enrichments in K, Rb, Cs and 25 to 93% depletions in Sr, Ca, Mg, Na and even higher depletions (96 to 99% decrease) in the quartz–adularia vein zone. Lanthanum, Ce, Pr, Hf, Zr, Sm, Eu, Gd, Tb and Ho also exhibit up to 50% depletions in the wall rock and even more so (up to 90% depletion for La and Nd) in the vein structure. Wall rock enrichment in Au, Ag, As, Hg and Sc is by factors of 60, 150, 88, 8 and 3, respectively. The ranges of REE in both the altered volcanic rocks and quartz–adularia veins are wide and may reflect either significant mobilization of REE during alteration and mineralization or their dilution by the metasomatic processes from fresh volcanic rocks through montmorillonite–illite–adularia-altered wallrock to quartz–adularia veins. High Rb/Sr ratios in adularia–illite-altered areas are closely related to the presence of K-rich alteration minerals. Low Rb/Sr ratios and corresponding low K values at Saganci are due to acid leaching of volcanic rocks. Positive correlation coefficients between Au and Ag, Pb, Zn, Cd, Cu

* Corresponding author. Dokuz Eylul University, Faculty of Engineering, Dept. of Geological Engineering, 35160 Buca, Tinaztepe Kampusu, Izmir, Turkey. Fax: +90 232 453 1129.
E-mail address: huseyin.yilmaz@deu.edu.tr (H. Yilmaz).

0169-1368/$ - see front matter
doi:10.1016/j.oregeorev.2006.10.007

and Sb in epithermal quartz veins, all of which are >0.51, are significant. Silver and Sb are remarkably enriched at higher levels of the deposit. No correlation occurs between Au and As or Ag and As.

The Ovacik quartz in Au–Ag-bearing veins has $\delta^{18}O$ values ranging from +9.5 to +15.7‰, whereas δD values of fluid inclusions in quartz range from −89 to −125‰. However, the Narlica quartz in Au–Ag bearing veins returned $\delta^{18}O$ values ranging from +5.9‰ to +8.3, whereas the δD values of fluid inclusion in quartz range from −82 to −99‰. $\delta^{18}O$ results indicate that ore-forming hydrothermal fluids at Ovacik and Narlica had $\delta^{18}O_{H2O}$ values ranging from −2.9 to +3.5‰ (average: −0.24‰) and from −2.96 to −0.6 (average −1.6), respectively. They are thus ^{18}O-enriched in comparison with present-day meteoric and hydrothermal meteoric waters (−5.4‰). $\delta^{18}O$, $\delta^{18}O_{H2O}$ and δD values suggest that mineralizing solutions were a mixture of meteoric and magmatic waters. The $\delta\ ^{34}S_{\Sigma sulfide}$ data at Ovacik and Narlica range from −2.1 to 5.3‰ (average: +1.7) and from −4.6 to +2.7‰ (average: −0.36), respectively. These $\delta\ ^{34}S_{\Sigma sulfide}$ values are consistent with a magmatic source for S.

Keywords: Gold; Hydrothermal alteration; Stable isotopes; Geochronology; Fluid inclusions; Ovacik, Turkey

1. Introduction

Basement rocks of Western Turkey consist of Paleozoic metamorphic rocks and Mesozoic mélange, comprising clastic and carbonate rocks. These basement rocks are cut by granitic and granodioritic intrusives, and are overlain mainly by calc-alkaline and minor alkaline volcanic rocks (Fig. 1), ranging in age from 35 to 23 Ma (Yilmaz, 1989; Ercan et al., 1995). The andesitic volcanic suite is represented by andesite, latite, dacite, rhyodacite lava dome facies, and related volcaniclastic sequences. North–south compression and crustal thickening, caused by the north-dipping subduction of the neo-Tethys oceanic crust beneath the Pontic arc, occurred between the Eocene and Early Miocene. This was followed by partial melting of the lower crust to produce anatectic granitic melts (Yilmaz, 1989) and subsequent downbending of the north-subducting slab. This process led to the ultimate detachment and loss of the northward-dipping slab, giving way to the establishment of an extensional tectonic regime with widespread Basin and Range-style deformation (orogenic collapse) in western Turkey (Wright, 1996). The Ovacik and Narlica gold–silver deposits occur in this geological framework within the Western Turkey magmatic arc complex, which forms a part of the northward-dipping Tethys subduction system. The magmatic rocks, which are of Eocene to Pliocene age, exhibit calc-alkaline to alkaline compositions and are tectonically linked to episodes of subduction and extension related to the northward movement of the African–Arabian plate.

The Ovacik–Narlica deposit, in the Bergama area, is the first documented example of low-sulfidation epithermal gold mineralization in the Western Anatolian Volcanic and Extensional (WAVE) province (Figs. 1 and 2). The province hosts several other epithermal deposits (measured and indicated ore reserves prior to mining are given in brackets), such as the quartz–adularia-type Efemçukuru (3.1 Mt at 14.6 g/t Au) and Kucukdere (1.4 Mt at 6.4 g/t Au) deposits and the porphyry-related high sulfidation Kisladag deposit (276 Mt at 1.2 g/t Au). The Ovacik–Narlica deposit is classified as a quartz–adularia-type or 'low sulfidation' gold deposit based on wall-rock and vein alteration assemblages (Yilmaz, 2002) and is similar to many deposits elsewhere in the world (e.g., White and Hedenquist, 1990, 1995; Hedenquist et al., 1996; Cooke and Simmons, 2000; Leach and Corbett, 2001; Simpson et al., 2001; Sillitoe and Hedenquist, 2003).

This paper presents an integrated geochronological, alteration, geochemical and isotope study of the Ovacik–Narlica deposit, which is one of the best exposed-low sulfidation occurrences in the Aegean region. Alongside a number of unpublished company reports, previous studies of gold mineralization at Ovacik include publications by Yilmaz (2002) and Sener (2003). These two papers deal with geological and mineralogical studies of the Ovacik gold deposit. The goal of the present investigation was to constrain the origin and evolution of the deposit in order to address fundamental questions regarding (1) the source(s) of fluids; and (2) the temporal and spatial relationship between, volcanism, adularia–illite (sericite) alteration, and Au mineralization. The enhancement of exploration criteria for similar epithermal deposits in Western Turkey was an additional aim of this study.

2. Mining and exploration history

Mining in the Bergama graben area started at the Narlica gold deposit around 600 B.C., during the reign of King Croesus. This gold occurrence is located at a higher elevation (270 m) than that of Ovacik (70 m). Substantial ancient mine workings and dumps were developed at Narlica over a 500 m strike length within a 1600 m long epithermal lode. Pottery from shallow pits, shafts and

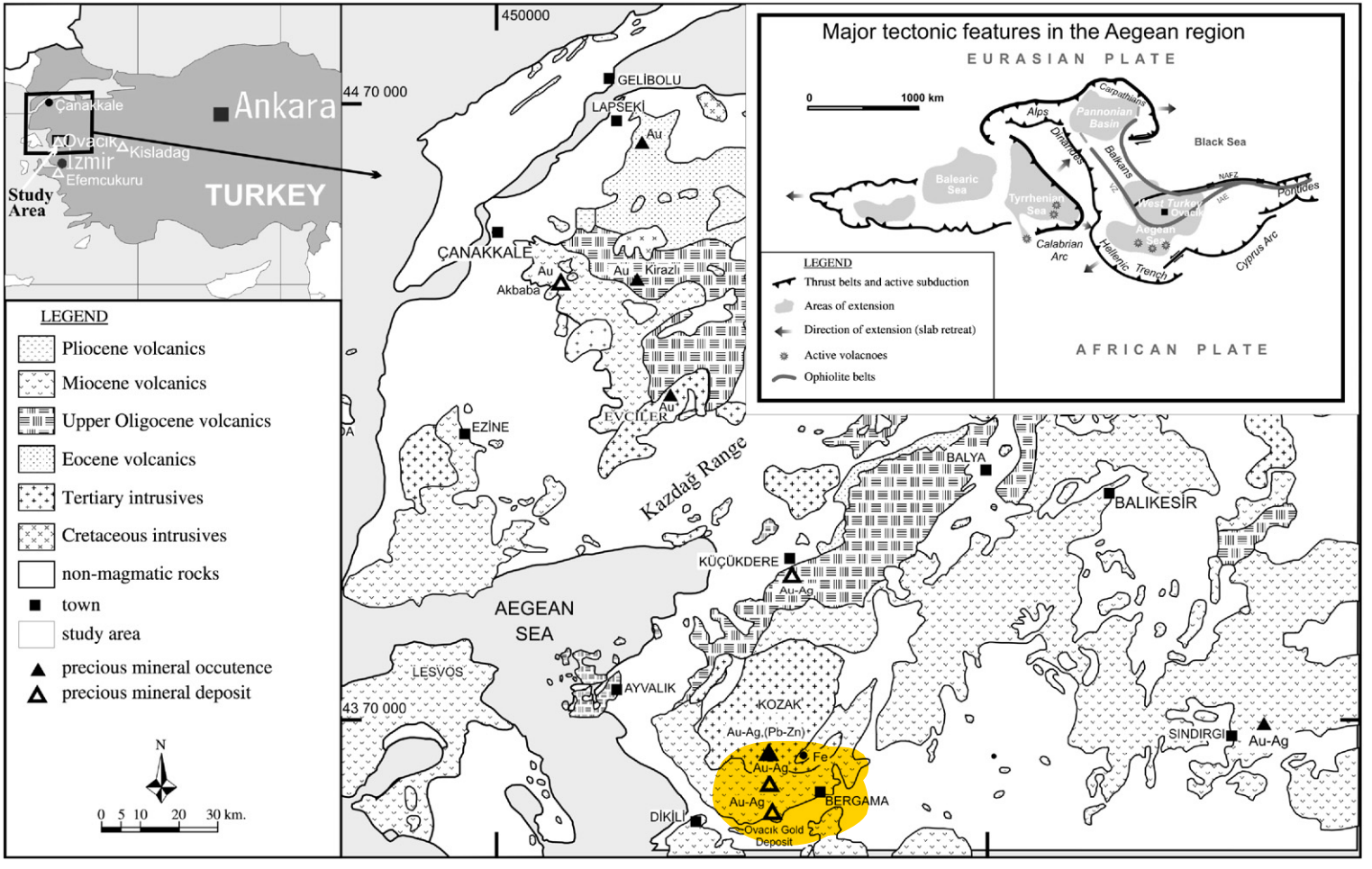

Fig. 1. Simplified geological map of the Tertiary volcanic and plutonic field of northwest Turkey and location of the study area and significant mineralization (volcanic and plutonic fields are modified from Ercan et al., 1984).

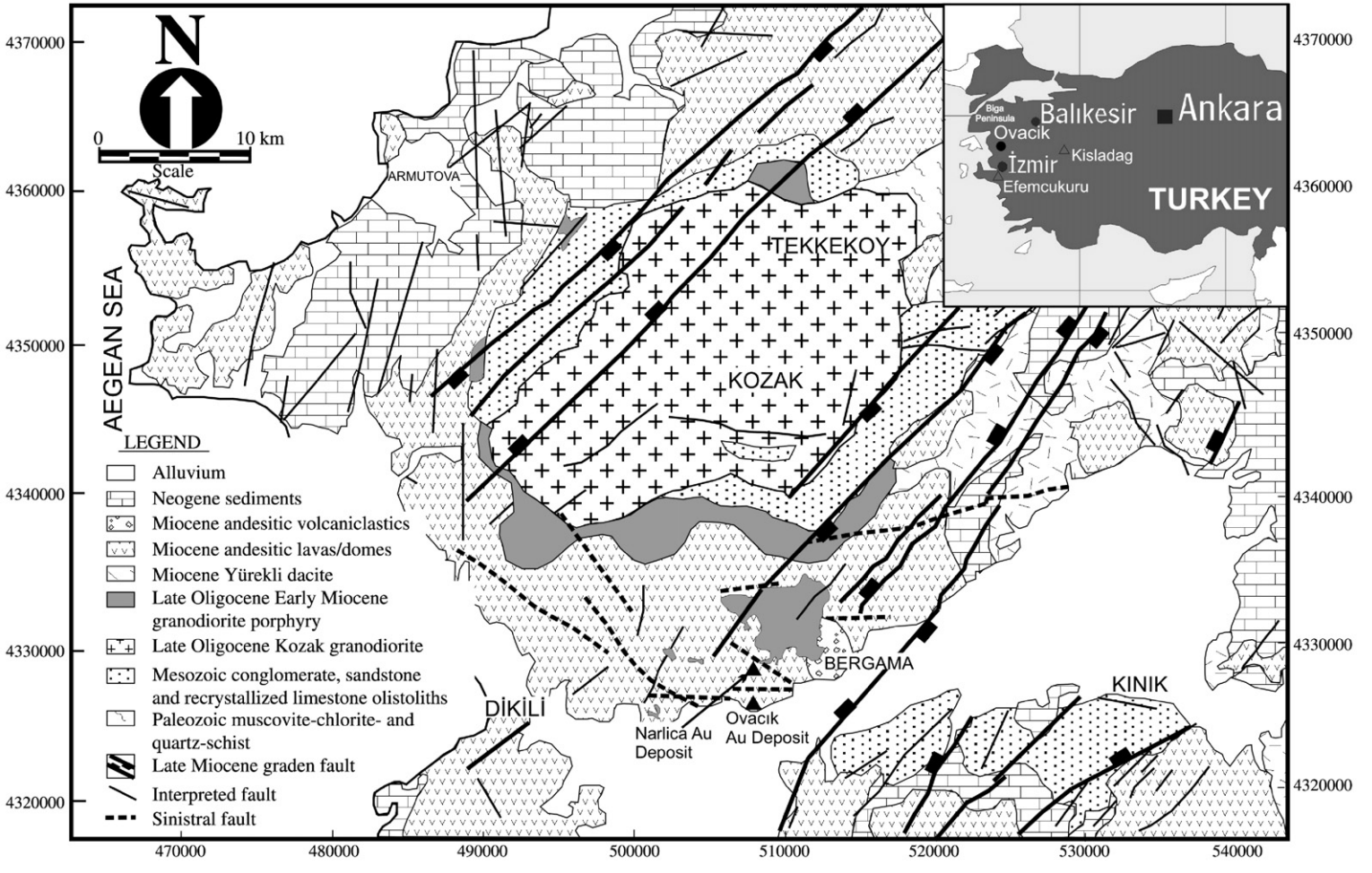

Fig. 2. Regional geologic map of Bergama–Dikili area, modified from Altunkaynak and Yilmaz (1998), Eurogold Madencilik AS unpublished data and Yilmaz (2002).

drives provides evidence that gold from epithermal quartz veins in the Ovacik area was further exploited during the Roman era (~400 A.D.). The Ovacik–Narlica Au–Ag epithermal deposit was rediscovered during a regional Bulk Leach Extractable Gold (BLEG) stream-sediment sampling program in 1988 and was the first economic deposit in the region to be identified by modern prospecting techniques. During the initial BLEG sampling program several anomalous gold values, ranging from 3 to 142 ppb Au, were returned. Follow-up of the 142 ppb BLEG Au anomaly in late 1988 resulted in the location of abundant quartz float in an area which is now known to contain the ancient mine dumps at Narlica. During further prospecting, several epithermal quartz veins were located near the village of Ovacik. Rockchip sampling from this vein returned high gold grades of up to 110 g/t. Since 1989, approximately 20,000 m of drilling has been undertaken by Normandy Mining Ltd. on and around the deposit area during definition of the Ovacik orebody. As of 2003, the Ovacik deposit contained a total reserve (proven + possible + probable) of 4.19 Mt at 7.6 g/t (31.87 t or 1.02 Moz contained gold), of which 2.4 Mt at 10 g/t (24 t) is mineable (Sener, 2003).

3. Geological setting

3.1. Regional geology

The Ovacik and other deposits of the Bergama Au–Ag ore field occur at the southeastern edge of the NE–SW-trending suite of subaerial volcano-plutonic rocks in the Bergama–Ivrindi–Balya districts. These units are bounded to the west by the Ayvalik–Edremit Graben and to the east by the Bergama Graben (Figs. 1 and 2).

The oldest units in the region are Paleozoic metamorphic rocks including low-grade muscovite, chlorite and quartz schists. Widespread magmatism occurred in western Turkey from the Late Oligocene to Early Miocene (Ercan et al., 1984; Yilmaz, 1989; Mckenzie and Yilmaz, 1991; Seyitoglu and Scott, 1991; Seyitoglu et al., 1997; Altunkaynak and Yilmaz, 1998; Bingol and Delaloye, 2000; Yilmaz et al., 2001; Yilmaz and Kracik, 2001). Altunkaynak and Yilmaz (1998) carried out detailed regional scale investigations of volcanism and structural features in the Bergama region, including in the Ovacik–Narlica area.

Magmatic activity in the area began with emplacement of the Upper Oligocene Kozak granodiorite pluton (Fig. 2). Coeval, sheeted, hypabyssal granodiorite porphyry intrusive rocks of Upper Oligocene to Lower Miocene age (Altunkaynak and Yilmaz, 1998) cut the metamorphic basement units and Mesozoic conglomerates, sandstone and recrytallized limestone olistoliths formed around the pluton (Fig. 2). These are, in turn, surrounded by extrusive rocks consisting of andesitic volcaniclastic rocks, undifferentiated intermediate volcanic lava flow/domes and the Yurekli dacite, which are partly contemporaneous with the emplacement of hypabyssal granodiorite porphyry intrusive rocks during the Early Miocene.

Two magmatic episodes are distinguished in Western Turkey. An initial intermediate to felsic calc-alkaline association formed during the Oligocene–Early Miocene (Yilmaz et al., 2001). In this period, granitic plutons were intruded to shallow levels (~4 km below surface) in the crust when the region was still undergoing N–S-directed compression. The magmatic rocks of this phase are commonly high-K calc-alkaline, and partly of shoshonitic and hybrid type (Yilmaz et al., 2001). Altunkaynak and Yilmaz (1998) suggested that lavas and sheeted high-level intrusions followed NE–SW and NS-trending oblique faults to reach the surface. Their compositions reveal crystallization from mantle-derived magmas contaminated by abundant crustal components. Based on the above factors, this magmatic event may be regarded as Tibetan-type magmatism (Yilmaz et al., 2001), with the geological signature of the magmas similar to that of arc-derived magmas. The second magmatic phase consisting of sporadically developed alkaline basalts occurred during the Late Miocene–Pliocene (Seyitoglu et al., 1997).

During the Neogene the region was affected by several extensional events (Zanchi et al., 1990, 1993). The earliest (NW–SE) extensional phase, which prevailed from Middle to Late Miocene, gave rise to NNE–SSW to NE–SW-trending grabens. This was followed by N–S extension during the Early Pliocene to Quaternary. The deposition of overlying Upper Miocene–Lower Pliocene successions was restricted to NE–SW-trending grabens. The Kozak horst is separated from surrounding grabens by a set of *en echelon*, oblique-slip and transtensional faults with NW–SE, NNE–SSW and N–S strike directions (Yilmaz et al., 2001). The graben-bounding faults display oblique-slip with an important component of major strike–slip displacement, formed under approximately N–S extension. The NW–SE-striking faults are predominant and dip steeply with an average angle of 70°. Yilmaz et al. (2001) suggested that the faults with a small component of strike–slip motion, sinistral to the west (Ovacik–Narlica area) and dextral to the east of Bergama along the Bergama graben margin, are compatible with an N–S extensional regime. The major faults dip steeply

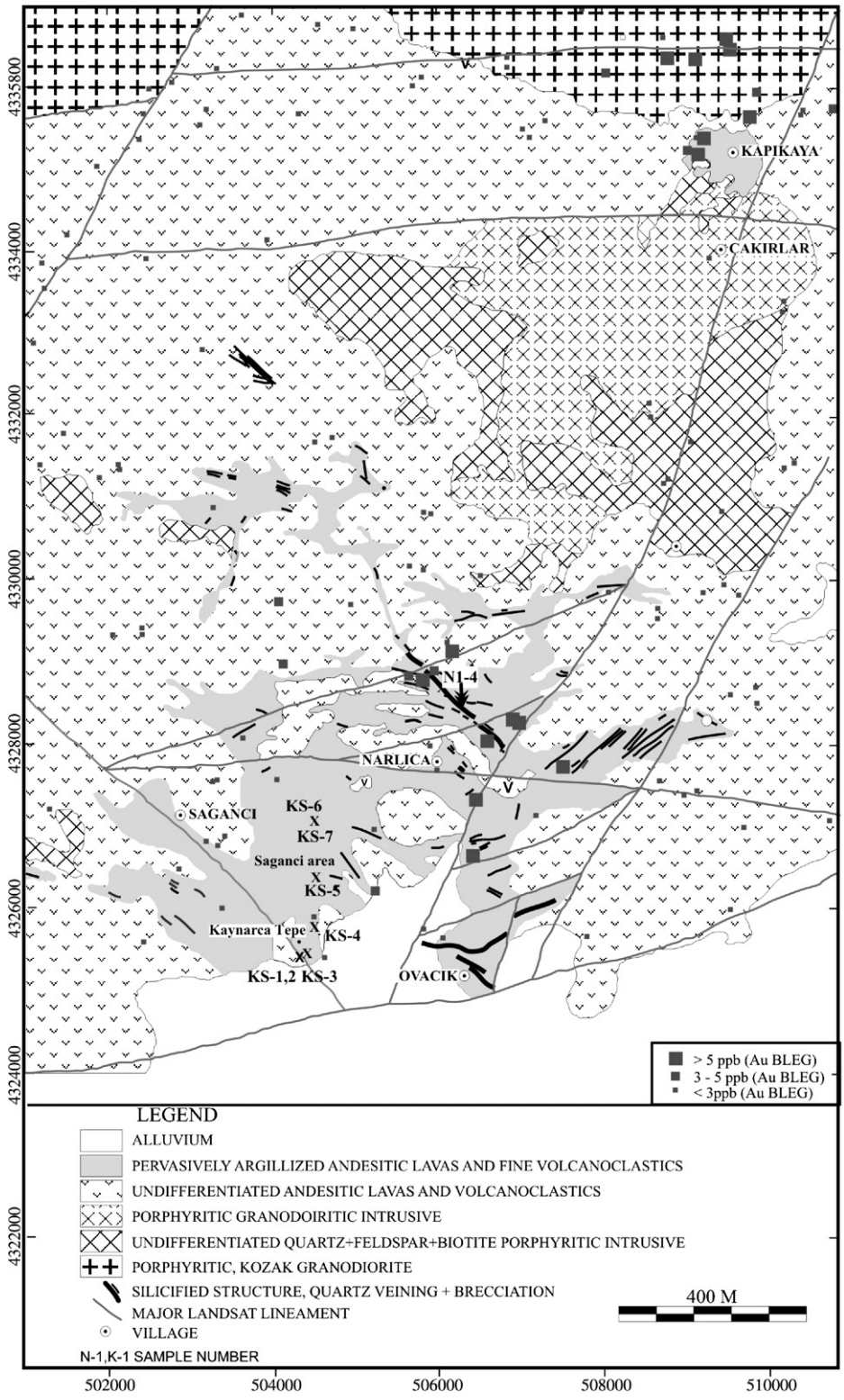

Fig. 3. Geologic map of the Ovacik area. Modified from Eurogold Madencilik AS (unpublished report) and Yilmaz (2002).

(>70°) to the south along the northern side of the Bergama graben.

3.2. Local geology

The Ovacik–Narlica area is underlain by Paleozoic metamorphic rocks and limestone, and is intruded by Kozak granodiorite pluton and porphyritic microdiorite to microgranodiorite intrusive (Fig. 3). Radiometric ages obtained from the plutonic, hypabyssal and calcalkaline volcanic rocks of the Kozak magmatic complex are overlapping, and range from 24 to 15 Ma (Altunkaynak and Yilmaz, 1998). The overlying rocks are porphyritic andesite lava, lava flow breccia, crystal-rich, coarse-to fine-grained volcanoclastic rocks, debris flows and fluviatile epiclastic rocks, followed by subaqueous shallow-water dacitic to rhyolitic lava dome flow facies, associated with various types of volcanoclastic rocks. Locally argillized and tourmalinized porphyritic microdiorite, microquartz-diorite and micro-granodiorite intrusions outcrops over an area of 25 km^2 beginning 1 km north of the Narlica deposit (Fig. 3).

In the Ovacik–Narlica area, lithologies consist of porphyritic biotite andesite with minor andesite breccia and debris flows. The primary mineralogy consists predominantly of large phenocrysts of altered plagioclase, feldspar, biotite and hornblende with accessory apatite and rare small zircon crystals in a fine-grained, recrystallized groundmass. According to the classification of Peccerillo and Taylor (1976), the volcanic rocks fall into the fields of K-rich andesite and dacite with minor latite andesite and trachyte (Ercan et al., 1984). The volcanic rocks are mainly calc-alkaline in composition and have a weakly shoshonitic character (Ercan et al., 1984). Early to Middle Miocene K/Ar ages were obtained from the lavas and vary between 21.9±1.4 and 15.3±0.3 Ma (MTA-JISCA, 1987; Ercan et al., 1995), corresponding mainly to the Early Miocene. K/Ar dating from porphyritic andesite lava domes within the immediate vicinity of the Ovacik ore deposit returned ages ranging from 19 Ma to 14 Ma (Aldanmaz et al., 2000), whereas fission-track dating of apatite phase from the Kozak granodirite yielded 25.7 Ma (Wright et al., 1996). $^{40}Ar/^{39}Ar$ dating from a fresh volcanoclastic outcrop sample 2 km NE of the Ovacik gold mine (this study; see below) returned a plateau age of 19.76±0.14 Ma.

NE–SW-trending prominent faults in the Ovacik–Narlica area are well presented, with most of the faults dipping towards SE. In addition, E–W to NW–SE faults dip steeply either NE or SW. Faults with similar trend and dip occur also in the Ovacik veined zone. These normal faults have a moderate sinistral strike–slip component and are oriented E–W to WNW–ESE, generally dipping to the north (Wright et al., 1996).

4. Characteristics of the vein system

4.1. Ovacik gold–silver deposit

The Ovacik gold–silver deposit consists of four epithermal quartz veins (Fig. 4). The two major lens-shaped veins forming the presently economic (and mined) part of the deposit, referred to as the "M" and "S" veins, display similar morphological and textural characteristics (Fig. 5), have a mapped strike length of 900 m, an average 8 m width, reach a maximum of 22 m and range in dip from 65 to 85° N, with a down-dip extension of about 200 m. Although the margins of the veins have transitional lateral boundaries from the main quartz lodes through stockwork and sheeted quartz veinlets to argillic alteration, the gold grades decrease rapidly from the vein to the country rock. The M vein has an average grade of 13.1 g/t Au, whereas the S vein has an average grade of 8.1 g/t Au.

The veins at Ovacik contain six main textural types of ores: (a) crustiform/colloform banded ore (Figs. 5 and 6A), which occurs in both the veins and as breccia clasts; (b) coarse, bladed carbonate (Fig. 6B), occurring as distinct bands or infilling vugs; (c) clast-supported crackle (shattered) breccia with angular monomictic fragments (Fig. 6C); (d) matrix-supported fluidized (milled) breccia with angular to subrounded polymictic fragments (Fig. 6D), in which the clasts consist mainly of quartz and adularia with common crustiform banding and quartz-cemented breccia; (e) cockade texture; formed from clasts of silicified wall rock overgrown by crustiform/colloform bands and cockades of chalcedonic quartz and adularia (Fig. 6E; and (f) a hanging wall zone of silicified porphyritic andesite (SiAn) and sheeted quartz veinlets (Fig. 6F, Sw).

4.2. Narlica gold–silver deposit

The Narlica gold deposit is located 3.5 km N of Ovacik and is also hosted by Miocene porphyritic andesitic to dacitic volcanic rocks (Fig. 3). The prospective zone at Narlica occurs associated with epithermal veins and veinlets along a main northwesterly-trending subvertical structure having a strike length of 1.6 km. Numerous E–W splays (mostly less than 2 m) from the main structure occur particularly in the vicinity of the central mineralized portion of the vein. The veins are silicified structures hosting dominant breccia and minor quartz lode infilling

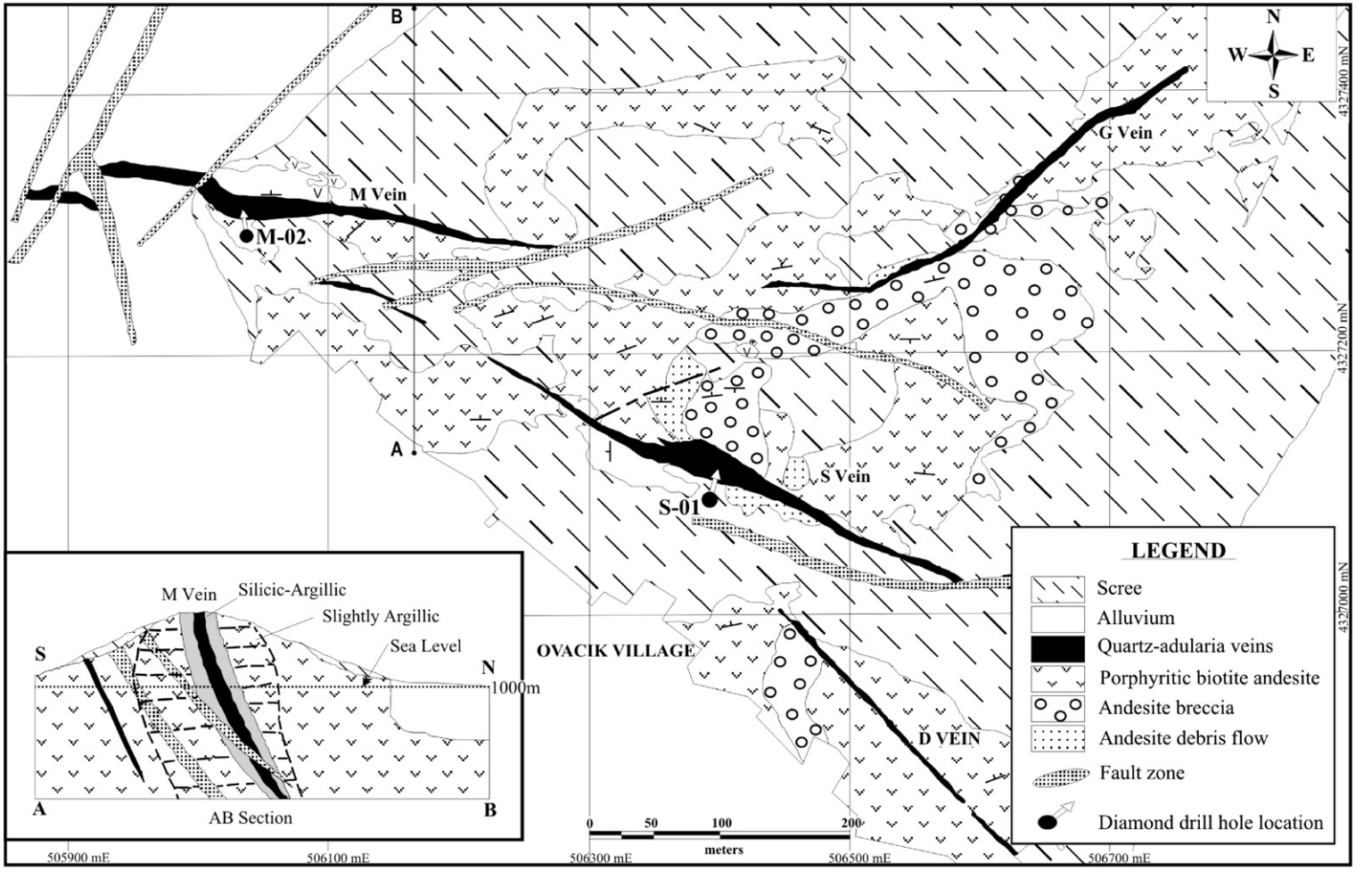

Fig. 4. Geologic map and cross-section of the Ovacik gold deposit (Yilmaz, 2002).

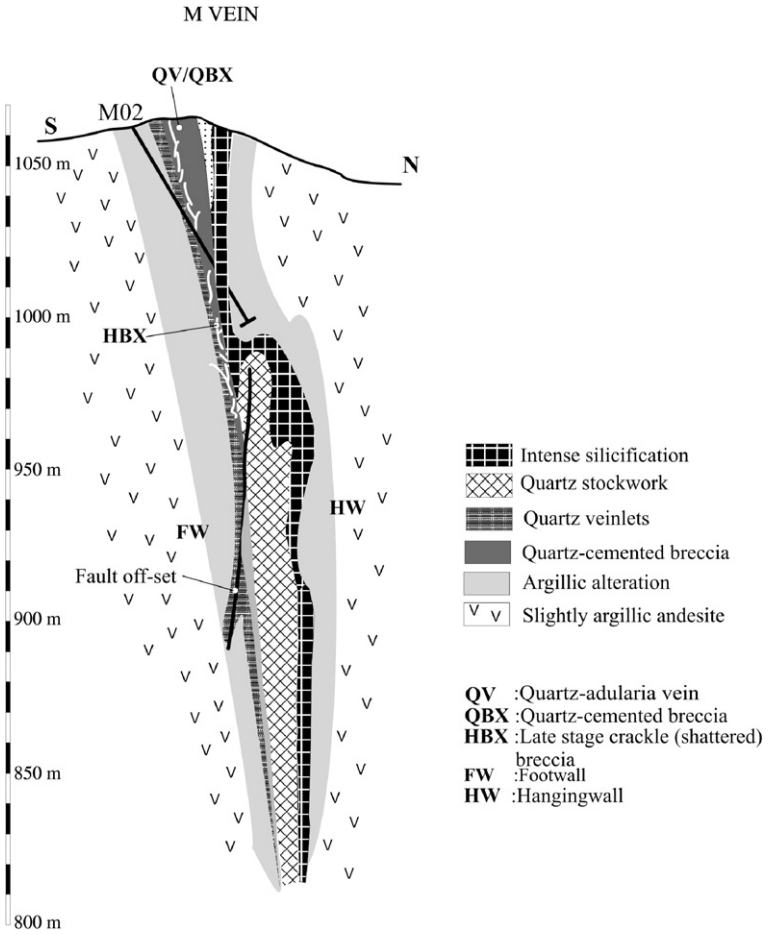

Fig. 5. Generalized cross-section of gold-rich M-vein at the Ovacik gold deposit.

within a sequence of lower Miocene andesitic to dacitic lavas and breccias. In the area, ancient workings up to 8 m wide are evident and dump and grab samples of wallrock range up to 75 g/t Au.

The zone contains narrow quartz veins (mostly less than 1 to 2 m), hydrobreccias, and zones of stockwork to sheeted veins focused around larger veins and in zones of structural intersections. The veins are dominated by crystalline quartz (Qtz ≫ Chal) consisting of fine to coarse sugary quartz, fine-grained comb quartz, druse-lined vugs, and locally coarse (up to 2 cm) euhedral quartz crystals with well developed growth zones. Bladed textures have been observed in a number of samples and faint crustiform banding occurs locally; minor amounts of amethyst occur in some veins. The hydrobreccia consists of angular to subrounded clasts composed of silicified and microveined andesite within a variable chalcedonic silica-pyrite to saccharoidal quartz matrix which is crosscut by late stage vuggy, comb-textured saccharoidal quartz veinlets. Pyrite content in the veins and the wall rock commonly exceeds 2%.

4.3. Saganci area

The Saganci area lies only 2 km NW of the Ovacik deposit and contains low-grade gold mineralization (<1 ppm Au), along with a distinctive alteration represented mainly by chalcedonic quartz and kaolinite, with minor mixed-layer smectite/illite mineral association (>13.4 Å). The Saganci area is located 1.5 km SE of Saganci village and contains a zone of shallow-dipping laminated chalcedonic quartz outcropping along a NW-trending structure for more than 200 m (Fig. 3). The chalcedony layers dip 15 to 45° (averaging 35°) to the SSW. Massive to laminated chalcedonic quartz appears in the form of white-pink and light brown bands. Brecciated chalcedony consists of layers with chalcedonic fragments 0.1 to 2 cm in size cemented in a chalcedonic matrix. Most of the fragments are flat and oriented parallel to layering.

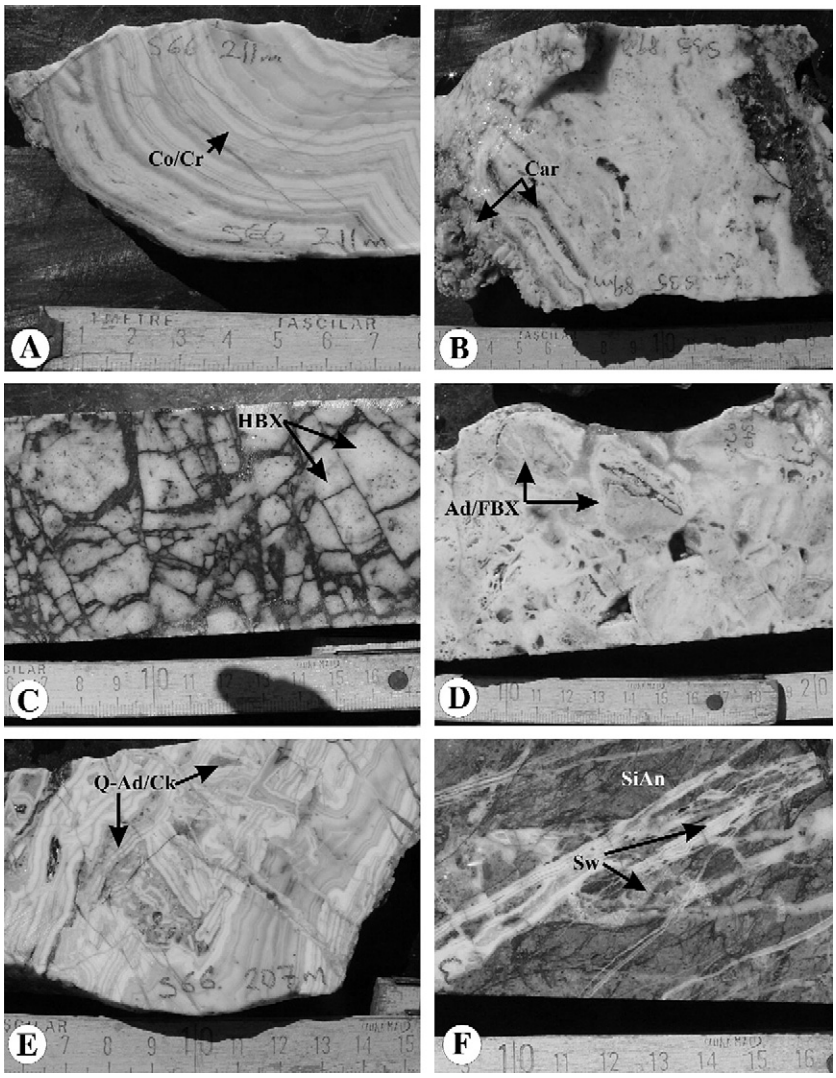

Fig. 6. Macroscopic primary epithermal quartz vein textures: A) Colloform/crustiform (Co/Cr) banded quartz–adularia vein. B) Coarse-banded chalcedonic quartz vein with bladed carbonate (Car) textures replaced by quartz; 27.8 g/t Au and 7.8 g/t Ag. C) Late-stage, clast-supported crackle/shattered breccia (HBX). D) Matrix-supported fluidized/milled (FBX) breccia with polymictic subangular clasts and silica–adularia (Ad)-sulfide matrix; 15.7 g/t Au and 47.7 g/t Ag. E) Clasts of silicified wall rock overgrown by crustiform/colloform bands and cockades (Ck) and chalcedonic quartz–adularia (Q–Ad). F) Hanging wall zone of silicified porphyritic andesite (SiAn) and sheeted quartz veinlets (Sw); 0.1 g/t Au and 0.2 g/t Ag.

This zone is interpreted to be a sinter and sinter-breccia deposit based on its physical appearance and nature, and the context of occurrence.

The continuous sedimentary-like clastic/brecciated layers within the deposit argue against a structurally controlled zone of silicification. It is, however, possible that this chalcedonic silicification could be replacing primary volcaniclastic beds, although evidence for such beds was not found in the immediate area. In active geothermal/epithermal systems, sinter breccias may form in areas of significant relief as sinter mounds periodically dry out and start to disintegrate as exposed silica layers crack and flake off. When the silica mound starts to grow again, the fragments are re-cemented and incorporated into the sinter deposit. The beds at Saganci do not contain reed casts or any obvious plant material or vertical growth structures that are diagnostic of young sinters, and evidence for 'pool sinters' is absent. Underlying the sinter beds, in the vicinity of ancient workings, are shallow-dipping zones and pods of argillized rocks (kaolinitic), chalcedonic silicification, and minor patches of gray pyritic silicification.

5. Vein mineralogy at Ovacik and Narlica gold deposits

5.1. Gangue mineralogy

The quartz veins in the Ovacik Au deposit consist mainly of fine to coarse-grained (Fig. 7A, E) quartz and adularia with minor carbonates and chalcedony in the vein (Fig. 7A, E). At least two episodes of quartz deposition (Fig. 7D, E) are recognized, as well as the formation of quartz after earlier-precipitated calcite. Adularia occurs as euhedral rhombs (Fig. 7A, E) either within breccia clasts or as a matrix in veins. The carbonates occurring as bands or infilling vugs (Fig. 7B) in the quartz vein are mainly calcite with lesser ankerite and siderite. Calcite is present as a network of intersecting blades separated by polyhedral cavities. Similarly-textured lattice quartz (Fig. 7C) may have originated as pseudomorphs after bladed calcite. Plagioclase phenocrysts in breccia fragments are invariably replaced by secondary albite or adularia (Fig. 7B), together with quartz and clays (Fig. 7A, E). In addition to these textures, clasts of silicified wallrock are overgrown by colloform bands (Fig. 7D). The adularia exhibits weak to intense

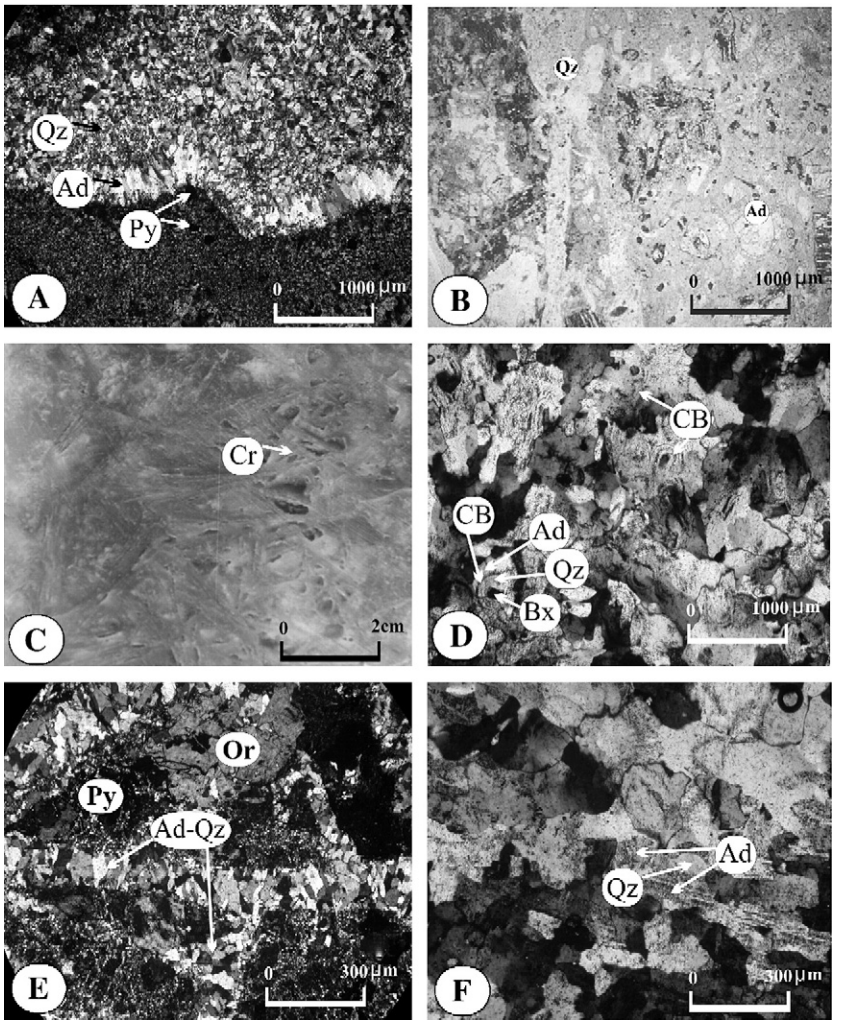

Fig. 7. Photomicrographs (under crossed Nichols; except C) of primary epithermal quartz textures: A) Colloform/crustiform banding texture; chalcedonic quartz (Qz), euhedral adularia (Ad) and pyrite (Py). B) Porphyritic dacite with potassic alteration, plagioclase is replaced by adularia (Ad) and wallrock is cut by sheeted stockwork quartz veinlets (Qz). C) Hand specimen showing a network of intersecting blades of calcite separated by polyhedral cavities: the similar texture of lattice-bladed quartz suggests it most likely originated as a pseudomorph of lattice-bladed calcite (carbonate replacement texture, Cr). D) Silicified wallrock breccia clasts (Bx) overgrown by fibrous colloform bands (CB) of adularia–quartz (Ad and Qz). E) Quartz–adularia stockwork veinlets cutting through the hanging wall: wallrock is commonly altered to fine quartz, adularia, and illite with minor remnants of orthoclase (Or); black opaque minerals are pyrite. F) Slightly-to moderately-argillized adularia (Ad) and unaltered quartz (Qz) from vein fillings.

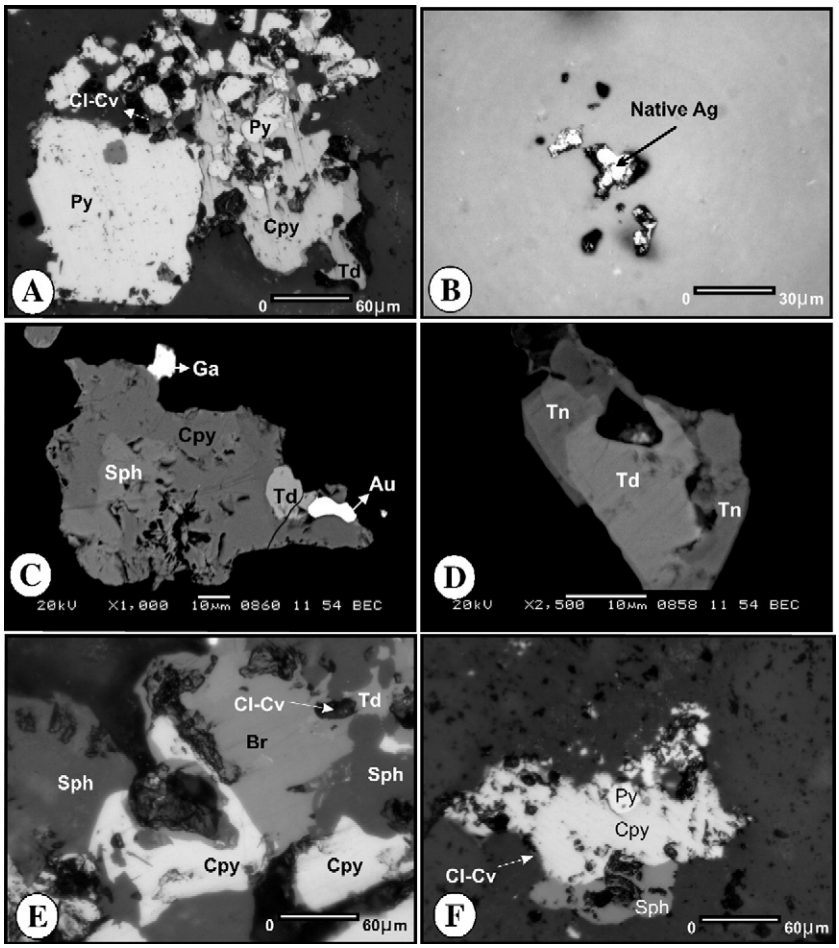

Fig. 8. Ore mineralogy (reflected plane-polarized light except C and D which are SEM-BSE images): A) Euhedral to subhedral pyrites (Py) surrounded by chalcopyrite (Cpy), rimmed by tetrahedrite (Td). Chalcocite–Covellite (Cl–Cv) occurs as an alteration product of chalcopyrite. B) Native silver in quartz gangue from shallow levels. C) Native gold (Au) associated with chalcopyrite (Cpy). Sphalerite (Sph), tetrahedrite (Td) and galena (Ga) replacing chalcopyrite D) Tennantite (Tn) surrounding tetrahedrite (Td). E) Chalcopyrite (Cpy) replaced by bornite (Br) and tetrahedrite (Td) replacing both Cpy and Br. Tetrahedrite (Td) and bornite (Br) are altered to chalcocite–covellite (Cl–Cv). F) Sphalerite (Sph) associated with chalcopyrite (Cpy) replacing pyrite (Py).

alteration to kandite (Fig. 7F). These textures are common in the M and S veins at Ovacik. The highest gold grades in both these veins are associated with banded quartz–adularia, clast-supported crackle (shattered) breccia and fluidized (milled) breccias; massive chalcedonic quartz and veins with carbonate replacement textures contain lesser or negligible gold. This does not mean that the above-mentioned quartz–adularia with banding/breccia textures invariably contain high Au and Ag grades; on the contrary, some part of quartz veins with very well developed colloform/crustiform banding in the S vein contain negligible gold. However, quartz veins without the above-mentioned textures always contain low precious metal grades.

Stockwork chalcedonic to crystalline quartz and adularia veining in silicified porphyritic andesite and dacite is common at the Narlica deposit. The microcrystalline groundmass of porphyritic andesite and dacite is replaced here by very fine chalcedonic quartz, adularia and illite.

5.2. Ore mineralogy

The epithermal system at the Ovacik Au deposit exhibits a distinctive mineralogical zoning within the western part of the system. The ore zone opaque minerals consist mainly of disseminated marcasite, pyrite and native silver; these are associated with relatively high Sb values, although no Sb minerals have been identified. At relatively deeper reference levels (1000 to 850 m, corresponding to 50 to 200 m below surface, the base metal content increases significantly and is characterized by pyrite and

chalcopyrite with minor bornite, tetrahedrite, sphalerite and galena. Arsenopyrite is also present in deeper parts of the system below the base metal zone (at depths of 200 m) and is often associated with pyrite. The ore minerals formed mostly as disseminations within subordinate veinlets, subsequent to the silica alteration across the deposit as a whole. Ore mineral assemblages identified in the Ovacik and Narlica deposits are typical of low- and intermediate-sulfidation epithermal systems (e.g., Hedenquist et al., 1996).

From surface outcrops to shallow levels of the mineralized veins, sulfides are represented mainly by pyrite and marcasite. Pyrite typically occurs as euhedral disseminated octahedral to pyritohedral crystals in barren quartz veins and, as anhedral grains (<0.03 to 1.0 mm in size) within mineralized quartz veins (Fig. 8A). Some subhedral pre-ore stage and early-ore stage pyrite crystals exhibit concentric zoning patterns with some weakly anisotropic (arsenic-bearing?) bands. Small arsenopyrite cores occur within some pyrite crystals. Marcasite occurs as subhedral to lamellar intergrowths with pyrite, or arranged with relict crystals of pyrite. Gold occurs as fine <0.05 mm grains of electrum (72% Au, 25% Ag, 3% Hg, Cu, Zn, Pb, As and Fe; Yilmaz, 2002) or in native form, precipitated between interstices of quartz crystals. No silver minerals were identified other than native silver at shallow levels (Fig. 8B). High-grade Au mineralization is typically accompanied by sulfide assemblages including base metal sulfides, the distribution of which is confined to the center of the M vein. In decreasing order of abundance, the major opaque minerals are pyrite, chalcopyrite, arsenopyrite, sphalerite, galena, (Ag-rich)

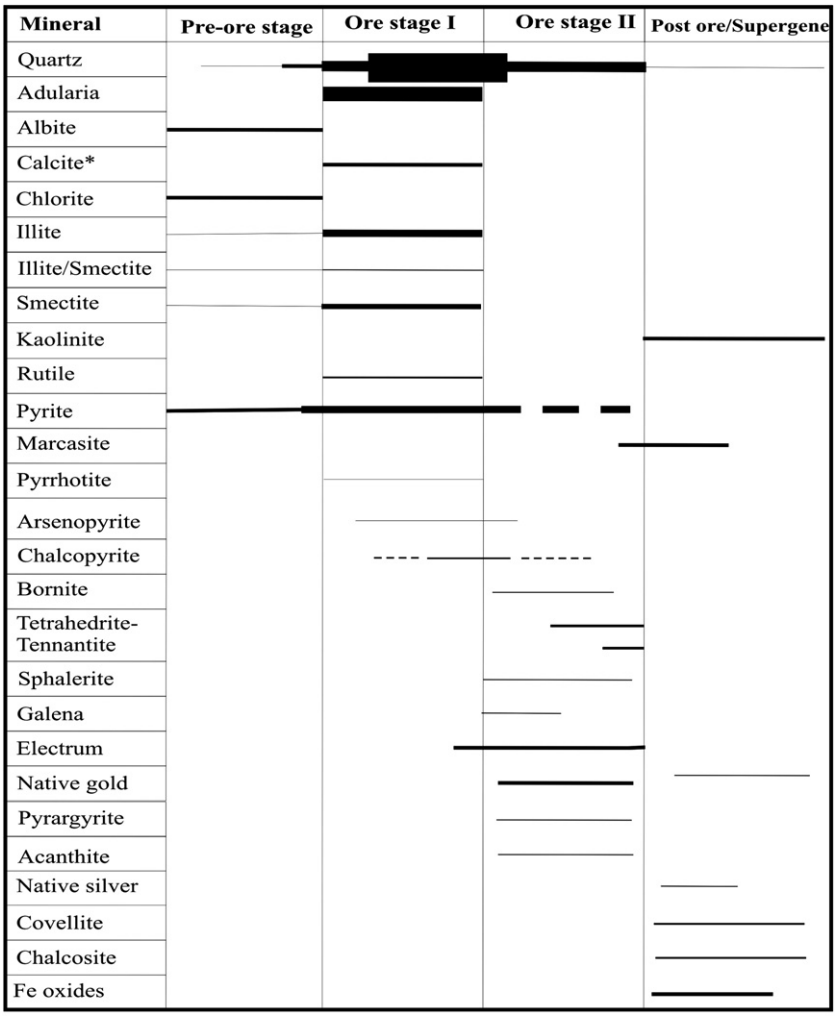

Fig. 9. Generalized paragenetic scheme for the Ovacik gold–silver deposit. Line width indicates abundance (fine: not abundant, thick: abundant).

Table 1
Summary of clay mineralogy proximal to Au-rich Ovacik and Narlica quartz–adularia veins, and Sagancı area

Drill hole number	Depth (m)	Whole rock and oriented clay analysis by XRD	Illite crystallinity index (mm)	Host rock
Ovacik				
M vein				
2	65	Quartz, adularia, illite, smectite (very minor), kaolinite (very minor).	1	Sericitized porphyritic andesite and sheeted quartz veinlets with colloform/crustiform textures.
3	107	Quartz, adularia, sericite, smectite (very minor), kaolinite (very minor).	none	Minor banded stringer quartz veinlets in silicified-argillized andesite.
6	89	Quartz, illite (minor), adularia (very minor), plagioclase (very minor), smectite (minor) , kaolinite (trace).	2	Slightly argillized porphyritic andesite.
21	34	Adularia, amorphous silica, quartz (minor), kaolinite (minor), smectite (very minor).	none	Hydrobrecciated pyrite-bearing andesite.
34	177.5	Quartz, adularia, illite, smectite (minor), amorphous silica (very minor).	2	Silicified porphyritic andesite with quartz veinlets and carbonate replacement texture.
51	118.5	Quartz, adularia, illite, smectite (minor), amorphous silica (very minor).	not clear	Quartz–pyrite-cemented andesite breccia with stockwork veining.
78	138	Quartz, adularia, illite (minor), smectite (trace).	1	Argillized andesite.
80	76	Quartz, adularia, illite (minor), kaolinite (minor), smectite (trace).	4	Fluidized quartz hydrobreccia.
117	110	Adularia, quartz, illite (minor), halloysite (minor), smectite (minor).	2.5	Argillized-silicified porphyritic andesite containing hairline pyrite veinlets.
132	194.6	Quartz, adularia, albite (minor), kaolinite (negligible), smectite (negligible).	none	Silicified porphyritic andesite with quartz veinlets and carbonate replacement texture.
149	159	Quartz, adularia, illite (trace), smectite (trace), hematite.	none	Quartz-pyrite hydrobreccia within silicified porphyritic andesite containing massive pyrite patches.
S Vein				
1	164	Quartz, adularia, illite (minor), smectite (minor), kaolinite (minor), hematite.	1	Silicified porphyritic andesite.
8	68	Adularia, illite, quartz,	0.5	Argillized porphyritic andesite.
9	54	Adularia, quartz, illite, smectite (minor), hematite.	1	Silicified porphyritic andesite containing sheeted quartz veinlets with colloform banding.
25	46	Quartz, adularia, illite (minor), mixed-layered clay (smectite/illite, minor).	2	Silicified porphyritic andesite.
53	75	Quartz, adularia, illite.	1	Highly silicified porphyritic andesite with minor pyrite.
66	206	Adularia, quartz, illite, smectite (very minor)	2	Argillized-silicified porphyritic andesite.
Narlica				
11	85.8	Quartz, adularia, kaolinite, illite (very minor), illite (very minor)	3	Crystalline quartz veinlets within slightly argillized andesite.
Sağancı area				
KS-1		Quartz, kaolinite (very minor), mixed-layered clay (illite/smectite:13.3 A°, 27.3 A°, very minor).	7	Clay-silica hydrobreccia with abundant iron-oxide staining.
KS-2		Quartz, highly crystalline kaolinite (minor), illite (very minor), mixed-layered clay (illite/smectite:13.2 A°, 28.5 A°, very minor).	10	Silicified and argillized dacite with minor iron-oxide staining.
KS-3		Quartz, kaolinite (minor)	none	Slightly silicified clayey andesite structure with minor quartz veinlets (N10W/90).
KS-4		Quartz, kaolinite.	none	E–W trending opalline quartz-clay structure.
KS-5		Quartz, kaolinite.	none	Argillized and silicified andesite.
KS-6		Quartz, kaolinite, hematite.	none	Argillized andesite adjacent to K70° W-trending silica structure.
KS-7		Quartz, kaolinite, mixed-layered clay (illite/smectite:13.4 A°, 31.6 A°)	9	Slightly hydrobrecciated silica–quartz–clay with trace pyrite.

Table 2
Results of $^{40}Ar/^{39}Ar$ analysis of Narlıca and Ovacık gold deposits

Step	*T**	^{36}Ar	^{37}Ar	^{38}Ar	^{39}Ar	^{40}Ar	% ^{40}Ar	% ^{39}Ar rlsd	Ca/K	$^{40}Ar/^{39}ArK$	Age (Ma)
N-1 (Narlýca), adularia, 20.40 *mg, J=0.001545±0.98%*											
1	600	5.972	0.087	1.698	41.065	1948.63	12.0	1.2	0.02	5.704323	15.83
2	675	2.494	0.113	1.561	87.489	1179.08	39.3	2.6	0.01	5.315000	14.75
3	750	1.849	0.109	2.465	170.154	1537.90	65.6	5.1	0.01	5.951207	16.51
4	810	0.940	0.067	2.289	173.031	1363.67	80.4	5.1	0	6.357212	17.63
5	865	0.743	0.054	2.473	184.330	1408.20	85.0	5.5	0	6.519540	18.08
6	915	0.640	0.047	2.475	191.143	1430.80	87.3	5.7	0	6.561578	18.20
7	965	0.644	0.042	2.694	208.162	1547.65	88.2	6.2	0	6.584773	18.26
8	1015	0.715	0.042	2.889	222.130	1657.03	87.8	6.6	0	6.573900	18.23
9	1065	0.802	0.049	2.882	217.493	1658.91	86.3	6.5	0	6.607243	18.32
10	1120	1.084	0.046	2.815	209.361	1679.82	81.7	6.2	0	6.576437	18.24
11	1180	2.057	0.056	3.134	218.752	2029.03	71.1	6.5	0	6.615217	18.35
12	1250	6.522	0.104	5.490	341.438	4121.12	54.6	10.1	0	6.625727	18.37
13	1320	14.568	0.156	10.115	589.814	8110.37	48.5	17.5	0	6.699307	18.58
14	1400	12.226	0.153	8.768	510.536	6940.56	49.5	15.2	0	6.759483	18.74
					Cumulative % ^{39}Ar released=			100.0		Total gas age=	18.15
										Plateau age=	18.29
										Isochron age=	18.17
M3-107, adularia (M veinı/Ovacik Au deposit), 20.63*mg, J=0.00190834±0.2898 %*											
1	610	5.47	0.012	1.253	0.158	1578.63	0.9	0.1	0.38	96.471497	304.86
2	670	5.357	0.014	1.498	0.441	1546.68	1.0	0.3	0.16	36.951729	122.93
3	740	15.149	0.024	3.723	2.764	4433.07	2.3	2.1	0.04	36.982824	123.03
4	810	4.200	0.036	0.956	8.636	1274.24	5.9	6.5	0.02	8.541346	29.17
5	880	1.539	0.028	0.630	29.478	611.55	29.4	22.1	0	5.884733	20.15
6	950	0.811	0.029	0.536	30.041	389.97	43.5	22.6	0	5.308173	18.18
7	1030	0.928	0.026	0.506	25.959	410.31	38.4	19.5	0	5.593733	19.16
8	1110	1.597	0.031	0.539	17.654	549.85	17.9	13.3	0.01	5.269152	18.05
9	1190	3.772	0.064	0.827	8.750	1118.06	3.6	6.6	0.04	4.400866	15.09
10	1270	6.140	0.117	1.258	4.676	1789.49	1.9	3.5	0.12	6.961736	23.81
11	1400	20.547	0.621	4.101	4.653	5950.86	1.2	3.5	0.66	16.771190	56.84
					Cumulative % 36Ar released			100.0		Total gas age=	23.71
										No plateau	
										No isochron	
M76-23, adularia (M vein/Ovacık Au deposit), 11.79 *mg, J=0.0019766±0.3132%*											
1	640	2.75	0.023	0.581	6.201	831.54	5.4	4.8	0.01	7.232402	25.61
2	680	0.723	0.023	0.226	7.894	256.85	20.3	6.1	0.01	6.426733	22.77
3	720	0.405	0.025	0.198	10.328	170.49	34.5	8.0	0.01	5.354646	18.99
4	760	0.247	0.028	0.196	12.147	134.44	52.0	9.4	0.01	5.311571	18.84
5	800	0.233	0.020	0.200	13.202	134.24	55.2	10.2	0.01	5.177552	18.37
6	835	0.183	0.022	0.187	12.340	116.83	61.4	9.6	0.01	5.285784	18.75
7	885	0.165	0.020	0.172	11.719	104.9	62.0	9.1	0.01	4.982112	17.68
8	945	0.187	0.021	0.159	11.101	110.85	57.4	8.6	0.01	5.118062	18.16
9	1020	0.287	0.028	0.225	13.95	152.54	49.6	10.8	0.01	5.017512	17.80
10	1095	0.44	0.041	0.259	14.143	193.81	33.3	11.0	0.01	4.693337	16.66
11	1245	1.34	0.135	0.327	5.704	414.79	7.7	4.4	0.09	5.511673	19.55
12	1320	3.3	0.326	0.690	3.725	945.81	0.2	2.9	0.34	0.576614	2.06
13	1400	6.88	0.928	1.469	6.519	2017.43	2.5	5.1	0.55	7.865757	27.83
					Cumulative % ^{39}Ar released			100.0		Total gas age=	18.85
										No plateau	
										No isochron	
DC-3 (Bergama) plagioclase, 16.59 mg, J=0.00195183±0.3146%											
1	600	0.72	4.960	0.406	11.329	269.99	24.9	5.0	1.68	5.782904	20.25
2	660	0.256	8.589	0.202	8.294	97.29	42.7	3.7	3.98	5.677514	19.88
3	720	0.169	18.111	0.175	8.925	97.29	60.1	3.9	7.81	5.839772	20.45

(continued on next page)

Table 2 (*continued*)

Step	*T**	^{36}Ar	^{37}Ar	^{38}Ar	^{39}Ar	^{40}Ar	% ^{40}Ar	% ^{39}Ar rlsd	Ca/K	^{40}Ar/ ^{39}ArK	Age (Ma)
4	790	0.142	32.799	0.198	11.586	1000.76	72.3	5.1	10.91	5.588797	19.57
5	860	0.125	48.235	0.219	14.805	1098.18	82.0	6.5	12.56	5.513298	19.31
6	920	0.115	54.896	0.236	16.398	116.95	86.6	7.2	12.91	5.573581	19.52
7	970	0.092	59.101	0.236	17.807	119.44	93.6	7.9	12.8	5.679812	19.89
8	1020	0.107	72.742	0.320	22.099	144.31	93.0	9.7	12.69	5.601142	19.62
9	1060	0.1	61.804	0.279	18.846	126.86	91.9	8.3	12.64	5.630713	19.72
10	1100	0.1	54.187	0.252	16.8	116.24	90.9	7.4	12.44	5.668326	19.85
11	1140	0.11	48.651	0.226	15.213	109.72	86.6	6.7	12.33	5.688713	19.92
12	1200	0.1	50.535	0.251	15.636	112.07	91.4	6.9	12.46	5.851836	20.49
13	1270	0.13	57.453	0.305	17.905	138.15	87.1	7.9	12.37	6.150645	21.53
14	1400	0.28	100.224	0.620	31.121	278.15	81.1	13.7	12.41	6.839423	23.92
					Cumulative % 39 Ar released			100.0		Total gas age=	20.53
										Plateau	19.76
										No isochron	

4 amu discrimination = 1.02879 ± 0.36%, 40/39K = 0.0001 ± 100.0%, 36/37Ca = 0.000288 ± 4.09%, 39/37Ca = 0.00071 ± 3.30%.
Isotope beams in mV, rlsd = released, error in age includes J error, all errors 1 sigma.
(^{36}Ar through ^{40}Ar are measured beam intensities, corrected for decay for the age calculations).
*Temperature in centigrade.

tetrahedrite, tennantite, bornite, native gold, electrum and achantite. Gold is found to be associated with chalcopyrite (Fig. 8C). Achantite and pyrargyrite occur as discrete fine-grained crystals in the quartz matrix. At the Ovacik gold deposit, tetrahedrite–tennantite is mainly represented by Sb–Ag-rich tetrahedrite (Fig. 8C; 26.7 to 29.6 wt.% Sb, 1.3 to 2.5 wt.% Ag, 29.5 to 33.9 wt.% Cu, 1.5 to 2.7 wt.% As), with minor As-rich tennantite (Fig. 8D; 14.6 to 19.6 wt.% As, 0.4 to 0.9 wt.% Ag, 33.9 to 34.8 wt.% Cu, 2.3 to 3.9 wt.% Sb). It is clear that some paragenetic overlap occurs between bornite and tetrahedrite, since these minerals enclose one another. Textural relationships indicate that the bornite–tetrahedrite association postdates the chalcopyrite (Fig. 8E). Covellite and chalcocite are present in partly oxidized zones. Galena is fine-to medium-grained (<50 to 100 μm) and occurs as anhedral aggregates associated with pyrite, chalcopyrite and sphalerite. Individual coarse sphalerite grains (300 μm) are more widespread than galena in the deposit. The sphalerite appears to partially replace pyrite, chalcopyrite and galena (Fig. 8E, F). Lack of chalcopyrite–pyrrhotite inclusion in sphalerite indicates that sphalerite precipitated at relatively low temperatures. Increasing temperature, Fe content and external sulfur fugacity have been previously considered as possible factors in explaining the occurrence of chalcopyrite and pyrrhotite inclusions within natural and synthetic sphalerite (Bortnikov et al., 1991; Bente and Doering, 1995; Lepetit et al., 2003).

Arsenopyrite-bearing veinlets exceeding 3 mm in thickness are significant in silicified volcanic rocks at deeper levels. In stringer veinlets, arsenopyrite often appears to be intergrown with pyrite and rutile. Arsenopyrite often displays growth-zoned pseudorhombic to acicular crystals.

On the basis of microstructural evidence, paragenetic relationships of the vein mineralization are subdivided into pre-ore, ore I, ore II and supergene stages (Fig. 9). The earliest phase of mineralization, which predates the gold mineralization, consists of microcrystalline barren quartz and pyrite. The main ore stage is characterized by deposition of medium- and fine-grained quartz, adularia, sulfides and precious metals. Gold-bearing quartz veins commonly exhibit colloform/crustiform banding, carbonate replacement and hydrothermal breccia textures. Lastly, the post-ore supergene mineral assemblage consists of native gold, native silver, copper sulfides and carbonates, iron oxides and supergene kaolinite.

The quartz veins at Narlica consist mainly of disseminated pyrite and marcasite with minor chalcopyrite, electrum and native silver. Pyrite appears to be the most common opaque mineral and forms dark sulfide-rich bands both within veins and vein breccias. The pyrite within veins occurs in clusters of elongate crystals that appear to have been originally deposited as marcasite. Marcasite generally forms in preference to pyrite where deposition is extremely rapid, and temperature and pH are low. Despite relatively high As contents in some samples, no arsenopyrite was observed. Instead, the arsenic appears to be largely contained within supergene scorodite which may have come from As-bearing marcasite. Gold occurs as small grains that are generally included in quartz, although in one Narlica sample, gold is located together with pyrite. The occurrence of gold within quartz rather than in pyrite suggests that much of the gold will be free milling.

6. Analytical methods and procedures

Clay identification for unoriented and oriented samples was accomplished using a Philips X-ray diffractometer which utilizes a nickel filter with CuKα radiation at 40 kV and 20 mA (Appendix A.1).

Adularia from quartz–adularia veins was selected for $^{40}Ar/^{39}Ar$ geochronology in order to establish the

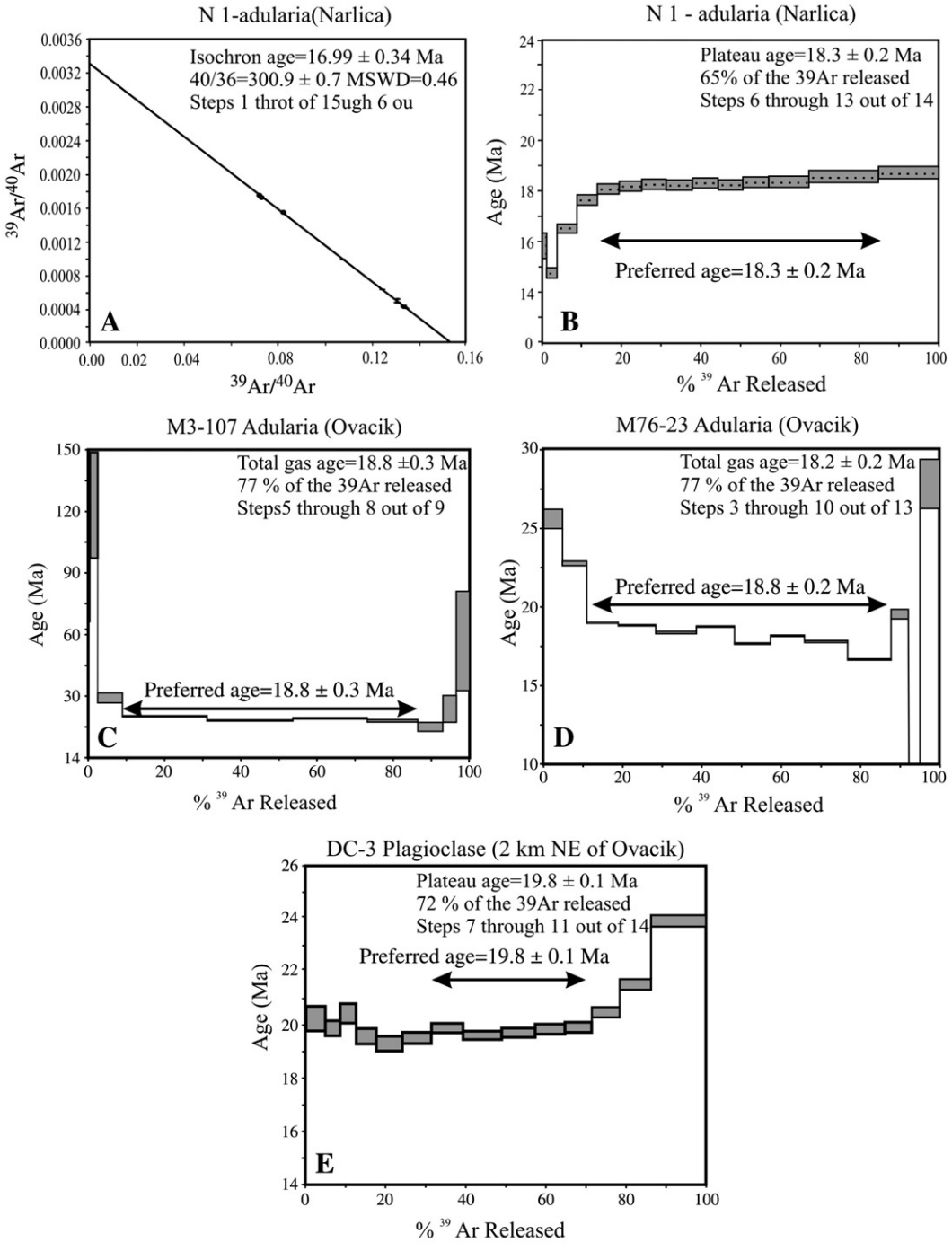

Fig. 10. Step-heating spectra of adularia from Narlica and Ovacik gold deposits, and associated volcanic rocks.

temporal relationship between magmatism, deformation and mineralization at Ovacik–Narlica. The sample was handpicked under binocular microscope to an estimated purity of >99%, and then cleaned in an ultrasonic bath with deionized water and acetone. 200 mg samples were irradiated at McMaster Nuclear Reactor at McMaster University, Ontario, Canada (Appendix A.2).

For geochemical analysis, 5 g of sample pulp were crushed to 100-mesh size and about 0.2 g was used for the ICP-MS determinations at ACME Laboratories, Canada. Fifteen elements were analyzed, including Mo, Cu, Pb, Zn, Ni, As, Cd, Sb, Bi, Ag, Au, Hg, Tl, Se and Sc, following a $HCl–HNO_3–H_2O$ leaching at 95 °C. For the remaining elements, including the major oxides (SiO_2, Al_2O_3, Fe_2O_3, MgO, CaO, Na_2O, P_2O_5 and MnO), rare earth and incompatible elements, the $LiBO_2$ fusion preparation method was used prior to ICP-MS analysis (Appendix A.3).

For microthermometric analysis, doubly-polished thin sections, approximately 100 μm thick, were prepared from more than 40 drill core samples from the Ovacik M and S veins. Of these, 11 samples, ranging from 13 to 200 m depth from surface, were suitable for investigation. A total of 203 fluid inclusions were studied: both homogenization temperatures (T_h) and melting temperatures of ice (T_m) were measured (Appendix A.4).

The $\delta^{18}O$ of the hydrothermal fluids ($\delta^{18}O_{H2O}$) associated with ore deposition was inferred from ^{18}O of quartz hosting the fluid inclusions (McInnes et al., 1990; Arribas et al., 1995). Oxygen isotope analyses were performed using a laser-based extraction technique using BrF_5 as the reagent, and isotope analyses were performed using molecular O_2, modified after the technique of Sharp (1990). Samples were heated using a Merchantek EO CO_2 laser, and the isotope analyses were performed using a Micromass IsoPrime stable isotope ratio mass spectrometer in dual inlet mode. Results are reported in $\delta^{18}O$ notation relative to Vienna-standard mean ocean water (V-SMOW) using value of $\delta^{18}O=+9.6$ for standard NBS-28. Reproducibility was ±0.1‰ and one standard was analyzed for every five samples (Appendix A.5).

The δD of the fluid ($\delta^{18}O_{H2O}$) was determined directly by the analysis of the water trapped within the fluid inclusions. Hydrogen isotope analyses of fluid inclusions were performed using a technique modified after Koziet (1997) and Hilkert et al. (1999), using a Eurovector model 3028 elemental analyzer interfaced to a Micromass IsoPrime stable isotope ratio mass spectrometer. The method of hydrogen isotope analysis was slightly modified by dropping a small portion of the sample (about 25 mg, much smaller than the old method) into a very high-temperature furnace (>1200 °C), where the inclusions burst immediately and the H_2O reacts with carbon to produce H_2 gas, which is then analyzed. In this technique, there is a continuous flow of He through the system, which rapidly removes the H_2 gas when it is formed. Replicate analyses indicate an uncertainty of ±1.0‰. Values are reported in common δD notation relative to V-SMOW using value of D=−66‰ for standard biotite NBS-30, and were reproduced to ±2‰.

Sulfur was extracted from bulk samples using Kiba reagent, after the technique of Sasaki et al. (1979). Sulfur isotope analyses were performed using the one-reactor column method of Fry et al. (2002), using the Isoprime mass spectrometer. $\delta^{34}S_{\Sigma sulfide}$ results are reported in the standard $\delta^{34}S_{\Sigma sulfide}$ notation relative to VCDT, and were reproduced typically to better than ±0.2‰.

7. Hydrothermal alteration

Silicification is best developed in the hanging wall of the veins at Ovacik, where it is associated with sheeted and stockwork-like quartz. The silicified zones are, in turn, enveloped by argillic alteration (Fig. 5). Within this envelope the original rock texture is mainly preserved. Propylitic alteration consisting mainly of albite, pyrite and chlorite with minor illite and smectite occurs in the outer zone. The argillic zone proximal to major quartz veins is dominated by quartz+adularia+illite±smectite with minor mixed layer illite/smectite and kandite-group (kaolinite) minerals (Table 1). Alteration minerals in the Ovacik deposit are similar to those of the Narlica deposit (Table 1).

Adularia is a characteristic mineral of low-sulfidation systems and at Ovacik occurs as massive replacement of metasomatized andesite or as progressive replacement of the plagioclase mainly in the hanging wall of the veins. Plagioclase phenocrysts are invariably replaced by secondary albite or adularia (Fig. 7B), together with quartz and clays. In the quartz veins, fine crystalline adularia–quartz layers are overgrown by relatively larger clear euhedral adularia and quartz crystals (Fig. 7A). Adularia is, in places, altered to clay, possibly by partial hydrothermal replacement of adularia needles (Fig. 7F) by kaolinite during supergene processes in the Ovacik veins.

8. Geochronology

8.1. Previous studies

Several workers have determined ages on volcano-plutonic rocks from Western Turkey by K/Ar methods

Table 3
Selected major and trace element geochemistry for samples from the Ovacik–Narlica gold deposit

Sample		SiO_2	Al2O3	Fe_2O_3	MgO	CaO	Na_2O	K2O	TiO2	P_2O_5	MnO	Cr	LOI
M 3-107	Silica-clay (illite–smectite)-	75.84	12.66	1.51	0.25	0.35	0.71	46166	4500	0.11	0.01	30	2.30
M 6-89	altered wall rock from Ovacik	66.24	16.43	3.28	0.62	0.34	0.38	58384	4700	0.16	0.01	24	2.60
M 21-34	gold deposit	72.07	13.15	3.34	0.19	0.34	0.38	58384	4700	0.16	0.01	24	2.60
M 34-177		72.80	12.10	2.97	0.46	0.49	0.91	50758	4000	0.17	0.01	30	3.12
M 78-138		66.63	14.70	3.14	0.68	0.64	0.61	72406	5100	0.18	0.01	36	3.80
M 78-139		90.26	4.28	1.52	0.20	0.18	0.13	18614	1400	0.05	0.02	12	0.70
M 109-106		92.97	1.36	3.74	0.04	0.09	0.04	4510	100	0.03	0.06	6	1.00
M 117-110		66.74	15.39	3.82	0.31	0.53	2.17	52644	5800	0.22	0.01	30	3.60
PD 1-36		78.91	9.56	2.37	0.05	0.06	0.12	51660	3500	0.11	0.02	96	1.90
PD 6-44.6		83.49	6.98	2.58	0.13	0.08	0.07	37064	2600	0.07	0.01	36	1.50
S 1-83		96.81	0.74	1.11	0.06	0.09	0.05	410	100	0.02	0.03	36	0.80
S 1-164		65.43	15.52	4.41	1.20	0.67	0.51	56826	5200	0.21	0.02	30	4.40
S 8-68		62.74	16.57	4.64	1.16	0.66	0.61	67487	6000	0.22	0.02	30	4.30
S 25-46		69.16	13.83	3.49	0.75	0.42	0.68	66559	4500	0.13	0.02	36	2.70
M 2-69	Mineralized quartz veins	95.16	1.34	0.89	0.03	0.11	0.11	5494	200	0.01	0.02	18	1.40
M 3-107.3	(Ovacık-Narlıca area)	94.72	1.59	1.49	0.02	0.07	0.04	5740	100	0.01	0.03	6	1.10
M 12-121.2		94.95	0.99	1.11	0.02	0.05	0.02	1968	100	0.01	0.02	24	2.40
M 17-123		96.40	0.91	1.11	0.02	0.05	0.03	1066	100	0.01	0.01	6	1.10
M 19-18		96.82	1.14	0.66	0.02	0.05	0.02	3198	100	0.01	0.02	12	0.50
M 21-44.5		95.30	1.58	1.10	0.06	0.07	0.03	4920	100	0.01	0.01	6	0.90
M 34-177.5		96.15	1.31	0.71	0.05	0.07	0.06	4674	200	0.02	0.02	12	0.80
M 35-46.5		97.66	0.33	1.44	0.04	0.05	0.01	164	100	0.01	0.02	6	0.40
M 51-118.5		82.40	7.39	3.55	0.14	0.40	0.40	28044	2300	0.21	0.06	24	1.70
M 55-166.6		97.63	0.55	0.82	0.03	0.04	0.03	328	100	0.02	0.02	12	0.80
M 71-76		80.94	8.96	2.02	0.17	0.11	0.15	55350	1600	0.06	0.02	18	0.70
M 76-23		94.08	2.36	1.19	0.06	0.08	0.04	10660	100	0.02	0.03	6	0.70
M 78-51.5		98.55	0.26	0.49	0.02	0.03	0.01	164	100	0.01	0.02	12	0.40
M 81-139.5		97.71	0.17	1.09	0.07	0.13	0.02	410	100	0.05	0.01	18	0.60
M 82-49.4		95.22	1.51	1.00	0.07	0.10	0.02	4510	100	0.02	0.02	6	1.40
M 101-45		96.08	1.23	1.03	0.03	0.06	0.05	2542	100	0.01	0.02	12	0.90
M 131-158.5		94.62	2.08	1.30	0.06	0.10	0.06	8200	400	0.03	0.02	18	0.70
M 132-194.6		74.42	10.80	4.51	0.17	0.37	0.72	52480	3800	0.15	0.02	24	1.50
M 149-159		84.45	4.33	5.01	0.09	0.17	0.12	18860	1300	0.06	0.01	12	3.80
MY 2		94.47	2.43	0.72	0.02	0.06	0.03	12054	100	0.01	0.03	18	0.60
MY 3		94.40	2.41	0.83	0.02	0.05	0.04	11480	100	0.01	0.03	6	0.60
N 1		83.77	6.89	2.40	0.05	0.06	0.10	40508	2500	0.09	0.04	36	1.00
N 2		96.18	0.79	1.59	0.03	0.13	0.03	574	100	0.05	0.09	6	1.00
N 4		92.88	3.34	1.10	0.05	0.06	0.03	9430	100	0.03	0.02	36	1.10
N 5		96.35	1.10	0.79	0.01	0.08	0.03	2706	100	0.01	0.06	6	1.10
PD 10-46		93.20	2.45	1.07	0.09	0.09	0.06	8774	600	0.02	0.03	18	1.50
PD 14-129.6		79.37	8.34	4.29	0.15	0.17	0.07	32472	2900	0.12	0.08	78	2.60
S 1-164		65.43	15.52	4.41	1.20	0.67	0.51	56826	5200	0.21	0.02	30	4.40
S 7-49.3		97.20	0.42	0.95	0.05	0.03	0.05	738	100	0.01	0.01	6	0.50
S 7-53.5		97.21	0.27	0.94	0.04	0.01	0.03	328	100	0.03	0.01	30	0.80
S 14-105		97.32	0.49	0.70	0.06	0.04	0.01	328	100	0.02	0.02	6	1.00
S 66-206		63.63	14.71	3.08	0.89	0.68	0.54	67158	4900	0.26	0.01	30	7.30
S 14-128		98.47	0.50	0.54	0.02	0.01	0.03	1312	100	0.01	0.02	18	0.60
S 25-46		69.16	13.83	3.49	0.75	0.42	0.68	66559	4500	0.13	0.02	36	2.70
S 35-89		95.81	0.81	1.91	0.05	0.05	0.01	902	100	0.02	0.02	18	0.90
S 40-92.35		96.63	1.05	0.54	0.06	0.07	0.01	2378	100	0.01	0.02	24	0.80
S 41-56.8		96.22	0.98	0.91	0.13	0.06	0.02	410	100	0.01	0.03	12	1.30
S 41-77.5		97.76	0.36	0.56	0.03	0.01	0.05	328	100	0.01	0.01	12	0.70
S 53-87.6		98.80	0.12	0.49	0.02	0.01	0.01	164	100	0.01	0.01	6	0.10
S 53-90		96.78	0.10	1.37	0.01	0.01	0.01	164	100	0.02	0.03	18	1.30
S 65-8		97.85	0.31	0.95	0.03	0.01	0.01	164	100	0.01	0.04	6	0.80
S 66-207		97.20	0.33	0.89	0.04	0.03	0.02	164	100	0.01	0.02	18	1.10
S 69-247		95.67	1.24	1.12	0.11	0.29	0.02	3362	100	0.01	0.02	6	1.00

(continued on next page)

Table 3 (*continued*)

Sample		SiO_2	Al2O3	Fe_2O_3	MgO	CaO	Na_2O	K2O	TiO2	P_2O_5	MnO	Cr	LOI
S 90-54		97.44	0.23	0.91	0.01	0.01	0.04	328	100	0.01	0.04	12	0.90
KS-1	Kandite (kaolinite)-	84.72	8.16	1.43	0.11	0.14	0.02	8774	5400	0.16	0.01	42	4.00
KS-2	altered Sagancı area	91.57	1.17	3.77	0.04	0.12	0.04	1640	7000	0.09	0.02	24	2.00
KS-3		70.04	12.71	8.46	0.03	0.13	0.02	1640	4300	0.27	0.01	24	7.60
KS-4		71.49	18.21	1.37	0.02	0.10	0.05	902	5600	0.29	0.01	36	7.60
KS-5		91.31	3.73	0.82	0.07	0.31	0.07	902	6300	0.05	0.04	12	2.50
KS-6		79.56	11.96	0.71	0.04	0.11	0.06	1066	5900	0.21	0.01	36	5.90
KS-7		85.80	3.44	4.37	0.15	0.13	0.05	5330	4600	0.24	0.01	42	4.20
COM-1		57.3	17.5	5.96	2.41	6.73	3.57	24600	5160	0.31	0.1	89	1.39

Sample	Silica-clay (illite–smectite)-altered wall rock from	TOT/C	S	SUM	Ni	Sc	Be	Co	Cs	Ga	Hf	Nb	Rb
M 3-107	Ovacik gold deposit	0.08	400	99.83	7	6	2	4	7.8	13.6	3.3	10.1	259
M 6-89		0.08	8600	99.83	9	11	2	9	10.3	18.3	4.7	12.3	336
M 21-34		0.08	8600	99.83	12	10	1	1	2.7	14.7	3.9	11.4	36
M 34-177		0.01	100	99.71	9	8	2	5	11.7	12.0	3.1	9.1	226
M 78-138		0.02	100	99.74	10	8	3	5	17.0	16.0	4.1	11.0	337
M 78-139		0.10	200	99.75	6	3	3	3	4.9	3.8	0.9	3.3	74
M 109-106		0.02	400	99.89	17	1	2	20	3.3	3.1	0.5	0.6	24
M 117-110		0.07	10800	99.79	13	10	2	14	8.2	14.7	4.6	11.4	292
PD 1-36		0.02	100	99.76	15	8	4	3	2.7	8.5	2.8	6.2	197
PD 6-44.6		0.05	2800	99.69	16	4	1	6	3.4	6.7	2.3	5.0	164
S 1-83		0.06	200	99.77	8	1	5	2	3.2	2.8	0.5	0.5	6
S 1-164		0.03	100	99.83	9	10	1	8	13.7	19.2	4.7	11.5	364
S 8-68		0.12	500	99.75	9	12	3	8	30.0	18.8	6.0	12.8	435
S 25-46		0.01	100	99.81	10	9	4	6	16.0	16.4	4.0	11.0	400
M 2-69	Mineralized quartz veins	0.01	300	99.76	6	1	7	1	5.5	5.2	0.5	0.6	38
M 3-107.3	(Ovacık-Narlıca area)	0.01	1500	99.77	4	1	3	2	3.2	2.4	0.5	0.6	36
M 12-121.2		0.03	1500	99.83	8	1	1	2	2.5	1.8	0.5	0.5	13
M 17-123		0.01	700	99.77	2	1	1	2	2.7	1.8	0.5	0.5	10
M 19-18		0.01	300	99.63	6	1	6	3	4.1	4.3	0.5	0.5	25
M 21-44.5		0.04	900	99.67	4	1	2	3	5.2	6.4	0.5	0.5	35
M 34-177.5		0.01	200	99.78	5	1	3	1	4.7	14.1	0.5	0.6	26
M 35-46.5		0.03	100	99.95	6	1	9	4	2.7	4.7	0.5	0.5	4
M 51-118.5		0.04	1300	99.91	17	6	2	13	6.9	10.3	1.9	5.0	123
M 55-166.6		0.01	100	99.98	5	1	2	3	4.6	5.8	0.5	0.5	7
M 71-76		0.03	300	100.04	9	3	3	4	9.0	7.3	1.3	3.5	281
M 76-23		0.02	200	99.86	5	1	27	3	5.9	5.2	0.5	0.5	66
M 78-51.5		0.01	100	99.79	7	1	2	1	2.0	6.3	0.5	0.5	3
M 81-139.5		0.04	100	99.90	6	1	3	2	2.6	1.6	0.5	0.5	3
M 82-49.4		0.04	200	99.91	7	1	10	4	4.1	3.8	0.5	0.5	26
M 101-45		0.02	2800	99.72	5	1	1	2	4.5	3.2	0.5	0.5	16
M 131-158.5		0.04	1000	100.02	6	1	4	2	3.6	5.7	0.5	1.1	40
M 132-194.6		0.03	300	99.44	10	7	4	4	9.4	12.3	2.8	8.3	222
M 149-159		0.09	28880	100.47	10	3	2	9	4.9	5.5	1.1	2.7	84
MY 2		0.02	200	99.85	8	1	4	2	5.4	4.4	0.5	0.5	76
MY 3		0.03	300	99.78	5	1	6	2	4.0	3.4	0.5	0.5	68
N 1		0.08	500	99.59	12	5	1	3	2.6	6.3	2.1	4.8	170
N 2		0.05	100	99.96	19	1	8	3	8.6	1.2	0.5	0.5	6
N 4		0.05	900	99.87	14	2	1	3	1.1	5.9	1.0	1.9	42
N 5		0.02	100	99.86	8	1	3	1	7.6	1.0	0.5	0.5	16
PD 10-46		0.04	200	99.64	7	2	2	2	3.1	2.5	0.7	1.2	46
PD 14-129.6		0.05	2000	99.45	30	9	3	11	6.2	10.0	2.5	6.3	194
S 1-164		0.03	100	99.83	9	10	1	8	13.7	19.2	4.7	11.5	364
S 7-49.3		0.03	200	99.32	2	1	4	1	1.9	3.1	0.5	0.5	4
S 7-53.5		0.01	100	99.37	8	1	1	1	1.6	4.8	0.5	0.5	2
S 14-105		0.01	200	99.71	3	1	4	1	2.3	5.2	0.5	0.5	3
S 66-206		0.04	200	99.78	7	7	2	5	12.6	18.8	3.9	11.2	352
S 14-128		0.07	200	100.35	10	1	2	5	2.7	3.3	0.5	0.5	9

Table 3 (*continued*)

Sample		SiO_2	Al2O3	Fe_2O_3	MgO	CaO	Na_2O	K2O	TiO2	P_2O_5	MnO	Cr	LOI
S 25-46		0.01	100	99.81	10	9	4	6	16.0	16.4	4.0	11.0	400
S 35-89		0.04	200	99.70	6	1	1	9	3.4	2.6	0.5	0.5	7
S 40-92.35		0.05	400	99.49	4	1	6	4	4.2	4.2	0.5	0.5	16
S 41-56.8		0.02	100	99.70	4	1	5	1	3.9	9.1	0.5	0.5	6
S 41-77.5		0.01	100	99.53	3	1	1	1	1.9	3.3	0.5	0.5	2
S 53-87.6		0.01	100	99.56	1	1	3	2	0.8	10.5	0.5	0.5	1
S 53-90		0.60	100	99.63	9	1	3	1	0.7	5.5	0.5	0.5	1
S 65-8		0.02	100	100.01	3	1	1	1	2.4	3.8	0.5	0.6	3
S 66-207		0.01	100	99.67	6	1	2	1	1.9	12.3	0.5	0.6	3
S 69-247		0.09	800	99.90	1	1	5	1	4.3	3.7	0.5	0.5	20
S 90-54		0.02	100	99.63	7	1	7	2	2.7	7.1	0.5	0.5	3
KS-1	Kandite (kaolinite)-	0.03	1400	100.36	1	7	1	1	2.7	14.7	3.9	11.9	36
KS-2	altered Sagancı area	0.22	2100	99.72	2	4	1	2	0.9	3.3	5.0	14.5	6
KS-3		0.09	2400	99.91	1	9	3	1	0.9	3.3	5.0	9.6	9
KS-4		0.09	1700	99.81	2	12	1	1	0.7	17.2	4.7	11.6	4
KS-5		0.10	700	99.63	9	2	1	3	1.2	4.1	3.5	11.0	8
KS-6		0.10	2400	99.26	2	11	1	1	0.5	15.0	4.3	11.7	4
KS-7		0.04	5800	99.50	4	8	3	1	0.9	4.8	2.9	6.7	16
COM-1		0.01	400	99.1	23	20	1.8	9	5.2	17.6	5.92	2.6	129

Sample	Silica-clay (illite–smectite)-	Sn	Sr	Ba	Ta	Th	U	V	Zr	Y	La	Ce	Pr
M 3-107	altered wall rock from	1	212	1173	0.9	20.9	3.4	99	114	10.5	39	68	6.6
M 6-89	Ovacik gold deposit	2	277	1355	1.0	27.0	5.0	112	149	17.6	54	97	9.5
M 21-34		2	1274	519	0.9	7.7	2.3	78	127	3.6	18	29	2.7
M 34-177		1	169	1028	0.8	23.6	4.4	234	107	15.6	40	70	7.2
M 78-138		2	152	1335	0.9	27.4	5.5	219	137	29.7	55	96	10.2
M 78-139		1	70	408	0.3	6.4	1.7	33	34	4.4	12	24	2.4
M 109-106		1	50	191	0.1	0.8	2.5	149	6	1.7	1	3	0.3
M 117-110		1	265	1171	1.0	27.3	8.0	109	166	23.9	51	91	9.4
PD 1-36		2	182	693	0.5	12.2	5.0	40	80	10.6	22	36	3.8
PD 6-44.6		1	106	681	0.4	10.4	4.1	31	69	8.1	18	35	3.7
S 1-83		1	27	336	0.1	0.2	0.1	19	3	0.5	1	1	0.1
S 1-164		3	108	1217	1.1	25.2	4.1	107	137	19.8	50	89	8.7
S 8-68		2	123	1309	1.1	29.4	4.5	105	206	21.6	56	97	10.0
S 25-46		1	160	1307	0.9	24.1	3.9	160	125	20.8	46	82	8.2
M 2-69	Mineralized quartz veins	1	36	203	0.1	1.3	0.3	10	9	1.0	2	3	0.4
M 3-107.3	(Ovacık-Narlıca area)	1	55	205	0.1	0.3	0.2	8	6	1.4	1	2	0.2
M 12-121.2		2	43	108	0.1	0.5	0.2	10	5	0.6	2	3	0.3
M 17-123		1	63	373	0.1	0.2	0.1	22	3	0.4	1	1	0.1
M 19-18		2	41	192	0.1	0.1	0.1	5	2	0.3	1	1	0.0
M 21-44.5		1	42	162	0.1	0.6	0.4	23	4	1.4	1	3	0.3
M 34-177.5		1	36	174	0.1	0.9	0.5	14	10	1.3	2	4	0.4
M 35-46.5		1	25	30	0.1	0.1	0.1	22	3	0.6	1	1	0.0
M 51-118.5		1	159	818	0.5	9.9	4.5	52	69	17.1	22	44	4.7
M 55-166.6		1	28	34	0.1	0.5	0.2	5	3	0.4	1	1	0.1
M 71-76		1	82	1132	0.3	7.0	2.3	77	55	6.7	12	24	2.5
M 76-23		1	60	341	0.1	0.2	0.1	17	2	1.2	1	2	0.2
M 78-51.5		1	12	38	0.1	0.1	0.1	5	1	0.2	1	1	0.0
M 81-139.5		1	9	14	0.1	0.3	1.1	24	6	0.4	1	1	0.1
M 82-49.4		1	48	214	0.1	0.1	0.3	22	2	1.8	1	2	0.1
M 101-45		1	55	127	0.1	0.1	0.1	7	2	1.9	2	3	0.3
M 131-158.5		1	63	241	0.1	2.1	0.7	21	12	2.6	4	7	0.7
M 132-194.6		2	195	1188	0.7	15.3	4.4	103	104	12.2	29	55	5.6
M 149-159		1	76	426	0.2	5.9	5.6	91	27	6.4	11	20	2.0
MY 2		1	39	176	0.1	0.1	0.1	6	2	0.6	1	1	0.0
MY 3		1	43	161	0.1	0.1	0.1	5	5	0.5	1	1	0.1
N 1		1	101	830	0.4	9.5	2.3	30	65	6.4	17	30	3.2
N 2		1	17	78	0.1	0.1	0.2	8	2	1.9	1	1	0.1

(continued on next page)

Table 3 (*continued*)

Sample		SiO_2	Al2O3	Fe_2O_3	MgO	CaO	Na_2O	K2O	TiO2	P_2O_5	MnO	Cr	LOI
N 4		1	39	279	0.1	3.5	1.5	42	31	2.4	6	11	1.2
N 5		1	23	74	0.1	0.1	0.2	5	2	0.5	1	1	0.1
PD 10-46		1	26	117	0.1	2.9	1.3	14	18	2.7	5	9	1.0
PD 14-129.6		1	105	850	0.5	14.7	10.3	77	86	17.2	23	44	4.7
S 1-164		3	108	1217	1.1	25.2	4.1	107	137	19.8	50	89	8.7
S 7-49.3		1	14	58	0.1	0.2	0.3	6	3	0.3	1	2	0.2
S 7-53.5		1	11	12	0.1	0.1	0.1	5	3	0.1	1	1	0.0
S 14-105		1	20	241	0.1	0.6	0.3	8	3	0.3	1	1	0.1
S 66-206		2	162	1434	0.9	24.1	3.9	108	145	19.9	52	93	9.3
S 14-128		2	19	19	0.1	0.1	0.1	5	1	0.1	1	1	0.0
S 25-46		1	160	1307	0.9	24.1	3.9	160	125	20.8	46	82	8.2
S 35-89		1	36	326	0.1	0.1	0.7	59	4	1.0	1	1	0.1
S 40-92.35		1	36	154	0.1	0.1	0.1	5	2	0.6	1	1	0.1
S 41-56.8		1	28	393	0.1	0.4	0.1	8	2	0.8	1	2	0.2
S 41-77.5		1	12	19	0.1	0.1	0.1	8	1	0.2	1	1	0.0
S 53-87.6		1	3	14	0.1	0.1	0.1	5	1	0.2	1	1	0.1
S 53-90		1	4	12	0.1	0.1	0.1	5	4	0.1	1	1	0.0
S 65-8		1	15	19	0.1	0.1	0.1	5	2	0.7	1	1	0.1
S 66-207		1	10	72	0.1	0.1	0.1	5	5	0.5	1	2	0.2
S 69-247		1	65	226	0.1	0.1	0.4	5	4	0.7	1	1	0.1
S 90-54		1	19	69	0.1	0.1	0.3	12	2	0.1	1	1	0.0
KS-1	Kandite (kaolinite)-	2	1275	519	0.9	7.7	2.3	78	127	3.6	18	29	2.7
KS-2	altered Sagancı area	1	37	2463	1.3	4.7	1.6	30	175	4.2	4	7	0.7
KS-3		1	1078	787	0.8	25.3	4.1	78	101	22.6	46	89	9.3
KS-4		1	2125	287	1.0	26.5	4.6	115	185	3.3	57	113	11.4
KS-5		2	107	1033	1.0	16.6	3.1	12	118	5.2	11	18	1.7
KS-6		2	1523	685	1.1	23.2	6.1	92	143	14.1	50	89	8.7
KS-7		2	220	2984	0.5	13.1	3.1	54	96	12.1	44	78	7.5
COM-1		1	984	1347	0.72	26	5.6	150	239	26	58	114	12.6

Sample		Nd	Sm	Eu	Gd	Tb	Dy	Ho	Er	Tm	Yb	Lu
M 3-107	Silica-clay (illite–smectite)-altered	24.6	3.6	0.7	2.8	0.34	1.96	0.36	0.96	0.15	1.02	0.14
M 6-89	wall rock from Ovacik gold deposit	37.3	5.7	1.2	4.4	0.65	3.52	0.60	1.68	0.27	1.67	0.29
M 21-34		11.8	2.6	0.7	2.5	0.22	0.90	0.13	0.37	0.09	0.66	0.10
M 34-177		27.1	4.4	0.7	3.0	0.51	2.70	0.48	1.40	0.21	1.50	0.24
M 78-138		37.1	6.2	1.4	4.7	0.76	4.57	0.91	2.68	0.45	3.10	0.44
M 78-139		8.3	1.4	0.3	0.9	0.14	0.85	0.15	0.40	0.05	0.41	0.06
M 109-106		0.9	0.3	0.1	0.3	0.04	0.32	0.05	0.18	0.05	0.20	0.02
M 117-110		36.8	5.2	1.2	4.5	0.70	3.78	0.80	2.29	0.41	2.59	0.35
PD 1-36		14.0	2.3	0.5	1.8	0.26	1.74	0.33	0.91	0.16	1.24	0.16
PD 6-44.6		12.8	2.1	0.6	1.6	0.27	1.57	0.26	0.79	0.13	0.87	0.12
S 1-83		0.4	0.1	0.1	0.1	0.01	0.07	0.05	0.05	0.05	0.06	0.01
S 1-164		33.7	6.0	1.2	4.2	0.59	3.36	0.72	1.89	0.30	2.20	0.31
S 8-68		35.8	6.0	1.4	4.8	0.67	3.49	0.76	2.06	0.33	1.87	0.30
S 25-46		32.5	5.4	1.1	4.2	0.66	3.68	0.70	1.93	0.33	2.14	0.33
M 2-69	Mineralized quartz veins (Ovacık–Narlıca area)	1.3	0.1	0.1	0.2	0.02	0.13	0.05	0.09	0.05	0.07	0.01
M 3-107.3		0.6	0.2	0.1	0.1	0.02	0.16	0.05	0.11	0.05	0.15	0.03
M 12-121.2		1.0	0.3	0.1	0.2	0.01	0.13	0.05	0.05	0.05	0.07	0.01
M 17-123		0.4	0.1	0.1	0.1	0.01	0.06	0.05	0.05	0.05	0.05	0.01
M 19-18		0.4	0.1	0.1	0.1	0.01	0.06	0.05	0.05	0.05	0.05	0.01
M 21-44.5		1.0	0.2	0.1	0.2	0.05	0.23	0.05	0.14	0.05	0.10	0.02
M 34-177.5		1.6	0.3	0.1	0.3	0.03	0.17	0.05	0.10	0.05	0.08	0.02
M 35-46.5		0.4	0.1	0.1	0.1	0.01	0.09	0.05	0.06	0.05	0.07	0.01
M 51-118.5		20.4	3.6	0.8	3.5	0.54	2.74	0.57	1.42	0.22	1.66	0.24
M 55-166.6		0.4	0.1	0.1	0.1	0.01	0.05	0.05	0.05	0.05	0.07	0.01
M 71-76		9.3	1.3	0.3	1.2	0.21	1.23	0.23	0.68	0.11	0.71	0.10
M 76-23		0.6	0.1	0.1	0.2	0.01	0.17	0.05	0.08	0.05	0.05	0.01

Table 3 (*continued*)

Sample		Nd	Sm	Eu	Gd	Tb	Dy	Ho	Er	Tm	Yb	Lu
M 78-51.5		0.4	0.1	0.1	0.1	0.01	0.05	0.05	0.05	0.05	0.05	0.01
M 81-139.5		0.4	0.1	0.1	0.1	0.01	0.08	0.05	0.05	0.05	0.05	0.01
M 82-49.4		0.7	0.1	0.1	0.2	0.04	0.27	0.05	0.10	0.05	0.14	0.02
M 101-45		1.3	0.2	0.1	0.3	0.04	0.19	0.05	0.11	0.05	0.13	0.02
M 131-158.5		2.5	0.6	0.1	0.4	0.08	0.38	0.08	0.18	0.05	0.18	0.03
M 132-194.6		21.8	3.2	0.8	2.6	0.37	2.16	0.41	1.04	0.17	1.15	0.17
M 149-159		8.9	1.5	0.3	1.1	0.17	0.88	0.19	0.59	0.08	0.59	0.07
MY 2		0.4	0.1	0.1	0.1	0.02	0.08	0.05	0.06	0.05	0.05	0.01
MY 3		0.4	0.1	0.1	0.1	0.01	0.05	0.05	0.05	0.05	0.05	0.01
N 1		11.8	1.7	0.5	1.2	0.19	1.03	0.21	0.62	0.10	0.80	0.11
N 2		0.6	0.1	0.1	0.3	0.04	0.24	0.06	0.16	0.05	0.15	0.01
N 4		4.7	0.8	0.1	0.6	0.06	0.47	0.10	0.23	0.05	0.19	0.03
N 5		0.4	0.1	0.1	0.1	0.01	0.09	0.05	0.05	0.05	0.05	0.01
PD 10-46		4.2	0.8	0.2	0.5	0.08	0.60	0.09	0.26	0.05	0.21	0.05
PD 14-129.6		19.0	3.1	0.8	3.1	0.46	2.66	0.52	1.47	0.22	1.67	0.22
S 1-164		33.7	6.0	1.2	4.2	0.59	3.36	0.72	1.89	0.30	2.20	0.31
S 7-49.3		0.5	0.1	0.1	0.1	0.01	0.05	0.05	0.05	0.05	0.07	0.01
S 7-53.5		0.4	0.1	0.1	0.1	0.01	0.05	0.05	0.05	0.05	0.05	0.01
S 14-105		0.4	0.1	0.1	0.1	0.01	0.07	0.05	0.06	0.05	0.07	0.01
S 66-206		36.2	5.6	1.1	4.2	0.64	3.27	0.68	1.86	0.28	1.82	0.29
S 14-128		0.4	0.1	0.1	0.1	0.01	0.05	0.05	0.05	0.05	0.05	0.01
S 25-46		32.5	5.4	1.1	4.2	0.66	3.68	0.70	1.93	0.33	2.14	0.33
S 35-89		0.4	0.2	0.1	0.2	0.02	0.11	0.05	0.09	0.05	0.15	0.01
S 40-92.35		0.4	0.1	0.1	0.1	0.01	0.12	0.05	0.05	0.05	0.09	0.01
S 41-56.8		0.7	0.1	0.1	0.1	0.01	0.11	0.05	0.06	0.05	0.11	0.01
S 41-77.5		0.4	0.1	0.1	0.1	0.01	0.05	0.05	0.05	0.05	0.09	0.01
S 53-87.6		0.4	0.1	0.1	0.1	0.01	0.05	0.05	0.05	0.05	0.08	0.01
S 53-90		0.4	0.1	0.1	0.1	0.01	0.05	0.05	0.05	0.05	0.05	0.01
S 65-8		0.5	0.1	0.1	0.1	0.02	0.14	0.05	0.09	0.05	0.10	0.01
S 66-207		0.7	0.2	0.1	0.2	0.03	0.05	0.05	0.05	0.05	0.09	0.01
S 69-247		0.4	0.1	0.1	0.1	0.02	0.06	0.05	0.05	0.05	0.05	0.01
S 90-54		0.4	0.1	0.1	0.1	0.01	0.05	0.05	0.05	0.05	0.06	0.01
KS-1	Kandite (kaolinite)-altered	11.8	2.6	0.7	2.5	0.22	0.90	0.13	0.37	0.09	0.66	0.10
KS-2	Sagancý area	3.3	0.5	0.1	0.6	0.13	0.79	0.17	0.55	0.80	0.65	0.12
KS-3		35.4	5.5	1.4	4.7	0.84	4.61	0.71	1.77	0.25	1.57	0.25
KS-4		41.4	4.6	0.7	1.8	0.14	0.69	0.11	0.37	0.06	0.38	0.09
KS-5		5.7	0.8	0.1	0.8	0.13	0.74	0.15	0.50	0.07	0.50	0.09
KS-6		31.7	4.9	1.0	3.5	0.38	2.28	0.44	1.49	0.28	1.96	0.36
KS-7		29.8	4.7	1.1	3.4	0.43	2.74	0.43	1.19	0.17	1.20	0.18
COM-1		45.6	7.8	1.8	5.67	0.77	4.47	0.86	2.54	0.35	1.85	0.32

Sample		Au	Ag	Cu	Pb	Zn	As	Sb	Hg	Tl	Bi	Se	Cd	Mo	W
M 3-107	Silica-clay (illite–smectite)-altered wall rock from Ovacik gold deposit	3	0.1	5	10	3	32	15.0	3.95	0.3	1.2	0.7	0.1	5.3	4
M 6-89		1	0.1	21	11	29	5	4.9	0.10	0.2	0.1	0.5	0.2	0.2	3
M 21-34		252	0.6	79	15	29	214	26.7	0.58	0.2	0.1	0.5	0.1	0.7	6
M 34-177		455	0.2	17	18	84	273	30.0	0.36	0.1	0.1	0.5	0.3	0.3	5
M 78-138		208	0.1	23	16	162	162	4.6	0.23	0.1	0.1	0.1	0.7	0.9	9
M 78-139		443	0.5	9	4	10	21	5.6	0.15	0.1	0.1	0.5	0.1	0.4	2
M 109-106		10617	4.8	49	87	47	595	47.7	0.67	0.4	0.1	1.8	4	1.2	2
M 117-110		411	0.5	35	21	27	379	8.0	0.73	0.9	0.1	2.2	0.1	0.4	7
PD 1-36		112	1.4	13	27	13	57	5.5	0.40	0.2	0.1	0.7	0.1	12.7	7
PD 6-44.6		831	3.3	13	22	21	179	5.1	0.46	0.4	0.1	0.5	0.1	23.4	7
S 1-83		352	0.6	8	2	5	12	10.6	0.10	0.1	0.1	0.5	0.1	4.1	16
S 1-164		29	0.1	13	11	24	16	12.1	0.18	0.2	0.1	0.5	0.1	0.1	2
S 8-68		209	0.1	7	17	47	38	16.1	0.14	0.4	0.1	0.5	0.1	0.3	4
S 25-46		11	0.1	17	15	42	113	94.1	0.07	0.3	0.1	0.5	0.1	0.3	9

(continued on next page)

Table 3 (*continued*)

Sample		Au	Ag	Cu	Pb	Zn	As	Sb	Hg	Tl	Bi	Se	Cd	Mo	W
M 2-69	Mineralized quartz veins (Ovacık–Narlıca area)	4866	11.1	21	17	19	16	20.3	0.30	0.1	0.1	0.5	0.2	3.2	14
M 3-107.3		65267	27.2	205	254	293	44	16.6	0.40	0.1	0.1	0.7	8.3	0.6	0
M 12-121.2		48207	26.8	307	168	121	37	17.0	0.73	0.1	0.1	0.6	3.9	4.1	16
M 17-123		44594	16.8	49	71	49	79	21.4	1.31	0.1	0.1	0.5	1.8	0.5	1
M 19-18		36026	26.2	41	43	19	12	25.9	0.35	0.1	0.1	0.5	0.3	2.1	9
M 21-44.5		15663	50.3	52	41	66	76	39.9	2.34	0.1	0.1	0.7	0.6	0.5	1
M 34-177.5		9136	48.5	32	28	42	21	42.3	2.09	0.1	0.1	0.5	0.5	2.1	10
M 35-46.5		1461	5.1	7	7	10	74	23.9	0.41	0.1	0.1	0.5	0.1	0.5	1
M 51-118.5		846	0.6	16	12	104	118	4.6	1.11	0.2	0.1	0.5	0.4	2.3	11
M 55-166.6		1106	4.7	10	3	3	5	7.3	0.26	0.1	0.1	0.5	0.1	0.4	1
M 71-76		6560	2.4	40	25	22	169	34.6	2.84	0.2	0.1	0.5	0.2	2.1	7
M 76-23		80173	91.8	34	72	11	58	97.7	1.05	0.1	0.1	0.5	0.4	0.6	1
M 78-51.5		4894	14.2	5	3	2	4	10.0	0.18	0.1	0.1	0.5	0.1	1.8	7
M 81-139.5		381	0.2	6	5	3	51	37.3	0.11	0.1	0.1	0.5	0.1	3.2	13
M 82-49.4		24558	100.0	108	84	84	64	62.4	1.77	0.1	0.1	0.8	2.6	0.6	1
M 101-45		74107	100.0	173	113	169	63	70.0	0.53	0.1	0.1	1.3	3	2.4	10
M 131-158.5		1780	1.7	24	34	52	64	14.9	0.32	0.1	0.1	0.5	0.8	2.4	10
M 132-194.6		4578	2.4	37	34	49	191	20.7	1.69	0.3	0.1	0.5	0.3	0.8	4
M 149-159		77887	29.0	54	221	119	1842	51.3	4.07	0.7	0.1	1.3	1.4	0.6	3
MY 2		45634	90.0	64	67	62	18	52.4	1.11	0.1	0.1	0.5	0.5	2.7	9
MY 3		38305	44.4	44	44	52	9	20.7	0.63	0.1	0.1	0.5	0.6	0.5	1
N 1		1263	2.5	20	18	15	61	5.3	0.11	0.2	0.1	0.5	0.1	4.9	13
N 2		7835	13.4	13	31	36	19	4.9	0.34	0.3	0.1	0.5	0.2	2.7	1
N 4		404	0.9	11	17	13	35	3.5	0.14	0.1	0.1	0.5	0.1	17.7	7
N 5		13879	4.4	3	15	10	3	0.9	0.36	0.2	0.1	0.5	0.1	1.3	1
PD 10-46		170	1.5	6	8	11	29	2.3	0.13	0.1	0.1	0.5	0.1	8.3	8
PD 14-129.6		4894	100.0	34	123	205	451	41.8	0.52	2.1	0.1	1.2	1.3	35.7	7
S 1-164		29	0.1	13	11	24	16	12.1	0.18	0.2	0.1	0.5	0.1	0.1	2
S 7-49.3		944	2.4	5	4	4	6	66.0	0.16	0.1	0.1	0.5	0.1	0.5	1
S 7-53.5		194	0.7	6	1	1	2	7.0	0.12	0.1	0.1	0.5	0.1	3.8	16
S 14-105		1448	2.7	5	2	4	8	9.4	0.10	0.1	0.1	0.5	0.1	0.4	0
S 66-206		56	0.1	7	7	15	25	8.8	0.08	0.2	0.1	7.0	0.1	0.2	3
S 14-128		4094	3.1	12	2	1	2	5.8	0.14	0.1	0.1	0.5	0.1	2.2	9
S 25-46		11	0.1	17	15	42	113	94.1	0.07	0.3	0.1	0.5	0.1	0.3	9
S 35-89		27865	7.8	20	20	13	235	121.8	0.67	0.1	0.1	0.5	0.2	1.5	2
S 40-92.35		15707	47.7	17	14	20	11	15.5	0.42	0.1	0.1	0.5	0.1	1.7	8
S 41-56.8		7754	21.3	6	5	6	11	16.0	0.80	0.1	0.1	0.5	0.1	0.5	1
S 41-77.5		1974	1.3	4	3	4	25	21.0	0.10	0.1	0.1	0.5	0.1	1.5	5
S 53-87.6		140	0.3	6	1	1	6	6.7	0.14	0.1	0.1	0.5	0.1	0.2	1
S 53-90		1369	3.0	9	1	1	2	11.0	0.08	0.1	0.1	0.5	0.1	5.6	22
S 65-8		804	5.5	5	3	1	5	10.9	0.25	0.1	0.1	0.5	0.1	0.4	1
S 66-207		108	0.2	6	2	3	6	17.4	0.09	0.1	0.1	0.5	0.1	3.1	14
S 69-247		3834	2.1	6	7	11	16	6.0	0.29	0.1	0.1	0.5	0.1	0.3	1
S 90-54		635	1.1	7	3	2	32	26.3	0.03	0.1	0.1	0.5	0.1	3.4	12
KS-1	Kandite (kaolinite)-altered Sagancı area	3	0.1	5	10	3	32	14.7	3.95	0.3	1.2	0.7	0.1	5.3	3
KS-2		5	0.1	21	10	17	189	32.5	2.95	0.2	1.3	1.8	0.1	17.3	3
KS-3		77	0.1	77	53	7	336	31.2	2.48	1.4	0.1	1.7	0.1	30.2	2
KS-4		1	0.1	9	12	4	35	2.1	3.80	0.5	0.1	0.5	0.1	0.7	4
KS-5		1	0.1	10	17	9	14	2.7	0.96	0.1	0.1	0.5	0.1	1.3	5
KS-6		2	0.1	8	7	6	48	2.3	0.30	0.1	0.1	0.7	0.1	3.6	3
KS-7		1	0.1	9	18	30	85	0.9	2.34	0.2	0.1	1.5	0.1	1.0	2
COM-1		4	4	40	39	40	2	0.2	0.07	1	0.01	0.14	0.2	1.1	2

For Mo, Cu, Pb, Zn, Ni, As, Cd, Sb, Bi, Ag, Au, Hg, Tl, Se a 0.5 g sample is leached with HCl–HNO3–H_20 at 95 °C, and analyzed by ICP-MS. For remaining elements 0.2 g sample fused by $LiBO_2$ and analysed by ICP-ES. SiO_2, Al_20_3, Fe_2O_3, MgO, CaO, Na_2O, P_2O_5, MnO, LOI, TOT/C, SUM in wt.%; Au in ppb limit; remaining elements in ppm altered wall rock. COM-1: arithmetic means of geochemical analysis from Kozak (Bergama; Altunkaynak and Yilmaz, 1998) and Evciler (Bayramiç; Genç, 1998) volcanics.

(Ercan et al., 1984; MTA-JISCA, 1987; Delaloye and Bingöl, 2000; Aldanmaz et al., 2000), and the Kozak intrusion has been dated using fission track methods (Wright et al., 1996). Despite this, no previous study has been published on the age of the associated gold mineralization in Western Turkey including Ovacik. The K/Ar dating from a porphyritic andesite lava dome returned ages ranging from 19 Ma to 14 Ma (Aldanmaz et al., 2000). In parallel to this work an average $^{40}Ar/^{39}Ar$ age of ~18.5 Ma was noted from the adularia minerals of the gold-bearing quartz veins at the Ovacik mine (Ebert, 2004).

8.2. $^{40}Ar/^{39}Ar$ results

One sample (N-1 with 4.94% K_2O) from the Narlica quartz–adularia vein yields both a plateau age (65% of the total ^{39}Ar released; Table 2; Fig. 10A,B) of 18.3±0.2 Ma and a total gas age of 18.2±0.2 Ma. A valid isochron is defined by steps 5–14 yielding an age of 18.2±0.2 Ma, indicating a small amount of excess argon ($^{40}Ar/^{36}Ar$ intercept of 302±1). Ca/K ratios were consistent throughout the step heating run, indicating a pure monomineralic unaltered sample.

Sample M3-107 (0.5% K_2O) produced a discordant age spectrum with high initial ages (up to ~300 Ma) followed by ages of ~18–20 Ma for ~10–90% of the gas released (Table 2, Fig. 10C), and ending with higher ages for the final ~10% of gas released. The total gas age is 23.7±0.3 Ma and there was no statistically valid isochron or plateau age defined for this sample. The Ca/K and radiogenic yields ($\%^{40}Ar$) vary systematically with age. Older ages in the initial and final ~10% of gas released correspond to higher Ca/K and very low radiogenic yields, whereas the more consistent ages of ~18–20 Ma for the ~10–90% of gas released, correspond to higher radiogenic yields and lower Ca/K, indicating that a high-K phase such as adularia is producing these ages. Thus, for this sample, the average of steps 5–8, yielding a mean age of 18.8±1.0 Ma, a weighted mean age of 18.8±0.3 Ma, and accounting for 77% of the total gas released, is the most reliable age estimate for this sample. This is likely to be a more reliable age estimate than the total gas age. However, since this is not a plateau age it should be considered to be only an estimate of the age of this sample.

Sample M76-23 (1.06% K_2O) produced a discordant age spectrum with high initial ages up to ~26 Ma for the first two steps, followed by ages of ~17 to 19 Ma for ~10 to 90% of gas released (Table 2, Fig. 10D), and both high and low ages during the final ~10% of gas released. The total gas age is 18.9±0.2 Ma. There was no statistically valid isochron or plateau age defined for this sample. A similar argument regarding interpretation of this sample as made above for M3-107 Quartz/Adularia may be made. Thus, steps 3 to 10, comprising 77% of the total gas released yield a mean age of 18.2±0.8 Ma, and a weighted mean age of 18.2±0.2 Ma. This is considered to be a more reliable age estimate for this sample than the total gas age.

One sample (DC-3) from dacitic pyroclastic rocks located 2 km NE of the Ovacik deposit produced a moderately discordant age spectrum with initial ages of ~20 Ma for the first ~70% gas released (Table 2, Fig. 10E), followed by older ages up to ~24 Ma. The total gas age is 20.5±0.1 Ma. Steps 7 to 11 (72% of the total gas released) define a plateau age of 19.8±0.1 Ma. There was no statistically valid isochron defined for this sample. Overall this is a generally well-behaved sample; however, there is a mild U-shape to the age spectrum. This may suggest that some excess argon is present, although this could not be confirmed via isochron analysis. If excess argon is present then the calculated ages may be overestimates. Thus the ages would be most conservatively considered to be maximums. With this in mind, the plateau age should be considered the most reliable age for this sample.

9. Geochemistry

Sampling of altered rocks in this study provides an ideal opportunity to investigate possible systematic variations in precious and base metals, REE, minor elements and major oxides in hydrothermally altered volcanic rocks that host quartz–adularia-type epithermal Au–Ag deposits (e.g., Palacios et al.,1986; Bierlein et al., 1999; Bi et al., 2004). Data for all samples are presented in Table 3. Fresh volcanic-normalized trace element patterns of wallrock (Fig. 11) and vein quartz (Fig. 12) from the Ovacik–Narlica Au deposits, and Saganci alteration (Fig. 13) are presented. Also shown were chondrite-normalized patterns (Fig. 14) and scatter diagrams (Figs. 15 and 16).

The degree of hydrothermal leaching of wallrock in the Ovacik–Narlica deposits is highly variable for major and trace elements. Rubidium and Cs are enriched by a factor of 2 whereas Pb, Cr, V, Ni, Zr and Cu show two-to three-fold depletions in altered wallrocks (Fig. 11). Of the major elements, K displays two-fold enrichment, while Mg is depleted by a factor of 5. Due to structurally-controlled pervasive alteration, Ca and Na are depleted in plagioclase, and Mg and Fe are leached from biotite whereas K, Rb and Cs are enriched in adularia or illite (Table 3, Fig. 11A, B). Trace elements

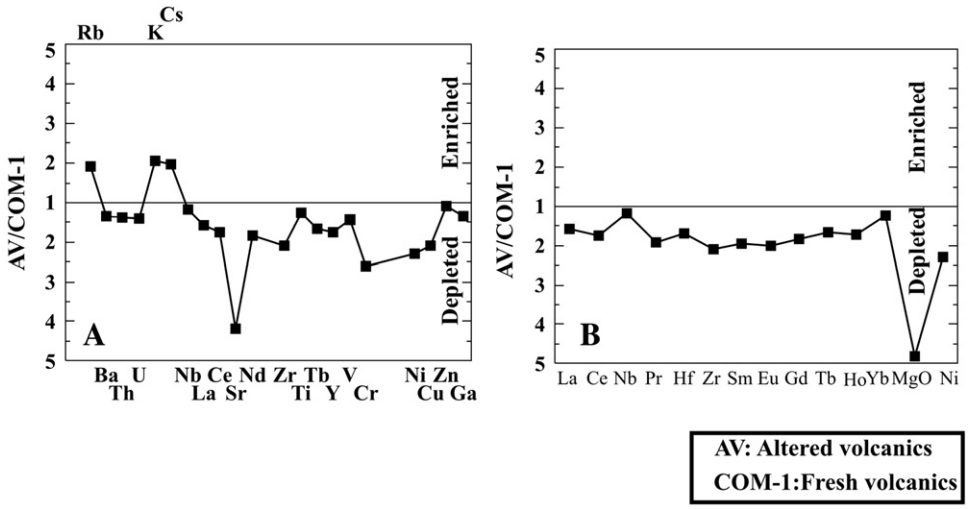

Fig. 11. Plot of (A) major and trace elements and (B) REE in altered wallrock at Ovacik and Narlica deposits, normalized against fresh rock (sample COM-1).

such as Ba, Th, U, Nb, La, Ce, Sr, Nd, Zr, Ti, Tb, Y and Cr are very low in mineralized quartz veins in the Ovacik–Narlica deposits. (Fig. 12A, B). The average concentration of Mg, Fe, Na and Ca (Fig. 12B) is also very low (Table 3). All REE in altered wallrock typically display a flat pattern, at ratios slightly less than unity relative to fresh rock, whereas LREE (La–Eu) concentrations in quartz veins are significantly lower than in the host volcanic rocks (Fig. 12B). A progressive relative enrichment from Eu through Gd, Tb, Ho to Yb appears, with decreasing depletion factors of 9 to 4 across these elements. Contents of Rb, K and Cs in the Saganci alteration zone are depleted by factors of about 11, 9 and 5 (Fig. 13), which is in contrast to the distribution of Rb, K and Cs in altered wall rocks at the Ovacik and Narlica deposits. Low Rb/Sr ratios and corresponding low K values within kaolinite-altered areas are due to acid leaching of K in volcanic rocks, whereas higher Rb/Sr ratios in adularia–illite-altered areas are correlative with these K-rich alteration minerals.

Fig. 14A–C depicts chondrite-normalized minor element and REE-profiles of fresh volcanic rocks, wallrock and quartz veins. The altered wallrock shows a

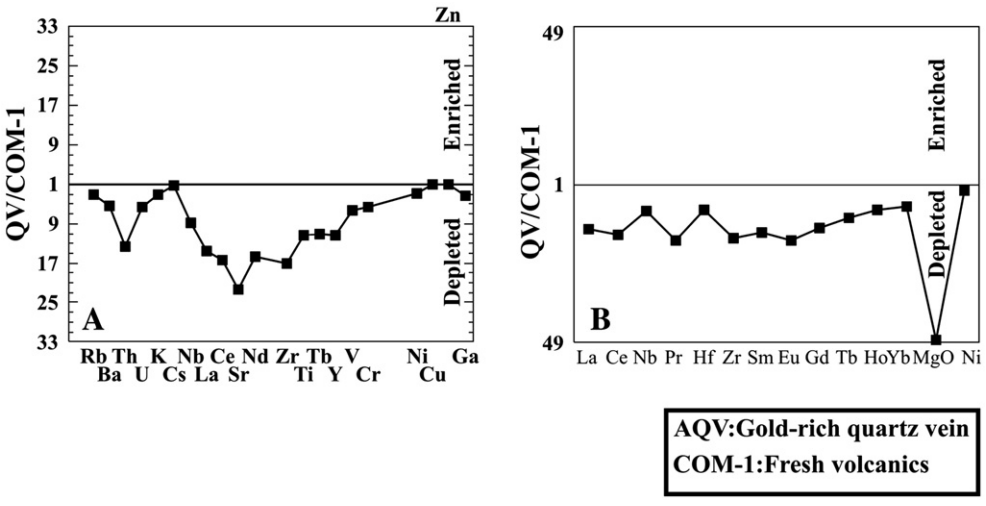

Fig. 12. Plot of (A) major trace and elements and (B) REE in quartz veins at Ovacik and Narlica deposits, normalized against fresh rock (sample COM-1).

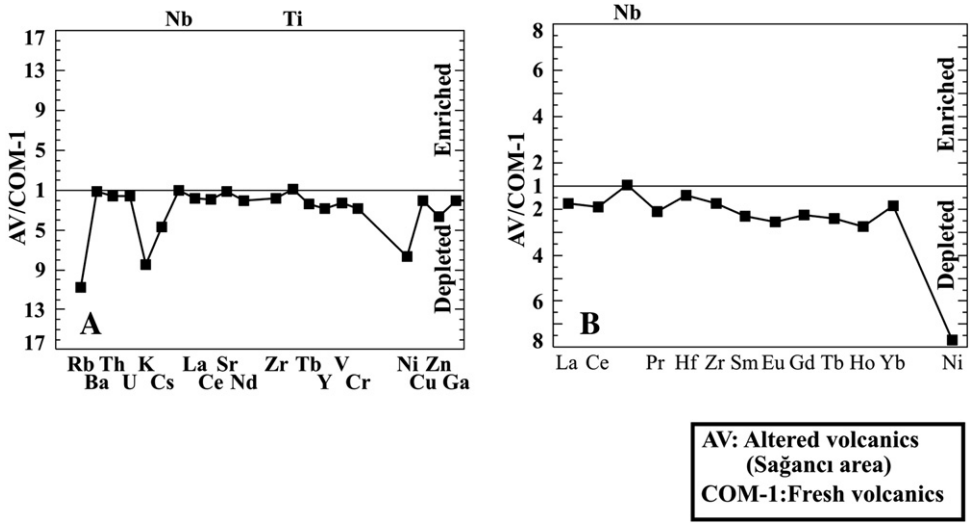

Fig. 13. Plot of (A) major and trace elements and REE from altered outcrop rocks in Saganci area, normalized against fresh rock (sample COM-1).

significant negative Sr anomaly (Fig. 14A), whereas the strong decrease in minor elements and REE are more apparent in the Narlica and Ovacik deposits (Fig. 14B). On the other hand, all REE chondrite-normalized patterns within altered volcanic rocks at Saganci, and altered wall rock and mineralized quartz veins in the Narlica and Ovacik deposits, show some systematic decrease relative to the COM-1 standard. Evidence for remobilization of REE (Fig. 14C) at Ovacik is provided by their consistent decrease from fresh volcanic rocks through montmorillonite–illite–adularia-altered wallrock to quartz–adularia veins. However, LREE concentrations are noticeably lower in the quartz–adularia veins (Figs. 12 13 and 14). Eu shows a very weak negative anomaly, probably inherited from Ca-plagioclase removal from the volcanic rocks (Bierlein et al., 1999).

The average Rb/Sr ratios of unaltered fresh volcanic rocks, the wallrocks of Ovacik–Narlica deposits and Ovacik–Narlica adularia–quartz veins are 0.13, 1.5 and 0.85, respectively. The average Rb/Sr ratio within the kandite (kaolinite)-altered Saganci area 1 km NW of the Ovacik gold deposit is 0.05 and corresponding K_2O value is 0.28%, whereas Rb/Sr ratios in the argillized-silicified wall-rocks at Ovacik and Narlica are 1.5 with corresponding K value of 4.6%. The average Rb/Sr ratio at the Ovacik–Narlica ore zones is 0.85% with associated 1.2% K_2O. A large variation in Rb/Sr following addition of K and Ca leaching of the wall rocks is typical for alteration in shallow low-sulfidation hydrothermal systems. Low Rb/Sr ratios and corresponding low K values recorded in the Saganci area are due to acid leaching of K and associated Rb in volcanic rocks, accompanied by development of kaolinite.

The wall rock at Ovacik and Narlica is enriched in Au, Ag, As, Hg, and Sc by factors of 60, 150, 88, 8 and 3, respectively. Geochemical relationships between Au–Ag and associated elements from mineralized epithermal quartz veins are presented in Table 4 and Figs. 15 and 16. Data from the Ovacik area show a moderate to strong association of Au with Ag, Pb, Zn, Cd, Cu, Sb in rockchip ore-grade samples (correlation coefficients are greater than 0.5). A strong association of Zn with Cu, Zn with Pb and Cu with Pb is also obvious. Correlation coefficients between Au and Cu are significant in the zone of base metal enrichment. It is interesting to note that there is no correlation between Au and As nor between Ag and As (Figs. 15 and 16). The lack of correlation between As and precious metals in the ore-grade Ovacik–Narlica rocks suggests that the elements may relate to different phases of mineralization. The As enrichments in the east of the M and the west of the S veins are persistent to a depth of 200 m below the surface, with rare arsenopyrite present. Nevertheless, the occurrence of the pre-ore stage or early-ore stage I arsenic-bearing pyrite at these depths may probably explain the lack of correlation between the As and Au or Ag. Moderate to strong correlations between Au or Ag and Pb, Zn, Cd, Cu and Sb suggest that all of these elements are related to the same mineralizing event (s). The association of tetrahedrite with enrichment in gold also supports this suggestion. Moderate correlation between Ag and Sb likely is due to concentration of silver within pyrargyrite and even more so with tetrahedrite.

At the Ovacik gold deposit, economic concentrations of Au and Ag along with associated base metal accumulations occur mainly in the M vein. It is important to consider that the Ag/Au ratio is close to unity. This is

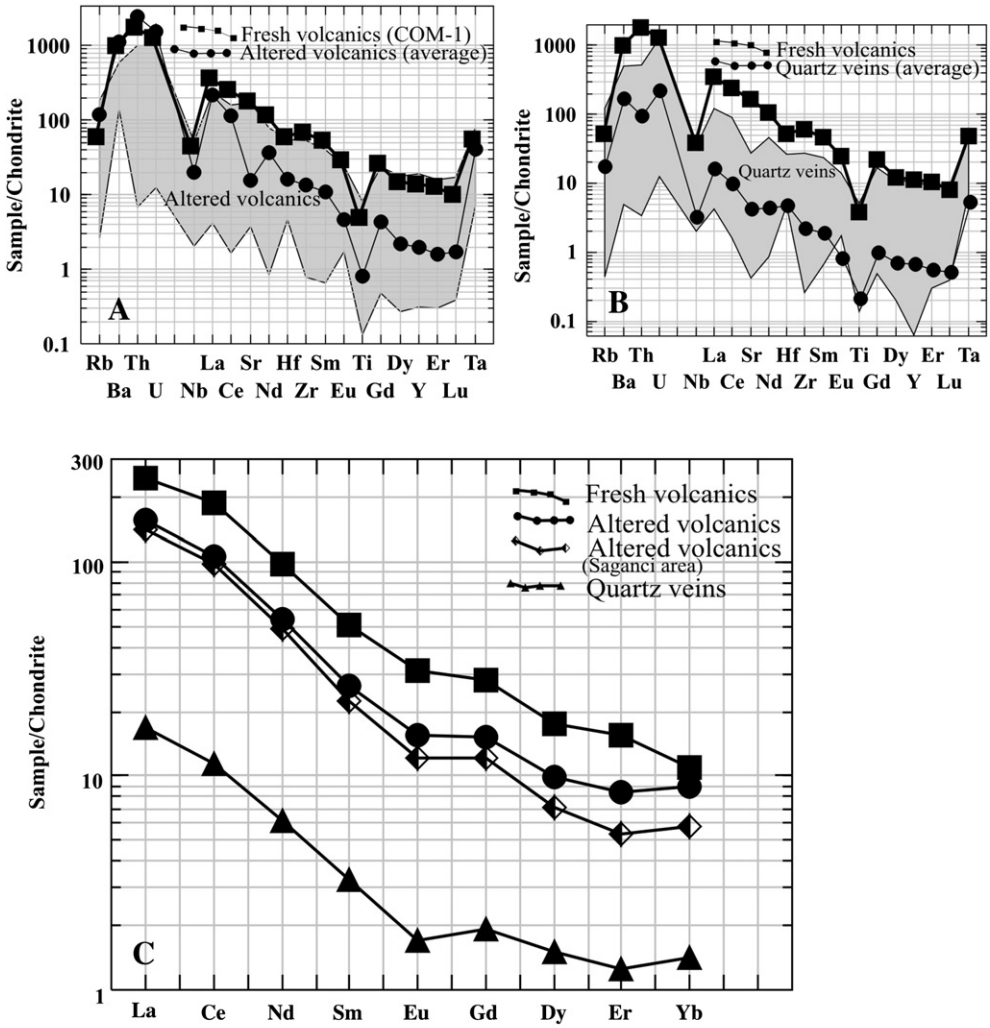

Fig. 14. Plot of chondrite-normalized REE concentrations of fresh volcanic rocks, altered wallrock, gold-mineralized quartz veins and weakly mineralized to barren volcanic rocks from Ovacik–Narlica–Saganci areas. A shows the range and average values of elements in altered volcanic rocks whereas B presents the range and average values of these elements in the mineralized quartz veins. E shows chondrite-normalized REE concentrations in the above-mentioned rocks. Normalized values are after Nakamura (1974).

important as an exploration guide in establishing the nature of the system, as well as elucidating metal enrichment and zoning. If epithermal systems with Ag/Au ratios (as is the case for Ovacik) are ~1, they contain mainly electrum and free gold, gold-thiosulfide complexes would have been dominant in the ore-forming fluids and the temperature of formation is less than 250 °C (Cole and Drummond, 1986).

10. Fluid inclusions

Most fluid inclusions studied were hosted by medium to coarse crystalline quartz (0.2 to 2.2 mm grain size), from colloform/crustiform bands with thicknesses ranging from a few mm to cm. Only two-phase liquid-rich inclusions, vapor (V) and liquid (L), containing approximately 15 to 20 vol.% vapor and 80 to 85 vol.% liquid (Fig. 17) were recognized. All fluid inclusion data are believed to have been obtained from primary fluid inclusions.

The homogenization temperatures first reported by Yilmaz (2002) ranged from 150 to 250 °C with a mode of 200 °C in both M and S veins. Within this data set, no correlation was found between the homogenization temperature and depth of formation. Yilmaz (2002) stated that the narrow range of salinities (from 7 to 8 wt.%

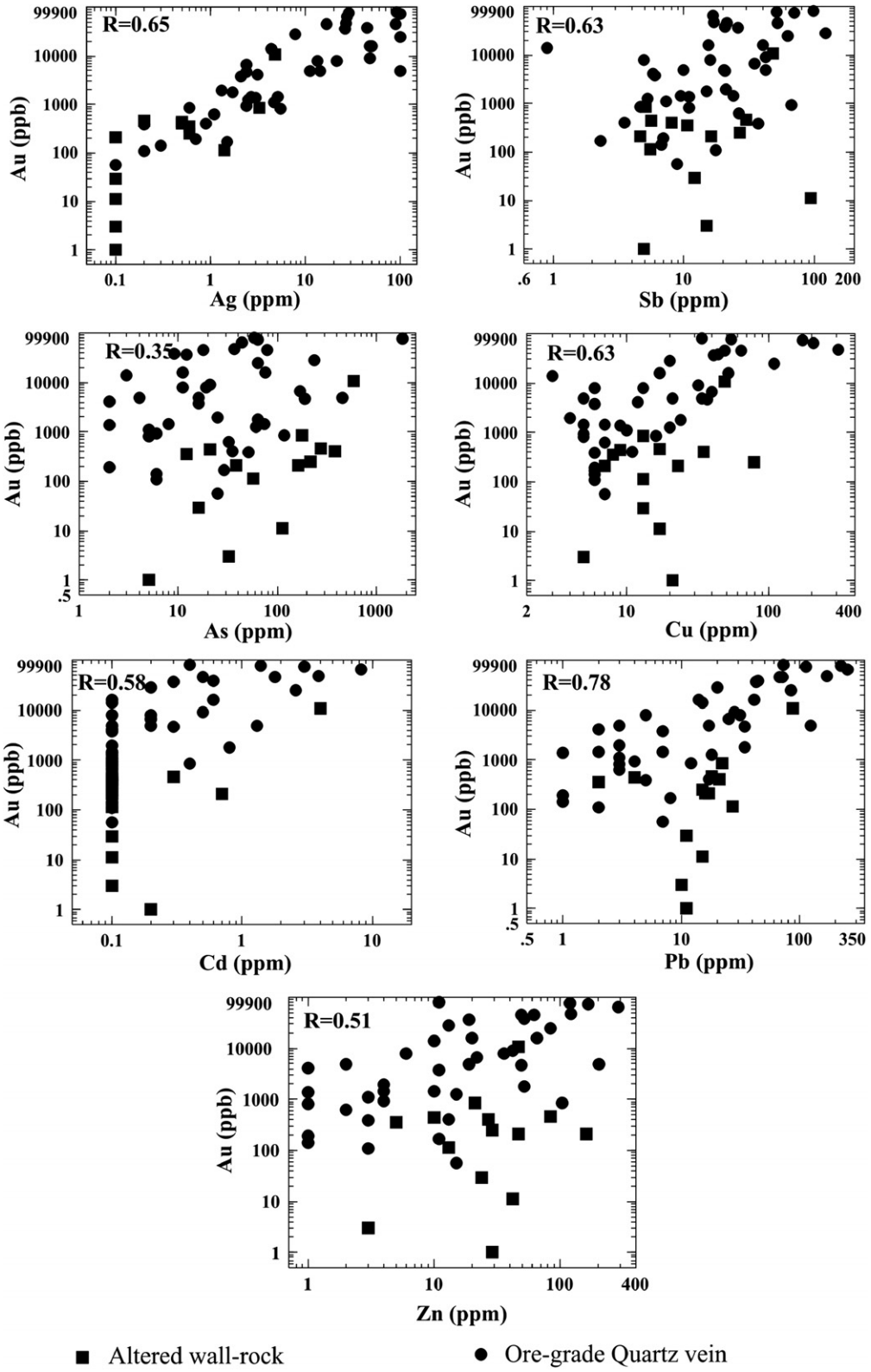

Fig. 15. Log–Log plot of concentrations of Au–Ag, Au–Sb, Au–As, Au–Cu, Au–Cd, Au–Pb and Au–Zn in drill core samples from Ovacik and Narlica deposits.

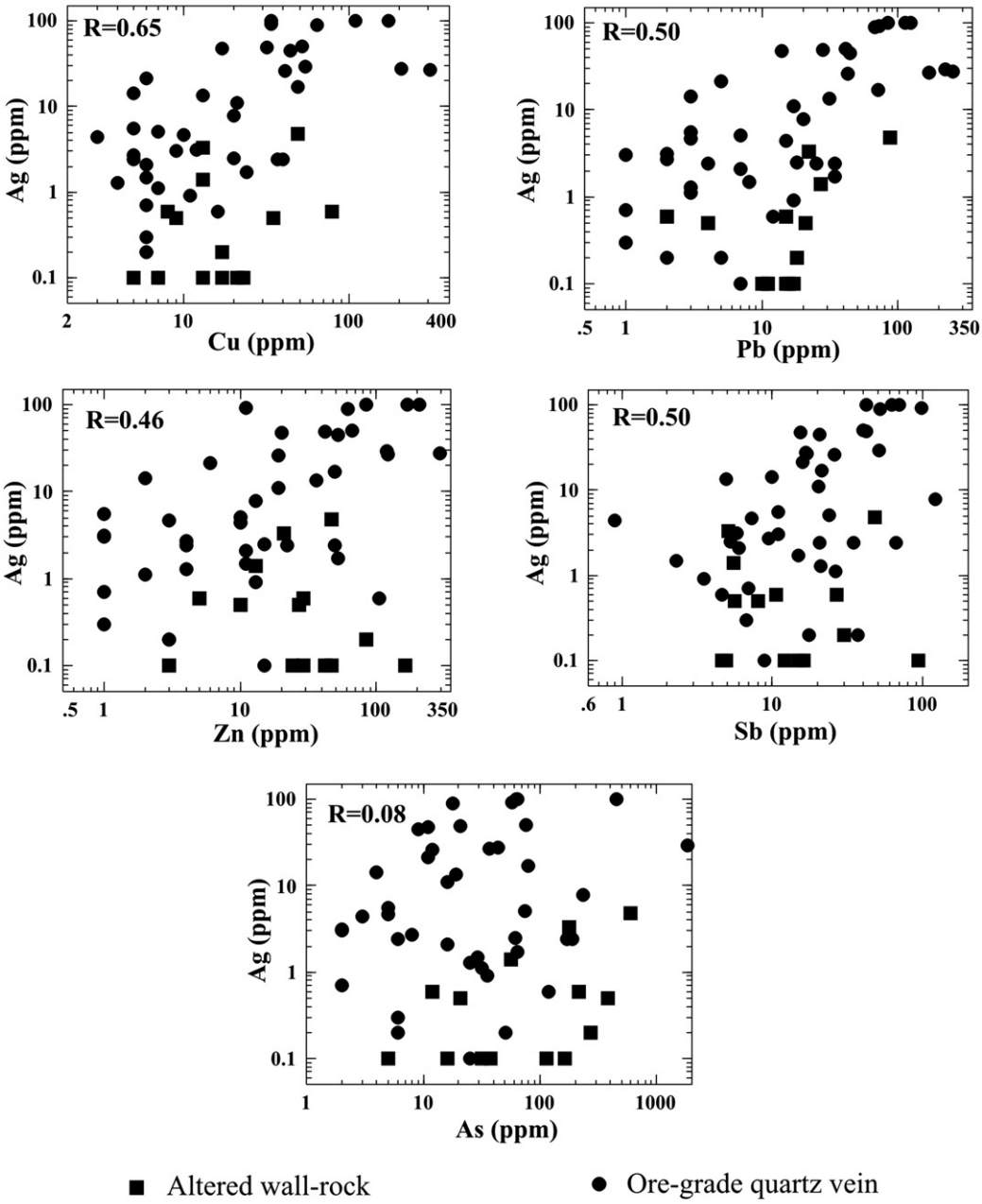

Fig. 16. Log–Log concentrations of Ag–Cu, Ag–Pb, Ag–Zn, Ag–Sb and Ag–As in drill core samples from Ovacik and Narlica deposits.

NaCl equiv.) is higher than in other quartz–adularia epithermal systems (e.g., Roedder, 1984; Heald et al., 1987). Ebert (2004) also measured salinities in 6 samples from the Ovacik deposit, ranging from 1.5 to 3.1 wt.% NaCl equiv., and from the Narlica deposit (0.17 to 0.83 wt.% NaCl equiv. in 7 samples). Homogenization temperatures obtained from 203 fluid inclusions in the present study returned relatively lower values ranging from 147 to 298 °C, with an average value of 190 °C (Table 5, Fig. 18). This is consistent with the secondary alteration minerals described earlier, the formation temperatures of which have been deduced from alteration studies of many geothermal systems (e.g., Browne, 1978; Reyes, 1990).

Table 4
Matrix of correlations between measured variable for Ovacik–Narlica deposits rockchip data set

	Au	Ag	Cu	Pb	Zn	As	Sb	Hg	Cd	Bi	Mo	Ba	Rb	Sr	Ga	Ta	Nb	K_2O	SiO_2	MgO	CaO	Na_2O
S	0.35	0.04	0.14	0.46	0.22	0.85	0.08	0.45	0.09	−0.03	−0.03	0.15	0.11	0.31	0.13	0.19	0.22	0.18	−0.26	0.04	0.15	0.25
La	−0.30	−0.26	−0.14	−0.13	0.14	0.11	−0.12	0.02	−0.17	0.20	0.02	0.94	0.95	0.37	0.86	0.97	0.97	0.93	−0.97	0.87	0.91	0.77
Na_2O	−0.23	−0.24	−0.07	−0.12	0.06	0.15	−0.08	0.10	−0.14	0.20	−0.14	0.70	0.68	0.36	0.64	0.77	0.76	0.68	−0.74	0.54	0.75	
CaO	−0.25	−0.24	−0.11	−0.12	0.17	0.12	−0.10	0.03	−0.13	0.13	−0.15	0.85	0.84	0.40	0.79	0.90	0.89	0.83	−0.90	0.88		
MgO	−0.26	−0.23	−0.15	−0.16	0.06	0.00	−0.05	−0.11	−0.16	0.04	−0.13	0.79	0.86	0.23	0.80	0.84	0.82	0.77	−0.83			
SiO_2	0.25	0.22	0.08	0.05	−0.17	−0.20	0.08	−0.10	0.13	−0.16	−0.06	−0.95	−0.94	−0.52	−0.84	−0.97	−0.98	−0.98				
K_2O	−0.26	−0.23	−0.09	−0.09	0.14	0.14	−0.07	0.12	−0.17	0.16	0.08	0.95	0.94	0.53	0.81	0.94	0.95					
Nb	−0.32	−0.27	−0.12	−0.13	0.11	0.12	−0.11	0.05	−0.18	0.23	0.05	0.92	0.91	0.57	0.87	0.99						
Ta	−0.32	−0.27	−0.12	−0.15	0.10	0.09	−0.11	0.05	−0.18	0.24	0.00	0.92	0.91	0.55	0.87							
Ga	−0.37	−0.21	−0.21	−0.24	0.02	0.03	−0.10	0.06	−0.26	0.17	−0.03	0.80	0.80	0.44								
Sr	−0.13	−0.13	0.10	−0.05	0.04	0.11	−0.02	0.07	−0.07	0.09	−0.03	0.36	0.26									
Rb	−0.23	−0.18	−0.13	−0.08	0.14	0.10	−0.04	0.10	−0.15	0.18	0.07	0.96										
Ba	−0.23	−0.20	−0.12	−0.07	0.16	0.14	−0.04	0.18	−0.14	0.22	0.07											
Mo	−0.14	0.20	−0.05	0.11	0.20	0.09	−0.09	−0.07	−0.03	0.05												
Bi	−0.08	−0.08	−0.07	−0.06	−0.09	−0.04	−0.05	0.51	−0.05													
Cd	0.58	0.33	0.79	0.84	0.77	0.17	0.15	0.11														
Hg	0.36	0.27	0.17	0.38	0.18	0.52	0.25															
Sb	0.48	0.50	0.19	0.28	0.16	0.25																
As	0.35	0.08	0.08	0.53	0.31																	
Zn	0.51	0.46	0.66	0.80																		
Pb	0.78	0.50	0.77																			
Cu	0.63	0.43																				
Ag	0.65																					

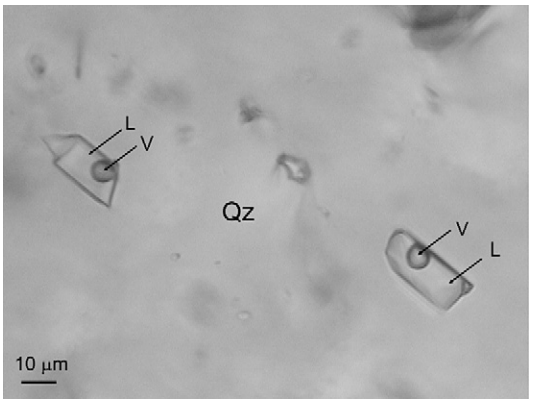

Fig. 17. Photomicrographs showing two-phase liquid-rich (L) fluid inclusions with vapor bubble (V) in quartz (Qz).

Fluid inclusions from crystalline quartz in the Narlica deposit returned homogenization temperatures up to 250 °C with a mean value of 235 °C. No phase changes were observed during the measurement of ice melting temperatures.

In the 26 suitable samples from the Ovacik deposit, only 4 of the fluid inclusions returned reliable ice melting temperature results (T_m): −0.4, −0.7, −0.8 and −1.2 °C. Only one of these (T_m: −0.8) was obtained from the M vein. These small values may be explained in large part by the presence of dissolved CO_2 in the fluid (Hedenquist and Browne, 1989). This limited data set indicates very low salinity values (<2 wt.% NaCl equiv.). There was no evidence for the presence of daughter minerals or visible CH_4. Somewhat unusually high T_h values were obtained from several inclusions in quartz from a few samples derived from the Ovacik deposit. This may be due to two-phase trapping and would indicate boiling (*cf.* White and Hedenquist, 1995). The possibility of boiling is also consistent with the presence of adularia in veins, the lattice-textured and bladed calcite, and extensive hydrothermal brecciation within a vertical zone of 200 m. However, it was not possible to confirm boiling in the majority of the fluid inclusions examined in this study.

11. Stable isotope studies

The isotopic compositions were calculated specifically for only four samples (Table 6) based on the average of several homogenization temperatures of low salinity inclusions from chalcedonic quartz in the M and S veins at Ovacik. The calculations of the fractionation factors at Narlica were made using the mean value of the fluid inclusion homogenization temperatures of Yilmaz (2002). Due to very low salinities (<2 wt.% NaCl equiv.), no correction factor (Horita et al., 1995) is added to the fractionation equation.

Table 6 shows the isotopic values of oxygen, hydrogen and sulfur for the Ovacik and Narlica samples. The $\delta^{18}O_{quartz}$ values in the M and S veins of the Ovacik deposit range from +9.5 to +15.7‰, whereas the calculated $\delta^{18}O_{H2O}$ values cover a relatively narrow interval from −3.5 to +3.5‰ (Table 6, Fig. 19). The average $\delta^{18}O_{H2O}$ value (−0.4‰) obtained for the M vein is relatively lower than that obtained for the S vein (0.0‰). However, individual values across the Ovacik ore zones do vary considerably. A plot of $\delta^{18}O_{quartz}$ and $\delta^{18}O_{H2O}$ values reveals a deposit-scale, subvertical zonation pattern (Fig. 20). The zonation in $\delta^{18}O$ values may reflect the fluid-flow directions of paleofluids and could be significant for exploration. Faure et al. (2002) suggested that the higher $\delta^{18}O$ values in the north in the Hishikari Au deposit, Japan, might indicate a greater proportion of magmatic source fluid in that part of the vein system. However, the M vein contains higher Au and lower $\delta^{18}O_{H2O}$ (Fig. 20) than the S vein. The average $\delta^{18}O_{quartz}$ and $\delta^{18}O_{H2O}$ values of the deeper Narlica deposit (+7.3 and −2.4‰) are relatively lower than that of the shallower Ovacik deposit (average of M and S veins: +12 and −0.2‰; Fig. 20). The geometry of the E–W-trending contoured long-section of oxygen isotope values, along with the E–W and NW–SE-trending steep

Table 5
Microthermometric data of fluid inclusions from the Ovacik and Narlica gold deposits

Vein	Sample number-depth (m)	Type	Mean T_h °C	Standard deviation	*N*	Min T_h °C	Max T_h °C
Ovacik Au deposit							
M	M35-146.5	L-V	182.7	18	20	166.7	235.0
M	M78-51.5	L-V	197.0	22	34	162.6	256.2
M	M81-139.5	L-V	201.7	30	47	147.6	298.3
Mean from M vein			196.4	26	101	147.6	298.3
S	S53-87.0	L-V	180.0	13	41	148.6	245.4
S	S41-77.5	L-V	179.7	12	22	159.1	197.2
S	S14-105.0	L-V	175.4	12	39	147.6	211.8
Mean from S vein			178.2	12	102	147.6	245.4
[a]*Narlica Au deposit*							
	PD5-15.25		*242*	[b]dna	*3*	*238*	*250*
	PD1-37		*228*	dna	*7*	*205*	*303*
	PD13-92		*240*	dna	*2*	*230*	*251*
Mean from Narlica			***236***		***12***	***205***	***303***

[a] Data from (Dag, 1993).
[b] dna: Raw data is not available.

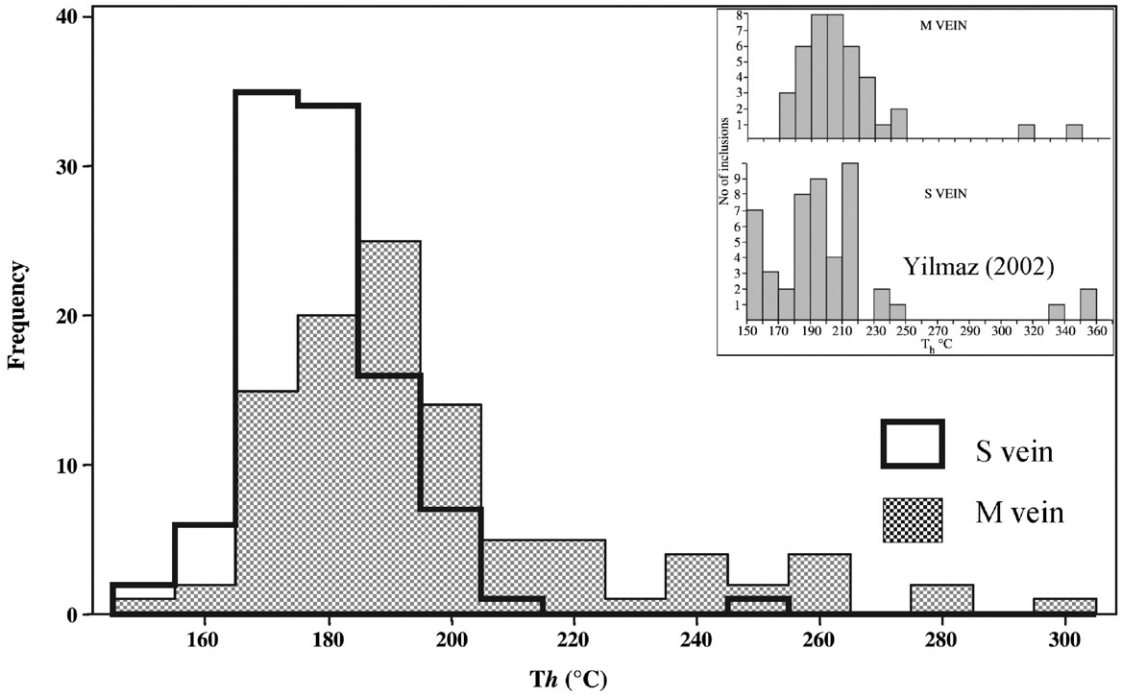

Fig. 18. Homogenization temperatures of primary fluid inclusions in quartz from M and S veins of the Ovacik gold deposit. T_h frequency histograms of M and S veins of the Ovacik Au deposit on the upper right corner of the figure is taken from Yilmaz (2002).

structures in the deposit, suggest that the ore-bearing fluids initially migrated upwards to the surface. There is a pronounced temperature gradient going from higher temperatures in the north of the deposit to lower temperatures in the south. This temperature gradient may be attributed mainly to the level of exposure. Although the oxygen isotope distributions at levels below RL900 m of the Ovacik deposit are relatively homogeneous, they exhibit significant lateral variations above this level (Fig. 20). These variations may range from −3.5 to +3.5‰ between the RL900 to RL1000 m levels in the M vein. Present-day geothermal water has $\delta^{18}O_{H2O}$ values ranging from −5.2 to −8.1‰, with an average of −6.8‰ (MTA-JISCA, 1987).

Quartz samples from the Ovacik veins yielded δD values in fluid inclusions that range from −92 to −117‰ with an average of 102‰; the Narlica deposit returned relatively higher δD values ranging from −82 to −97‰ with an average of −92.5‰ (Table 6, Fig. 19). The fluid inclusions in quartz have low δD values (−35.2 to −50.7‰) compared with present day geothermal waters (average δD: −42‰), which can not be adequately explained by fluid mixing or water-rock interaction. Six samples of illite associated with gold mineralization have δD values ranging from −88 to −111‰, with an average of −97‰; corresponding calculated δD_{H2O} values range from −66 to 86‰ with an average of −71‰. This variation shows that there are problems associated with δD analysis, which are caused by significantly adsorbed and loosely-bound water, primary vs. secondary inclusions, and anomalously low δD values of fluid inclusions along with some of the structural water (Faure et al., 2002). The δD analysis of illite (Sheppard and Gilg, 1996) from such samples appears to partially overcome this problem.

The $\delta^{34}S_{\Sigma sulfide}$ values in bulk samples from Ovacik and Narlica (Table 6, Fig. 19) range from −2.10 to 5.3‰ (average 1.7‰ for the M vein and 2.2‰ for the S vein), and from −4.6 to 2.7‰ (average: −0.4), respectively. The average $\delta^{34}S_{\Sigma sulfide}$ values are very tightly clustered near zero which is the value of bulk sulfur in the magmatic system (Rye, 1993). Average $\delta^{34}S_{\Sigma sulfide}$ values point to a magmatic source for the sulfur (Seal and Rye, 1992; Sherlock et al., 1995).

Fig. 21 shows plots of δD *vs.* $\delta^{18}O_{H2O}$ values for the Ovacik and Narlica deposits on a diagram which is a combination of two separate diagrams prepared for low sulfidation deposits by Hedenquist et al. (1996). Fluids in istopic equilibrium with hydrothermal quartz (at 200 °C for Ovacik and 230 °C for Narlica) are highly enriched in $\delta^{18}O$ with respect to the meteoric water line (MWL; Fig. 21). Oxygen and hydrogen isotope values indicate

Table 6
Stable O, H ve S isotope values of Ovacýk and Narlýca gold deposits

Drill hole number	Depth (m)	$\delta^{18}O_{quartz}$ ‰	$\delta^{18}O_{H2O}$ ‰	δD-fluid inclusion ‰	δD-clay ‰	$\delta^{34}S$-Σsulfide ‰	$\delta^{34}S$–H_2O ‰	*E* (m)	RL (m)	Explanation
Ovacik gold deposit										
M vein, drill core samples										
2	69	12.47	0.27[a]	−97		3.00	2.12[b]	6059	1000	Quartz vein with minor colloform/crustiform texture.
2	65				−91					Sericitized porphyry andesite and sheeted quartz veinlets with colloform/crustiform texture.
3	107.3	9.73	−2.47	−109		1.30	0.42	6018	957	Minor banded stringer quartz veinlets in silicified-argillized andesite.
21					−95					Pyritized andesite hydrobreccia.
101	45	10.20	−2.00	−98		1.40	0.52	6000	1000	Pyritic quartz hydrobreccia with abundant vug infill and banding textures.
109	106	9.46	−2.74	−110		−0.30	−1.18	5957	946	Hematitic quartz hydrobreccia with minor vug infill texture.
109	107				−98					Strongly silicified andesite with stockwork veinlets and pyritic quartz-breccia.
12	121.2	11.21	−0.99	*		3.40	2.52	5900	937	Quartz-pyrite-cemented vein breccia with minor carbonate replacement and vug infill textures.
131	158.5	11.04	−1.16	−97		1.00	0.12	6139	960	Quartz-cemented silicified andesite hydrobreccia.
132	194.6	10.94	−1.26	−103		0.10	−0.78	6018	857	Silicified porphyritic andesite with quartz veinlets and carbonate replacement textures.
17	123	9.80	−2.40	−114		2.70	−1.82	6117	887	Massive quartz vein with minor vug infill texture.
19	18	11.32	−0.88	−102		2.40	1.52	5997	1016	Quartz vein/breccia with colloform/crustiform texture.
21	44.5	11.53	−0.67	−97		1.80	0.92	5946	997	Pyritic quartz-adularia vein with colloform/crustiform texture.
34	177.5	14.33	2.13	−89		1.90	1.02	6117	879	Andesite with minor clay, silica and quartz.
35	46.5	12.26	0.06	−97		2.60	1.72	6039	1033	Quartz vein breccia with angel wings texture.
51	118.5	11.39	−0.81	−102		−1.90	−2.78	5900	940	Quartz–pyrite-cemented andesite breccia with stockwork veining.
55	16.5	13.20	1.00	−90		2.10	1.22	6096	1033	Quartz–adularia vein breccia with minor carbonate replacement and colloform/crustiform textures.
71	76	9.34	−2.86	−107		**	**	6112	970	Intensely silicified, hydrobrecciated andesite with minor vug infill texture.
76	23	11.26	−0.94	−97		0.50	−0.38	6016	1024	Quartz–adularia vein with colloform/crustiform, vug infill and carbonate replacement textures.
78	51.5	11.82	−0.38	*		−2.10	−2.98	6074	721	Massive chalcedony quartz with minor vug infill texture.
78	139	11.63	−0.57	−101		3.30	2.42	6081	1046	Silicified andesite hydrobreccia.
81	139.5	15.71	3.51	−125		**	**	6157	1005	Quartz–cemented hydrobreccia with abundant vug infill texture.
82	49.4	11.72	−0.48	−103		1.90	1.02	5919	989	Quartz–cemented hydrobreccia with abundant vug infill texture.
MY−2	110	12.78	0.58	−97		2.60	1.72	5880	990	Quartz–adularia vein with alternating fine to coarse banded colloform/crustiform texture and locally crystalline quartz.
MY−3	110	11.20	−1.00	−107		1.20	0.32	5870	985	Quartz–adularia vein with colloform/crustiform texture, intercalated with massive to brecciated chalcedony.
S vein, drill core samples										
1	83	10.61	−1.59	−109		2.40	1.52	6378	1008	Silicified andesite containing quartz veinlets with banded texture.
7	49.3	11.97	−0.23	−112		5.30	4.42	6519	1022	Massive to mill-brecciated chalcedony quartz vein with hematite matrix having minor vug infill texture.
7	53.5	11.69	−0.51	−101		**	**	6519	1018	Quartz-cemented hydrobreccia with minor cockade banding.
9	54				−96					Silicified porphyritic andesite and sheeted quartz veinlets with colloform texture.

Table 6 (*continued*)

Drill hole number	Depth (m)	$\delta^{18}O_{quartz}$ ‰	$\delta^{18}O_{H2O}$ ‰	δD-fluid inclusion ‰	δD-clay ‰	$\delta^{34}S$-Σsulfide ‰	$\delta^{34}S$–H_2O ‰	*E* (m)	RL (m)	Explanation
14	105	13.35	1.15	−108		3.00	2.12	6398	989	Quartz–adularia vein with colloform/crustiform banding.
14	128	14.49	2.29	−96		3.80	2.92	6398	965	Quartz hydrobreccia with moderately abundant colloform/crustiform banding.
35	89	11.60	−0.60	−117		−2.10	−2.98	6218	980	Quartz–adularia vein with banded and carbonate replacement textures.
40	92.35	12.75	0.55	−97		1.80	−2.68	6221	1035	Fluidized/milled quartz hydrobreccia with pyrite, abundant vug infill and minor colloform/crustiform textures.
41	56.8	10.58	−1.62	−99		1.80	0.90	6201	995	Massive chalcedony.
41	77.5	13.89	1.69	*		2.10	1.22	6201	973	Massive chalcedony.
42	12				−111					Quartz vein hydrobreccia with minor banded texture.
53	87.6	13.33	1.13	*		1.40	0.5	6461	1005	Massive chalcedony abundant vug infil and colloform/crustiform textures.
53	90	11.83	−0.37	−92		2.80	1.92	6461	995	Quartz vein with colloform/crustiform texture.
65	8	14.38	2.18	−108		**	**	6299	976	Quartz-cemented hydrobreccia with minor colloform/crustiform, vug infill and carbonate replacement textures.
66	207	15.10	2.90	−93		1.20	0.32	6399	852	Quartz-adularia vein/breccia with late stage vug infill texture.
90	54	15.26	3.06	−99		3.30	2.42	6458	916	Limonitic, partially massive quartz–adularia vein/breccia with minor colloform/crustiform texture.
Narlica gold deposit										
PD vein, outcrop sample										
N-1	0	7.22	−2.23	−95		2.30	1.42			Quartz/andesite hydrobreccia with rare banded and abundant vug infill textures.
N-2	0	7.91	−1.54	−90		**	**			Quartz vein with minor vug infill texture.
N-4	0	6.90	−2.25	−97		2.70	1.82			Quartz/andesite hyrobreccia with moderately abundant pyrite.
N-5	0	7.02	−2.43	−91		**	**			Quartz vein with abundant vug infill, and minor carbonate replacement and banded textures.
PD vein, drill core sample										
1	36	5.93	−3.52	−82		−4.00	−4.88			Crystalline quartz veinlets with vuginfill texture in silicified-argillized andesite.
14	129.6	7.24	−2.21	−89		0.70	−0.18			Crystalline quartz veinlets within altered andesite.
6	45	7.96	−1.43	−99		−4.60	−5.48			Quartz–pyrite-cemented silicified andesite hydrobreccia.
10	46	8.30	−1.10	−97		0.70	−0.18			Pyritic crystalline quartz hydrobreccia.
11	85.5				−88					Crystalline quartz stringer veinlets within altered andesite.

*: Water concentrations are too low for a reliable analysis. **:Sulfur concentrations are to low for a reliable analysis.

a: Calculated from Clayton et al. (1972).

b: Calculated from Ohmoto and Rye (1979); calculated for Ovacik at 200 °C and for Narlica at 250 °C.

that meteoric water-derived fluids appear to be dominant at the Ovacik deposit, with a lesser contribution of magmatic fluids. Such a significant shift cannot be caused by boiling of meteoric water alone. However, this ^{18}O-fluid shift might also have been due to fluid-rock isotopic exchange. Kodera et al. (2005), for example, have suggested that boiling away half of an aqueous fluid would result in a maximum relative $\delta^{18}O$ enrichment of 1.2‰ in the fluid and a maximum relative δD depletion of 4‰ in the remaining aqueous fluid. Boiling away of 90% of liquid would result in a maximum $\delta^{18}O$ enrichment of 3.9‰ in the fluid and a maximum relative δD depletion of 13‰. The variation in the samples reported here, (about 6‰ for $\delta^{18}O$ and 25‰ for δD in the fluids), therefore,

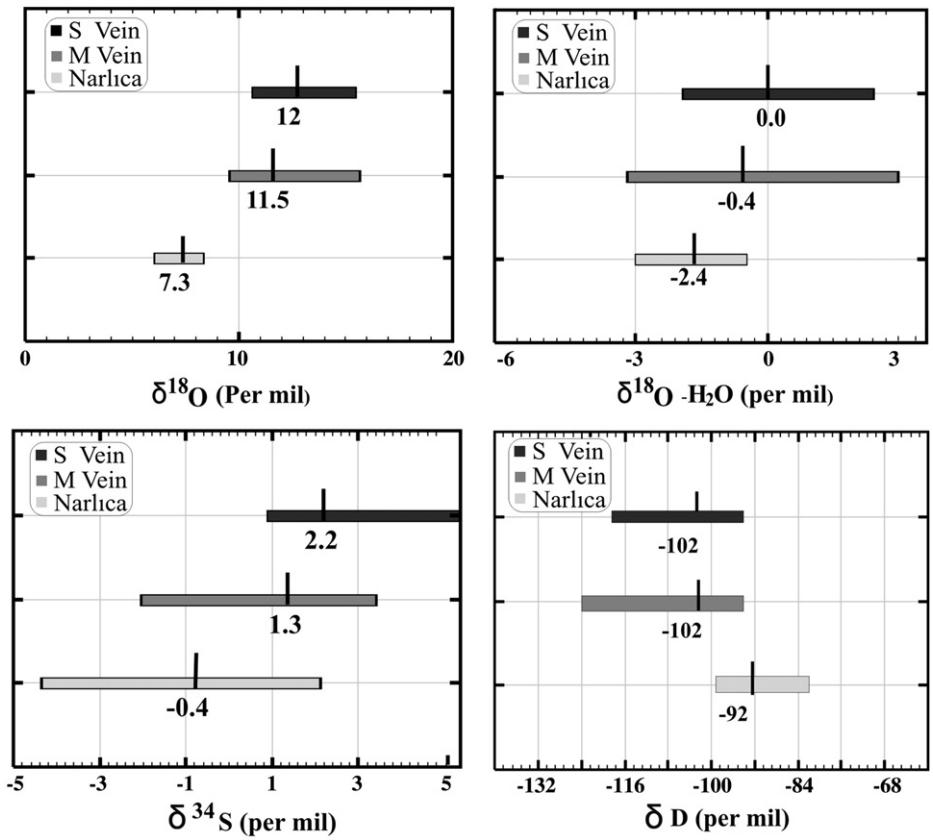

Fig. 19. Range (bars) and average (numbers) of $\delta^{18}O_{quartz}$, calculated $\delta^{18}O_{H2O}$, $\delta^{34}S_{\Sigma sulfide}$, and δD_{H2O} values within the Ovacik (S and M veins) and Narlica deposits.

demonstrate that the end stages of open system boiling and fractionation could not have been reached everywhere in the system.

Hedenquist and Lowenstern (1994) suggested that waters precipitating barren quartz in low sulfidation deposits commonly show an O-shift from local meteoric water values. In contrast, high-grade ore samples (e.g., the Comstock Lode epithermal gold deposit — solid star in Fig. 21) display both O- and D-isotopic shifts from local meteoric water, likely caused by a magmatic water

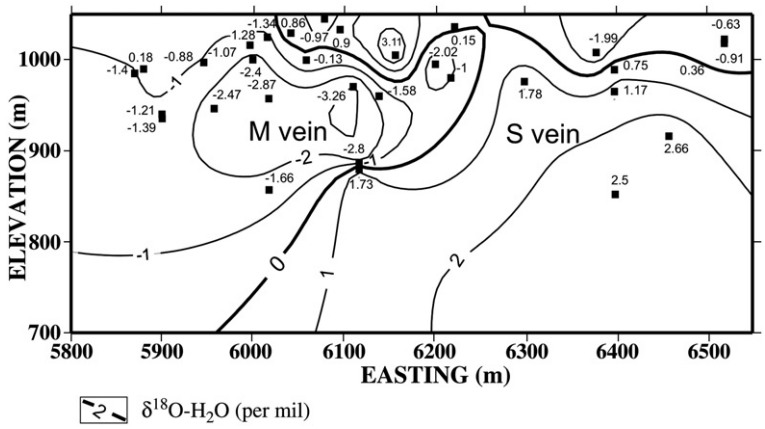

Fig. 20. Contoured values of $\delta^{18}O_{H2O}$ in M and S veins of the Ovacik deposit plotted by Surfer software.

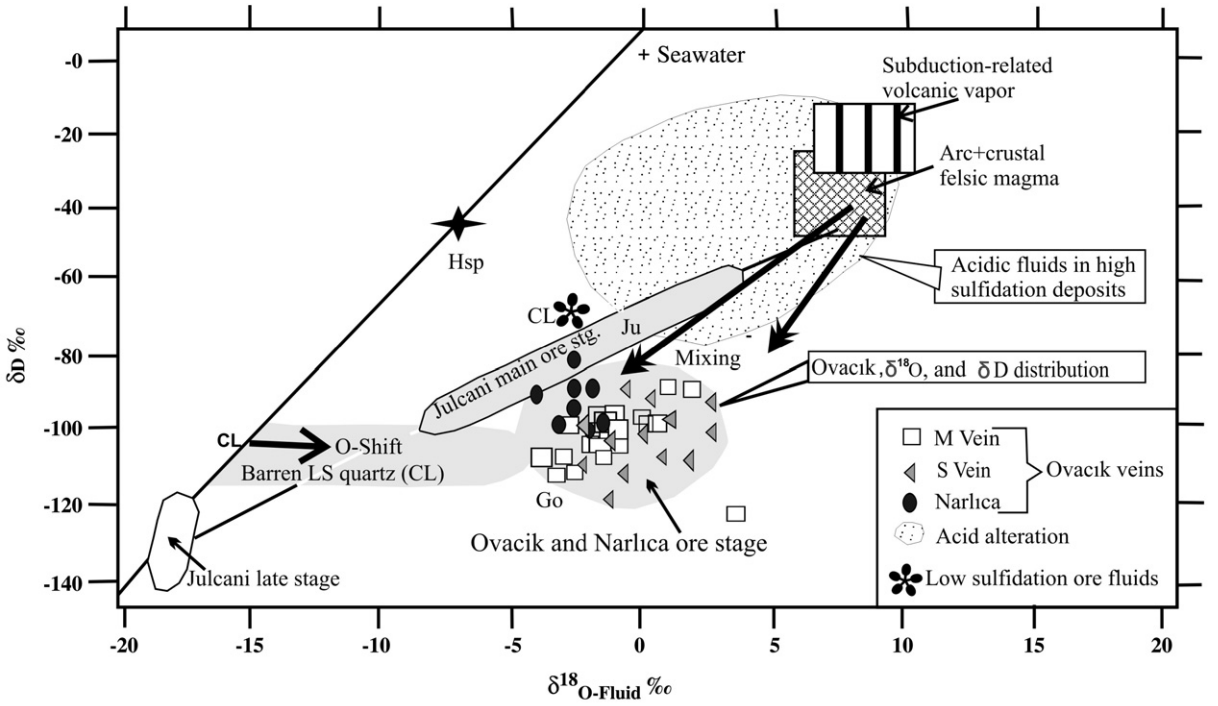

Fig. 21. Summary diagram showing the variation in $\delta^{18}O_{H2O}$ and δD isotopic compositions of hydrothermal fluids in the Ovacik and Narlica deposits, others elsewhere in the world. Ju: Julcani, Go: Goldfield, CL: Comstock Lode, M and S veins in Ovacik, Nr: Narlica. HSp: Hot springs at Ovacik (MTA-JISCA, 1987). In LS deposits, gangue quartz indicates hydrothermal fluids are O-shifted meteoric water in origin, though in some deposits there is evidence for a large magmatic water component associated with the highest grade of Au ore (Modified from Hedenquist et al., 1996).

component. Precipitation of high-grade gold ore in the Ovacik deposit (particularly in M vein, Fig. 21) might have been result of a moderate O- and D-isotopic shift from local meteoric water (likely caused by minor magmatic water). The average $\delta^{34}S_{\Sigma sulfide}$ compositions in the M (1.3‰) and S (2.2‰) veins also support this suggestion.

Development of hydrobrecciation and hydrothermal alteration increases the permeability of the epithermal system and facilitates the circulation of meteoric water towards deeper levels. Penetration of meteoric water toward deeper levels in the Ovacik Au deposit gave rise to a decrease in temperature and Cl^- activity, and a pH increase of the metal-bearing hydrothermal fluids. Such changes in the physico-chemical conditions may have contributed to precipitation of Cu, Pb and Zn sulfides by destabilization of base metal chloride complexes (e.g., $CuCl^{-2}$). In the western portion of the Ovacik deposit (M vein), high Cu+Pb+Zn and Au, and relatively low Ag values, correlate with the lowest $\delta^{18}O_{quartz}$ and $\delta^{18}O_{H2O}$ isotope values (Figs. 19 and 22). In particular, the coincidence of maximum Au and base metal contents with minimum $\delta^{18}O_{H2O}$‰ isotope values are highly significant from the exploration point of view.

12. Discussion and results

The Ovacik and Narlica Au deposits are good examples of quartz–adularia-type low-sulfidation epithermal gold deposits, as evidenced by the recognition of chalcedonic quartz, adularia, illite and mixed-layered illite/smectite minerals along with dominant colloform/crustiform banding and carbonate replacement textures.

Changes in the crystal morphology of the pyrite at the Ovacik mine, from cubes through octahedra to gel-pyrite, generally coincides with the changes from barren to mineralized rocks (e.g., Mauk et al., 1998). Therefore, crystal morphology of the pyrite may be a useful indicator during exploration. Descending acid-sulfate waters (<240 °C) following gold mineralization play an important role in supergene marcasite precipitation from fluids with pH below 5.0 and 3.9 (Murowchick, 1992), associated with replacement of adularia by kandite (Schoen et al., 1973; Murowchıck and Barnes, 1986; Simpson et al., 2001).

Fig. 23 summarizes the temperature estimates for the systems at Ovacik and Narlica. In the Saganci area northwest of Ovacik, clay mineralogy (presence of

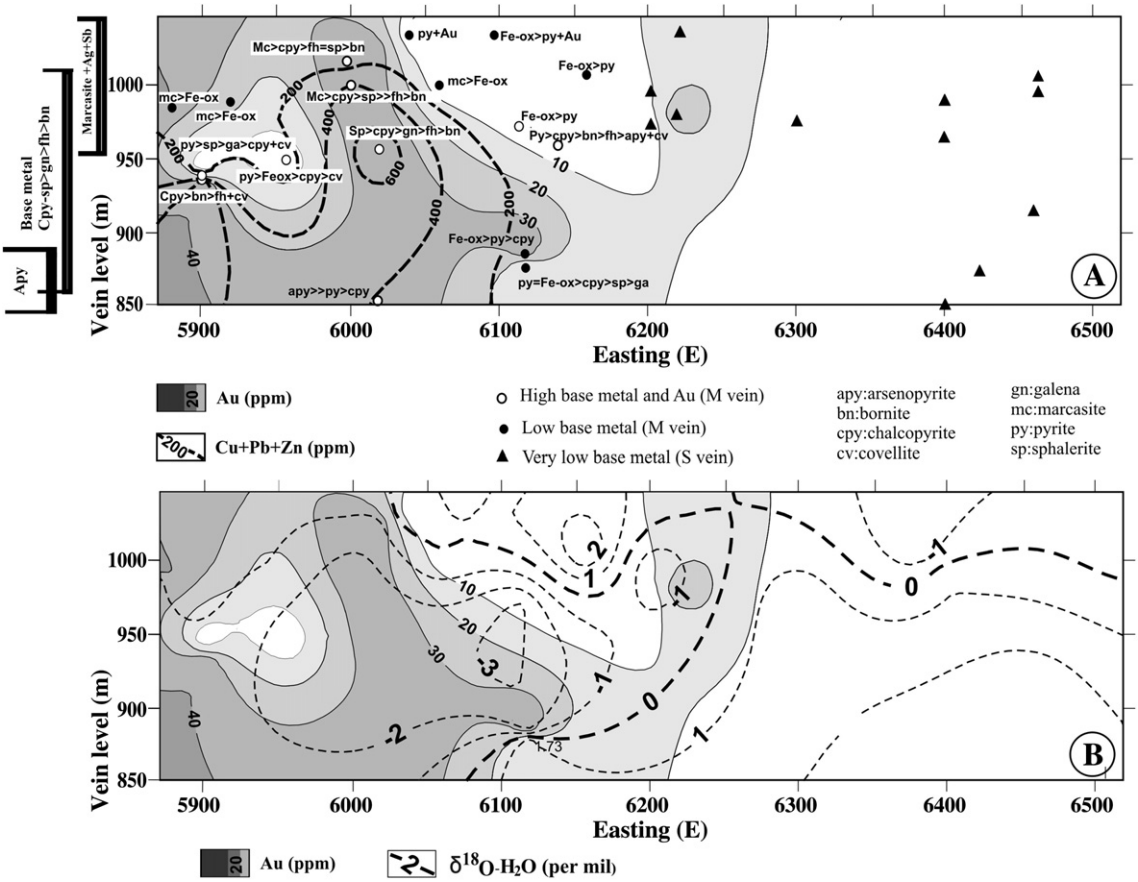

Fig. 22. Relationship between distribution of A) total Cu+Pb+Zn base metal and sulfide minerals, and high-grade Au and B) $\delta^{18}O_{H2O}$ and high-grade Au in the Ovacik gold deposit.

mixed-layered smectite/illite >13.4 Å) and sinter breccias indicate that (Figs. 3 and 23) alteration/mineralization formed at temperatures below 140 °C, indicating the very high levels of an epithermal system, and implicitly gold potential at depth. The Ovacik mineralization formed mainly at temperatures of ca. 170–200 °C (based on the presence of illite/illite with high crystallinity index and adularia; *cf.* Henley and Ellis, 1983; Reyes, 1990). The Narlica deposit probably formed between 220 and 300 °C, based on the dominance of crystalline quartz. This in turn suggests higher temperature of formation and lesser gold potential at depths.

Chalcedony in a typical epithermal system is deposited mainly below about 180 °C (Fournier, 1985). The Ovacik mineralization (chalcedony>quartz with colloform/crustiform, sugary quartz, cockade, bladed) developed at relatively higher temperatures whereas Narlica formed at the highest temperatures among the studied deposits (quartz>chalcedony with similar textures to those of the Ovacik deposit).

In the wallrock alteration zone at the Ovacik deposit, K, Rb and Cs are enriched with respect to fresh rocks, whereas Mg, Na, Ca, Sr are significantly depleted. Ca and Na were removed from plagioclase, and Mg and Fe from biotite, whereas K, Rb and Cs enrichment is associated with the crystallisation of adularia or illite/sericite. Trace elements such as Rb, Ba, Th, U, Cs, Nb, La, Ce, Sr, Nd, Zr, Ti, Tb, Y, Cr, V and Ni in mineralized quartz veins form very negative anomalies. Rare earth element contents in the altered wallrock generally show moderate depletions with respect to unaltered rock and suggest that in the volume and/or geochemistry of hydrothermal fluids was insufficient to cause significant remobilization of the rare earth elements. Large variation in Rb/Sr is due to changes in the concentration of both elements and follows the K-addition and Ca-leaching typical of wall-rock alteration of igneous rocks in shallow hydrothermal systems (Arribas et al., 1995). Evidence for remobilization of REE at Ovacik (Fig. 14C) is provided by their consistent decrease from fresh volcanic rocks through montmorillonite–illite–adularia-

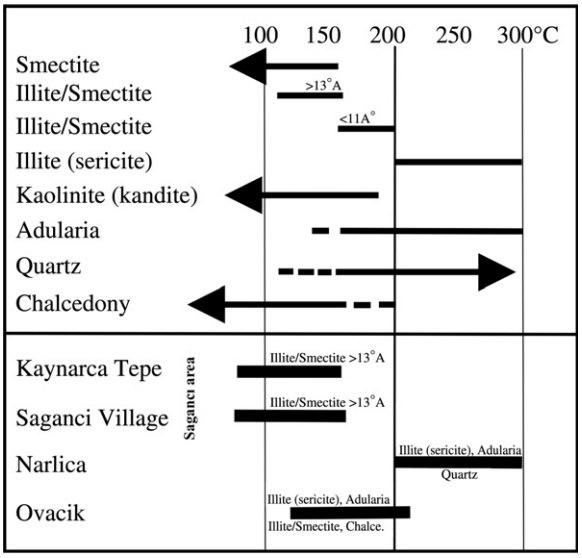

Fig. 23. Generalized temperature estimates for prospects in the Ovacik district based on clay mineralogy proximal to and away from mineralized zones. Temperature ranges of the hydrothermal minerals are from Henley and Ellis (1983), Reyes (1990), and White and Hedenquist (1995).

altered wallrock to quartz–adularia veins. An alternative explanation to this consistent decrease of REE from fresh volcanic rocks through montmorillonite–illite–adularia-altered wallrock to quartz–adularia veins may be dilution by metasomatic processes. Bierlein et al. (1999) suggested that no significant change of REE was likely to occur during illitic alteration, which also represented the predominant alteration style associated with mesothermal lode-gold deposits in central Victoria. This is because low concentrations of REE released during the breakdown of feldspar will re-precipitate and are fixed at constant inter-REE ratios by illite. This might have been the mechanism controlling the distribution of REE in the Ovacik and Narlica deposits.

Strong positive correlation coefficients ($R=0.51$ to 0.72) between Au and Ag, Pb, Zn, Cd, Cu, Sb and weak to moderately strong correlation coefficients ($R=0.43$ to 0.55) between Ag and Cu, Pb, Zn, Sb suggest that these metals are related to the same mineralizing event. In contrast, lack of correlation between As and Au (or Ag) in the ore deposits suggests that these elements may be related to different stages of the mineralization event. An alternative explanation to this is that As-rich minerals are concentrated at different levels.

The presence of liquid-rich inclusions with vapor, variable liquid-to-vapor ratios and relatively large ranges in homogenization temperatures at Ovacik are potential indicators of phase separation (i.e., boiling) in the hydrothermal system (*cf.* White and Hedenquist, 1995). Fluid inclusion data from the Ovacik Au deposit suggest that the ore-forming fluids were low salinity (<2 wt.% NaCl equiv.) Fluid inclusion homogenization temperatures range from 150 °C to 250 °C, with most of the data from Ovacik below 200 °C and that from Narlica indicating temperatures in excess of 211 °C. The Ag/Au ratio close to unity is consistent with the presence of minor base metal sulfide, achantite/sulfosalts and abundant electrum as the major mineralogical host for gold.

Fluids which are in isotopic equilibrium with hydrothermal quartz at about 200 °C are highly enriched in ^{18}O and depleted in D with respect to meteoric water. Oxygen and hydrogen isotope values indicate that fluids with both meteoric and magmatic origin were important components in the formation of the Ovacik gold deposit. The association of a large $\delta^{18}O$ depletion halo with high-grade gold at Ovacik and Narlica may be considered important. The spatial association of epithermal orebodies and mapped $\delta^{18}O$ anomalies is very marked in several areas, and has been noted, for example, at the Yankee Fork deposit, Idaho (Criss et al., 1985). This may prove to be a significant asset in exploration, as well as in further understanding the controls upon ore location.

The adularia sample from the Narlica deposit yield an excellent plateau and it therefore, appears to have been undisturbed since crystallization and rapid cooling whereas the adularia samples from Ovacik deposit exhibits no statistically valid isochron or plateau age, indicating somewhat thermal disturbance after crystallization. Thus, a weighted mean age of 18.2±0.2 Ma is considered to be a more reliable estimate for these samples than the total gas age for the Ovacik deposit. The age data presented here suggest that extension-related mineralization in the area took place at 18± 0.2 Ma in volcanic rocks having an age of 19.7 Ma. These findings are in contrast with earlier suggestions (Zanchi et al., 1990, 1993) that the rocks, and implicitly the deposits, are of approximately Mid–Late Miocene age.

Early Miocene extensional tectonism with earlier or associated synchronous Early Miocene calc-alkaline magmatism was responsible for the formation of N–S and NE–SW-trending grabens (Zanchi et al., 1993) accompanied by movement of variable degrees of a sinistral strike–slip component (Fig. 24) and is generally oriented E–W to NW–SE (Wright et al., 1996). Of four gold deposits in the Izmir region, those of current economic importance occur in quartz vein systems (Ovacik, Efemçukuru) or quartz stockwork (Kisladag)

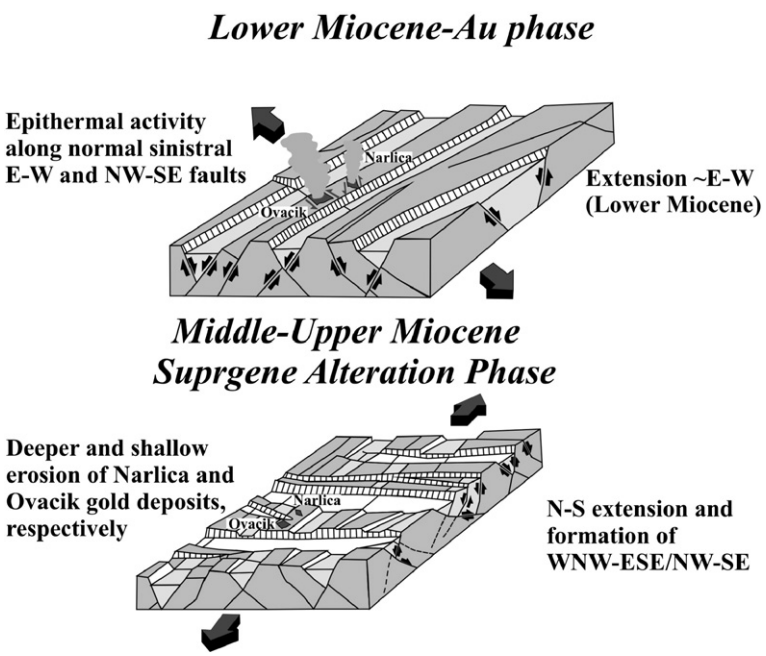

Fig. 24. Position of gold depositions at the Ovacik and Narlica in relation to tectonic evolution of western Turkey (modified from Zanchi et al., 1993; Wright et al., 1996). A) Development of NE-trending major grabens associated with gold mineralization and B) Changes in tectonic regime resulting in development of E–W-trending grabens. This tectonic change resulted in cessation of both extensional and hydrothermal activity in NE-trending grabens, thus ending the mineralization event at Ovacik and Narlica.

with strong NW–SE and E–W trends. Other deposits of this type should be sought with similar tectonic setting.

Acknowledgements

This study was financially supported by the National Research Council of Turkey (TUBITAK) under grant No: 103Y003. The authors are grateful to the staff of Normandy Gold Mine, Ovacik/Bergama for their help during core sampling and field work. We thank Ferenc Molnár and Peter Kodera for their detailed and thorough comments. Language review by Kerim Sener is greatly appreciated.

Appendix A

A.1. Radiocrystallography

Two analytical procedures were used for this study: 1) a standard procedure used to determine the mineral components of an unknown powdered sample, and 2) a technique known as the ‘clay-adapted’ procedure used to indicate the nature of the clay and main minerals present in the sample. The diffractometer used was an automated PW3710 instrument. The CuKα radiation source is supplied by Cu tube from a graphite back monochromator. Experimental conditions were: (a) for the spectra of powder in a pellet prepared from sample crushed to <40 μm, 2θ scanning 4° to 9° for a velocity of 0.02° of 2θ/s; and (b) for clay fractions <2 μm on oriented sections, 2θ scanning of 2° to 36° for a velocity of 0.02° of 2θ/s and on a fixed sample, whereby each sample was analyzed untreated, treated with glycol, and heated to 500 °C for 4 h.

A.2. $^{40}Ar/^{39}Ar$ dating

The $^{40}Ar/^{39}Ar$ technique was applied following procedures applied at the University of Nevada, Las Vegas, which have been outlined by Staudacher et al. (1978). Synthetic K-glass and optical grade CaF_2 were included in the irradiation packages to monitor neutron induced argon interferences from K and Ca. Loaded tubes were packed in an Al container for irradiation. 200 mg samples were irradiated at McMaster Nuclear Reactor at McMaster University, Ontario, Canada. The samples have been in-core for 7 h in the 5C position where they were surrounded by fuel rods on all four sides. J factors were determined by fusion of 3–5 individual crystals of neutron fluence monitors which gave reproducibility of 0.10 to 0.40% at each standard position. An error in J between 0.54 and 0.98% was used

in age calculations. Samples analyzed by the furnace step-heating method utilized a double vacuum resistance furnace similar to the Staudacher et al. (1978) design. Reactive gases were removed by three GP-50 SAES getters prior to being admitted to a MAP 215-50 mass spectrometer by expansion. Mass spectrometer discrimination and sensitivity was monitored by repeated analysis of atmospheric argon aliquots from an on-line pipette system. Measured $^{40}Ar/^{36}Ar$ ratios were 287.23±0.36% during this work, thus a discrimination correction of 1.02879 (4 AMU) was applied to measured isotope ratios. An age of 27.9 Ma (Steven et al., 1978; Cebula et al., 1986) was used for the Fish Canyon Tuff sanidine flux monitor in calculating ages for samples.

For $^{40}Ar/^{39}Ar$ analysis, a plateau segment consists of 3 or more contiguous gas fractions having analytically indistinguishable ages (i.e., all plateau steps overlap in age at $\pm 2\sigma$ analytical error) and comprising a significant portion of the total gas released (typically >50%). Total gas (integrated) ages are calculated by weighting by the amount of ^{39}Ar released, whereas plateau ages are weighted by the inverse of the variance. For each sample inverse isochronal diagrams are examined to check for the effects of excess argon. Reliable isochrones are based on the MSWD criteria of Wendt and Carl (1991) and, as for plateaus, must comprise contiguous steps and a significant fraction of the total gas released. All analytical data are reported at the 1σ confidence level.

A.3. Geochemical analysis

Approximately 500 g samples of fresh wallrock and vein quartz material were collected for analysis. These samples were crushed. Off these, 5 g of sample pulp was crushed to 100-mesh size and about 0.2 g was used for the ICP-MS determinations at ACME Laboratories, Canada. Detection limits for MgO, CaO, Na_2O, MnO and Cr_2O_3 were 0.01%. Detection limits for SiO_2, Al_2O_3, K_2O and Fe_2O_3 were 0.04, 0.03, 0.04 and 0.04 wt.%, respectively. Au has the lowest detection limit as 0.5 ppb. Detection limits for Ba, Co, Ga, Hf, Nb, Rb, Se, Sr, Zr, La and Ce were 0.5 ppm, and for Eu, Gd, Dy, Ho, Er, Tm and Yb were 0.05 ppm. The detection limits for Ag, Bi, Cd, Cs, Cu, Hg, Mo, Ni, Pb, Sb, Ta, Th, Tl, U, W, Y, Sm, Te and Lu were 0.1 ppm. Detection limits are 100 ppm for Ti, 5 ppm for V, 1 ppm for Zn, As, Sc, Sn and Zn, and 0.4 ppm for Nd. Detection limit for Pr is 0.02. LOI (Loss on Ignition), C and S were analyzed by Leco (Macro Carbon, Hydrogen, Nitrogen, Sulphur analysis). Major and trace element concentrations were normalized to those of sample "COM-1". Sample COM-1 represents the arithmetic mean of 15 samples with andesitic to dacitic compositions from the Ovacik district (Altunkaynak and Yilmaz, 1998) and the Evciler area (Genç, 1998), and were chosen to represent unaltered rock compositions in the diagrams. A total of 50 samples were analyzed from the Ovacik deposit for the above-mentioned elements; 8 and 7 samples from the Saganci area and the Narlica deposit, respectively, were also analyzed.

A.4. Fluid-inclusion microthermometry

Heating and freezing measurement were performed on a USGS gas-flow heating/freezing system mounted on a Leitz microscope at the Department of Geography and Geology, Auburn University, USA. The stage was calibrated using synthetic fluid inclusion standards manufactured by Synflinc Inc. For the low temperature calibration of the stage pure H_2O (0 °C), a synthetic fluid inclusion standard containing H_2O and CO_2 (−56.6 °C) and chlorobenzene (−45.6 °C) were used. The accuracy is ±2 °C below 300 °C and ±0.2 °C on freezing. Each measurement was repeated three times and was recorded as an average of the three. Photographs of the fluid inclusions were taken prior to microthermometric study in order to record the original vapor and fluid ratio for comparison with those which underwent heating and freezing processes.

A.5. Stable isotope (oxygen, hydrogen and sulfur) analysis

Oxygen isotope analyses were performed at the University of Nevada, Reno, USA using a laser-based extraction technique using BrF_5 as the reagent, and isotope analyses were performed using molecular O_2, modified after the technique of Sharp (1990). Results are reported in $\delta^{18}O$ notations relative to Vienna-standard mean ocean water (V-SMOW) using value of $\delta^{18}O = +9.6$ for standard NBS28. Reproducibility was ±0.1‰ and one standard was analyzed for every five samples.

Hydrogen isotope analyses from fluid inclusions were performed using a technique modified after Koziet (1997) and Hilkert et al. (1999), using a Eurovector model 3028 elemental analyzer interfaced to a Micromass IsoPrime stable isotope ratio mass spectrometer.

Oxygen isotopic compositions of hydrothermal waters in equilibrium with quartz were calculated using an extrapolation of the fractionation equation of Matsuhisa et al., 1979 whereas hydrogen isotopic compositions of hydrothermal waters in equilibrium with illite were calculated using Sheppard and Gilg

(1996) fractionation equation. Reliable fluid inclusion homogenization temperatures are not available from every sample of the quartz veins at Ovacik. Where no microthermometric data were available, the calculation of the fractionation factors for these samples was made using the mean value of the homogenization temperatures of fluid inclusions obtained from this study. However, the isotopic compositions were calculated specifically for only four samples based on the average of several homogenization temperatures of low salinity inclusions from chalcedonic quartz in the Ovacik M and S veins. The calculations of the fractionation factors at Narlica were made using the mean value of the homogenization temperatures of fluid inclusions data from Yilmaz (2002). Due to very low salinities (<2 Eq. % NaCl), no correction factor (Horita et al., 1995) is added to the fractionation equation. Whole-rock sulfur isotope compositions were determined from 38 samples over a sampling depth range from the surface to 200 m.

References

Aldanmaz, E., Pearce, J.A., Thirlwall, M.F., Mitchell, J.G., 2000. Petrogenetic evolution of late Cenozoic, post-collision volcanism in western Anatolia, Turkey. Journal of Volcanology and Geothermal Research 102, 67–95.

Altunkaynak, Ş., Yilmaz, Y., 1998. The Mount Kozak magmatic complex, Western Anatolia. Journal of Volcanology and Geothermal Research 85, 211–231.

Arribas Jr., A., Cunningham, O., Rytuba, J., Rye, O., Kelly, W., Podwysocki, W., Mckee, E., Tosdal, R., 1995. Geology, geochronology, fluid inclusions, and isotope geochemistry of Rodalquilar Au alunite deposit, Spain. Economic Geology 90, 795–822.

Bente, K., Doering, Th., 1995. Experimental studies on the solid-state diffusion of Cu+In in ZnS and on ''disease'', DIS (diffusion induced segregations), in sphalerite and their geological applications. Mineralogy and Petrology 53, 285–305.

Bi, X., Hu, R., Cornell, D.H., 2004. The alkaline porphyry associated Yao'an gold deposit, Yunnan, China: rare earth element and stable isotope evidence for magmatic-hydrothermal ore formation. Mineralium Deposita 39, 21–30.

Bierlein, F.P., Waldron, H.M., Arne, D.C., 1999. Behaviour of rare earth and high field strength elements during hydrothermal alteration of meta-turbidites associated with mesothermal gold mineralization in central Victoria, Australia. Journal of Geochemical Exploration 67, 109–125.

Bingol, E., Delaloye, M., 2000. Granotoids from western and northern Anatolia: geochemistry and modeling of geodynamic evolution. International Geological Review 42, 241–268.

Bortnikov, N.S., Genkin, A.D., Dobrovolskaya, M.G., Muravitskaya, G.N., Filiminova, A.A., 1991. The nature of chalcopyrite inclusions in sphalerite: exolution, coprecipitation, or disease. Economic Geology 86, 1070–1082.

Browne, P.R.L., 1978. Hydrothermal alteration in active geothermal fields. Annual Review of Earth and Planetary Science 6, 229–250.

Cebula, G.T., Kunk, M.J., Mehnert, H.H., Naeser, J.D., Obradovıch, J.D., Sutter, J.F., 1986. The Fish Canyon Tuff, a potential standard for the $^{40}Ar/^{39}Ar$ and fission-track dating methods. Terra Cognita 6, 139.

Clayton, R.N., O'Neıl, J.R., Mayeda, T., 1972. Oxygen isotope exchange between quartz and water. Journal of Geophysical Research 77, 3057–3067.

Cole, D.R., Drummond, S.E., 1986. The effect of transport and boiling on Ag/Au ratios in hydrothermal solutions: a preliminary assessment and possible implications of the formation of epithermal precious-metal ore deposits. Journal of Geochemical Exploration 25, 45–79.

Cooke, D.R., Simmons, S.R., 2000. Characteristics and genesis of epithermal gold deposits. Reviews in Economic Geology 13, 221–244.

Criss, R.E., Champion, D.E., McIntyre, H., 1985. Oxygen isotope, aeromagnetic, and gravity anomalies associated with hydrothermally altered zones in the Yankee Fork mining district, Custer County, Idaho. Economic Geology 80, 1277–1296.

Dag, N., 1993. Fluid inclusion study on Narlica prospect. Unpublished company report, Eurogold, Turkey, 11 pp.

Delaloye, M., Bingöl, E., 2000. Granitoids from western and northwestern Anatolia: Geochemistry and modeling of geodynamic evolution. International Geology Review 42, 241–268.

Ebert, S., 2004. Ovacik Normandy Gold Mine, Turkey. Unpublished company reports, Normandy, Turkey, 18 pp.

Ercan, T., Turkecan, A., Akyürek, B., Günay, E., Cevikbaş, A., Ateş, M., Can, B., Erkan, M., Ozkırışçı, E., 1984. The geology of Dikili–Bergama–Çandarlý area (Western Anatolia) and petrology of the magmatic rocks. Jeoloji Mühendisliği Dergisi 20, 47–60 (In Turkish with English abstract).

Ercan, T., Satir, M., Steinitz, G., Dora, A., Sarifakioglu, E., Adis, C., Walter, H.J., Yıldırım, T., 1995. Biga yarimadasi ile Gokceada, Bozcaada ve Tavsan adalarindaki (KB Anadolu) Tersiyer volkanizmasinin ozellikleri. Maden Tetkik ve Arama Enstitusu Dergisi 117, 55–86 (in Turkish with English Abstract).

Faure, K., Matsuhisa, Y., Metsugi, H., Mizota, C., Hayashi, S., 2002. The Hishikari au–ag deposit, Japan: oxygen and hydrogen isotope evidence in determining the source of paleohydrothermal fluids. Economic Geology 97, 481–498.

Fournier, R.O., 1985. The behavior of silica in hydrothermal solutions. Reviews in Economic Geology 2, 45–61.

Fry, B., Silva, S.R., Kendall, C., Anderson, R.K., 2002. Oxygen isotope corrections for online $d^{34}S$ analysis. Rapid Communications in Mass Spectrometry 16, 854–858.

Genç, S.C., 1998. Evolution of the Bayramiç magmatic complex, northwestern Anatolia. Journal of Volcanology and Geothermal Research 85, 233–249.

Heald, P., Foley, N.K., Hayba, D.O., 1987. Comparative anatomy of volcanic-hosted epithermal deposits: acid-sulfate and adularia–illite types. Economic Geology 82, 1–26.

Hedenquist, J.W., Browne, P.R.L., 1989. The evolution of the Waiotopu geothermal system, New Zealand, based on the chemical and isotopic composition of its fluids, mineral and rocks. Geochimica et Cosmochimica Acta 53, 2235–2257.

Hedenquist, J.W., Lowenstern, J.B., 1994. The roles of magmas in the formation of hydrothermal ore deposits. Nature 370, 519–527.

Hedenquist, J.W., Izawa, E., Arribas, A., White, N.C., 1996. Hydrothermal systems in volcanic arcs, origin of the exploration for epithermal gold deposits: a short course at Mineral Resource Department. Geological Survey of Japan, Higashi 1-1-3, Tsukuba 305, Japan. 139 pp.

Henley, R.W., Ellis, A.J., 1983. Geothermal systems ancient and modern: a geochemical review. Earth Science Reviews 19, 1–50.

Hilkert, A.W., Douthitt, C.B., Schlüter, H.J., Brand, W.A., 1999. Isotope ratio monitoring gas chromatography/mass spectrometry

of D/H by high temperature conversion isotope ratio mass spectrometry. Rapid Communications in Mass Spectrometry 13, 1226–1230.

Horita, J., Cole, D.R., Weslowski, D.J., 1995. The activity-composition relationship of oxygen and hydrogen isotopes in aqueous salt solutions: III. Vapor–liquid water equilibriation of NaCl solutions to 350 °C. Geochimica et Cosmochimica Acta 59, 1139–1151.

Kodera, P., Lexa, J., Rankin, A.H., Fallick, A.E., 2005. Epithermal gold veins in a caldera setting: Banska Hodrusa, Slovakia. Mineralium Deposita 39, 921–943.

Koziet, J., 1997. Isotope ratio mass spectrometric method for the on-line determination of oxygen-18 in organic matter. Journal of Mass Spectrometry 32, 103–108.

Leach, T.M., Corbett, G.J., 2001. Characteristics of low sulfidation Au–Cu systems in the southwest Pacific. Pacific Rim Congress 95, 19–22 November 1995, Auckland, New Zealand, Proceedings. The Australasian Institute of Mining and Metallurgy, pp. 327–332.

Lepetit, P., Bente, K., Doering, T., Luckhaus, S., 2003. Crystal chemistry of Fe-containing sphalerites. Physics and Chemistry of Minerals 30, 185–191.

Matsuhisa, Y., Goldsmith, J.R., Clayton, R.N., 1979. Oxygen isotopic fractionation in the system quartz–albite–anorthite–water. Geochimica et Cosmochimica Acta 43, 1131–1140.

Mauk, J.L., Hoskin, P.W.O., Seal II, R.R., 1998. Morphology of pyrite and marcasite at the Golden Cross mine, New Zealand. In: Arehart, G.B., Hulston, J.R. (Eds.), Water–rock interaction, vol. 9. Balkema, Rotterdam, pp. 557–560.

McInnes, B.I.A., Crocket, J.H., Goodfellow, W.D., 1990. The Laforma deposit, an atypical epithermal-Au system at Free Gold Mountain, Yukon Territory, Canada. Journal of Geochemical Exploration 36, 73–102.

Mckenzie, D., Yilmaz, Y., 1991. Deformation and volcanism in western Turkey and Aegean. Bulletin of the Technical University of Istanbul 44, 345–373.

MTA-JISCA, 1987. The prefeasibilty study on the Dikili–Bergama geothermal development. Final project report. Japan International Cooperation Agency. 128 pp.

Murowchick, J.B., 1992. Marcasite inversion and the retrographic determination of pyrite ancestry. Economic Geology 87, 1141–1152.

Murowchıck, J.B., Barnes, H.L., 1986. Marcasite precipitation from hydrothermal solutions. Geochimica et Cosmochimica Acta 50, 2615–2629.

Nakamura, N., 1974. Determination of REE, Ba, Fe, Mg, Na and K in carbonaceous and ordinary chondrites. Geochimica et Cosmochimica Acta 38, 757–773.

Ohmoto, H., Rye, R.O., 1979. In: Barnes, H.L. (Ed.), Geochemistry of Hydrothermal Ore Deposits. Wiley, New York, pp. 509–567.

Palacios, C.M., Hein, U.F., Dulski, P., 1986. Behavior of rare earth elements during hydrothermal alteration at the Buena Esperanza copper–silver deposit, north Chile. Earth and Planetary Science Letters 80, 208–216.

Peccerillo, A., Taylor, J.R., 1976. Geochemistry of Upper Cretaceous volcanic rocks from the Pontic chain, Northern Turkey. Bulletin of Volcanology 39, 557–56.

Reyes, A.G., 1990. Petrology of Philippine geothermal systems and the application of alteration mineralogy to their assessment. Journal of Volcanology and Geothermal Research 43, 279–309.

Roedder, E., 1984. Fluid inclusions. Reviews in Mineralogy 12 644 pp.

Rye, R., 1993. Evolution of magmatic fluids in the epithermal environment. The stable isotope perspective. Economic Geology 88, 733–753.

Sasaki, A., Arikawa, Y., Folinsbee, R.E., 1979. Kiba reagent meethod of sulfur extraction applied to isotopic work. Bulletin of the Geological Survey of Japan 30, 241–245.

Schoen, R., White, D.E., Hemley, J.J., 1973. Argillization by descending acid at the Steamboat springs, Nevada. Clays and Clay Minerals 22, 1–22.

Seal II, R.R., Rye, O., 1992. Stable isotope of water-rock interaction and ore formation, Bayhorse base and precious metal district, Idaho, USA. Economic Geology 87, 271–287.

Sener, A.K., 2003. Preliminary study of low-sulfidation epithermal Ovacik gold–silver deposit. In: Eliopoulos, D.G., et al. (Ed.), Mineral Exploration and Sustainable Development. Millpress, Rotterdam, pp. 519–522.

Seyitoglu, G., Scott, B., 1991. Late Cenozoic crustal extension and basin formation in west Turkey. Geological Magazine 128, 155–166.

Seyitoglu, G., Anderson, D., Nowell, G., Scott, B., 1997. The evolution from Miocene potassic to Quaternary sodic magmatism in Western Turkey: implications for enrichment processes in lithospheric mantle. Journal of Volcanology and Geothermal Research 76, 127–147.

Sharp, Z.D., 1990. A laser-based microanalytical method for the in situ determination of oxygen isotope ratios of silicates and oxides. Geochimica et Cosmochimica Acta 54, 1353–1357.

Sheppard, S.M.F., Gilg, H.A., 1996. Stable isotope geochemistry of clay minerals. Clays and Clay Minerals 22, 1–24.

Sherlock, R.L., Tosdal, R.M., Lehrman, N.J., Graney, J.R., Losh, S., Jowett, E.C., Kesler, S.E., 1995. Origin of the McLaughlin mine sheeted vein complex: metal zoning, fluid inclusion and isotopic evidence. Economic Geology 90, 2156–2181.

Sillitoe, R.H., Hedenquist, J.W., 2003. Linkages between volcanotectonic settings, ore-fluid compositions, and epithermal precious-metal deposits. In: Simmons, S.F., Graham, I. (Eds.), Volcanic, geothermal, and ore-forming fluids: rulers and witnesses of processes within the earth, vol. 10. Society of Economic Geologists Special Publication, pp. 315–343.

Simpson, M.P., Mauk, J.L., Simmons, S.T., 2001. Hydrothermal alteration and hydrologic evolution of the Golden Cross epithermal Au–Ag deposit, New Zealand. Economic Geology 96, 773–796.

Staudacher, T.H., Jessberger, E.K., Dorflinger, D., Kiko, J., 1978. A refined ultrahigh-vacuum furnace for rare gas analysis. Journal of Physics E: Scientific Instruments 11, 782–784.

Steven, T.A., Mehnert, H.H., Obrodovich, J.D., 1978. Age of volcanic activity in the San Juan Mountains, Colorado. U.S. Geological Survey Professional Paper 575-D, 47–55.

Wendt, I., Carl, C., 1991. The statistical distribution of the mean squared weighted deviation. Chemical Geology 86, 275–285.

White, N.C., Hedenquist, J.W., 1990. Epithermal environments and styles of mineralization: variation and their causes, and guide lines for exploration. Journal of Geochemical Exploration 36, 445–474.

White, N.C., Hedenquist, J.W., 1995. Epithermal gold deposits. Styles, characteristics and exploration. SEG Newsletter 27, 1–13.

Wright, J., 1996. Mineralization associated with volcanic terrains: the Mesozoic–Cenozoic Alpine collision zone. Normandy Mining Group Geological Conference, 18–25 November, Darwin, Northern Territory, Australia, Report No: CR21049.

Wright, J., Piantone, H., Cassard, D., Özaslan, G., 1996. Results of 1995 field program, Western Anatolia. LaSource Project Generation Group-N2344, Orleans, France.

Yilmaz, Y., 1989. The origin of young volcanic rocks of western Turkey. In: Sengor, A.C.M. (Ed.), Tectonic Evolution of the Tethyan Region. Kluver Academic Publishers, pp. 159–189.

Yilmaz, H., 2002. Ovacik gold deposit—An example of quartz–adularia-type gold mineralization in Turkey. Economic Geology 97, 1829–1839.

Yilmaz, Y., Kracik, Z., 2001. Geology of the northern side of the Gulf of Edremit and its tectonic development of the Aegean grabens. Geodinamica Acta 14, 31–43.

Yilmaz, Y., Genç, S.C., Karacik, Z., Altunkaynak, S., 2001. Two contrasting magmatic association of NW Anatolia and tectonic significance. Journal of Geodynamics 31, 243–271.

Zanchi, A., Kissel, C., Tipirdamaz, C., 1990. Continental deformation in western Turkey: a structural and paleomagnetic approach. In abstract International Earth Science Congress on Aegean Regions, October 1–6, 1990. Dokuz Eylul University, İzmir, Turkey, pp. 357–367.

Zanchi, A., Kissel, C., Tipirdamaz, C., 1993. Late Cenozoic and quaternary brittle continental deformation in western Turkey. Bulletin Sociéte Geologique de France 164, 507–517.